2017

Rational Design of High Temperature Water-Gas Shift Catalysts with Non-Toxic Earth-Abundant Elements

Minghui Zhu
Lehigh University

Rational Design of High Temperature Water-Gas Shift Catalysts with Non-Toxic Earth-Abundant Elements

by

Minghui Zhu

A Dissertation
Presented to the Graduate and Research Committee of Lehigh University
in Candidacy for the Degree of
Doctor of Philosophy

in

Chemical Engineering

Lehigh University

January 2017

CERTIFICATE OF APPROVAL

Approved and recommended for acceptance as a dissertation in partial fulfillment of the requirements for the degree of Doctor of Philosophy.

_____
Date

_____
Accepted Date

Dissertation Director:

_____
Dr. Israel E. Wachs
Lehigh University

Committee Members:

_____
Dr. James T. Hsu
Lehigh University

_____
Dr. Hugo S. Caram
Lehigh University

_____
Dr. Mark A. Snyder
Lehigh University

_____
Dr. Jonas Baltrusaitis
Lehigh University

_____
Dr. Anatoly Frenkel
Yeshiva University

ACKNOWLEDGEMENTS

I would like to give special thanks to my advisor Professor Israel E. Wachs for giving me the opportunity to join his research group and for his guidance throughout my years at Lehigh University. His passionate attitude and knowledge about catalysis research field was inspirational and has opened my eyes to how research needs to be approached and conducted.

I would like to thank all the members in my lab group for their help and support throughout the years: Jih-Mirn Jehng, Michael E. Ford, Chip Roberts, Julie Molinari, Peter Phivilay, Yadan Tang, Christopher J. Keturakis, Soe Lwin, Anisha Chakrabarti, Özgen Yalçin, Benjamin Moskowitz.

Among all my colleagues in the lab, I would like to emphasize the contribution from Christopher J. Keturakis who graduated since Jan 2016. Chris joined the group since 2007 as undergraduate student and started the project on Water-Gas Shift Reaction. His fundamental work initiated our interest in this topic and contributed to the following research. Chris is also an expert in this topic and has given me many valuable suggestions and guidance on my Ph.D. research.

This dissertation wouldn’t have been possible without the help from my collaborators. I would like to thank Dr. Tulio Rocha from Fritz Haber Institute-Berlin

to perform the cutting edge Near Ambient Pressure – XPS measurement. I would like to thank Dr. Thomas Lunkenbein and Professor Axel Knop-Gericke from Fritz Haber Institute-Berlin for the TEM measurement. I would like to thank Dr. Yuanyuan Li and Dr. Nebojsa Marinkovic from for teaching me how to perform the in situ XAS measurement in Brookhaven National Laboratory. I also would like to thank Prof. Anatoly Frenkel from Yeshiva University for all the beamline accessibilities.

Most of all I would like to thank my friends and family for their loving support, always encouraging and motivating me to do my best. Without my parents and the rest of my family, I would not have accomplished as much as I have in my life. This work is dedicated to them and I am thankful for everything that they have given me.

TABLE OF CONTENTS

LIST OF TABLES

CHAPTER 1

CHAPTER 3

CHAPTER 5

LIST OF FIGURES

CHAPTER 1

CHAPTER 2

CHAPTER 3

CHAPTER 4

CHAPTER 5

ABSTRACT

The copper promoted chromium-iron oxide has for decades been used as the commercial catalyst for production of H_2 via the High Temperature-Water Gas Shift reaction (HT-WGS). The wide operation temperature range, high activity and robust thermostability has made this catalyst the catalyst of choice for HT-WGS. The toxic nature of hexavalent chromium has motivated extensive research to develop non-chromium HT-WGS catalysts. The lack of fundamental understanding of this HT-WGS catalyst system (catalyst structure under working conditions, reaction mechanism and copper/chromium promotion mechanism), however, have hampered the developed of Cr-free catalysts.

The objectives of the dissertation were (1) to resolve the fundamentals of copper and chromium promotion mechanisms for the HT-WGS reaction, and (2) then apply the new fundamental insights to guide the rational design of chromium-free iron oxide-based HT-WGS catalysts. Temperature programmed surface reaction (TPSR) was employed to resolve the decades long debate regarding the HT-WGS reaction mechanism on iron oxide-based catalysts. Isotope $C^{16}O_2/C^{18}O_2$ switch experiments provided insights on the nature of active sites and the participation of surface oxygen, which allowed for the first time to calculate the Turnover Frequency (TOF) of iron

oxide-based HT-WGS catalysts. To understand the structure of copper promoted chromium-iron oxide catalyst under reaction condition, a series of modern characterization techniques were employed (XRD, *in situ* Raman spectroscopy, Near Ambient Pressure X-ray Photoelectron Spectroscopy (NAP-XPS), High-Sensitivity Low-Energy Ion Scattering (HS-LEIS) Spectroscopy, *in situ* X-ray Absorption Spectroscopy and TEM-EDX). The activated catalysts were chemically probed with CO-Temperature Programmed Reduction (TPR) to examine the effects of copper and chromium on the catalyst activity for removing oxygen by CO, which is the rate-determining-step. These findings provided critical insights into the promotion mechanisms of copper and chromium. Finally, based on the fundamental understanding of the existing commercial catalysis system, new chromium-free, environmentally friendly iron oxide based HT-WGS catalysts were rationally designed.

CHAPTER 1

Overview of Iron-Based Catalysts for the High Temperature Water-Gas Shift (HT-WGS) Reaction

1.1 Introduction

The United States Congress has determined that hydrogen energy is expected to solve many of our energy needs, resulting in the Energy Policy Act of 2005 and the Energy Independence and Security Act of 2007 [1-4]. According to the Department of Energy (DOE), "hydrogen and fuel cells offer a broad range of benefits for the environment, for our nation's energy security, and for our domestic economy, including: reduced greenhouse gas emissions; reduced oil consumption; expanded use of renewable power (through use of hydrogen for energy storage and transmission); highly efficient energy conversion; fuel flexibility (use of diverse, domestic fuels, including clean and renewable fuels); reduced air pollution; and highly reliable grid-support."[4]

Most hydrogen ($\geq$ 80%) is currently produced by steam methane reforming (SMR) followed by the water-gas shift (WGS) reaction:

SMR: $CH_4 + H_2O \leftrightarrow 3H_2 + CO$ (1)

WGS: $H_2O + CO \leftrightarrow H_2 + CO_2$ (2)

and the remaining hydrogen (≤ 20%) is produced as a by-product of chemical processes [1]. Even though the SMR-WGS process for H_2 production is based on non-sustainable methane and produces global warming CO_2 as a byproduct, this process will continue as the dominant technology for the foreseeable future given its cost-effective economics and the abundance of shale gas in the USA. The infrastructure for supplying H_2 for fuel-cell powered automobiles that are being rolled out by automotive companies in the USA is already being put into place by the California Energy Commission and is based on either on-site production at filling stations or centralized locations that will produce H_2 via the conventional SMR-WGS process [5].

The water-gas shift reaction (WGS) is a moderately exothermic reversible reaction that is thermodynamically favored at low temperatures and kinetically favored at high temperatures. Thus, the reaction is industrially performed in several stages with different catalysts to optimize the greater CO equilibrium conversion attained at lower temperatures [1, 6]. The high temperature shift (HTS) reaction is performed at ~350-450ºC with iron oxide-based catalysts and the low temperature shift (LTS) reaction is performed at ~190-250ºC with copper-zinc oxide-based catalysts. Additionally, there has been research into medium temperature shift (MTS) catalysts and sulfur tolerant "sour gas" shift catalysts [6]. The water-gas shift reaction has received much attention

in the catalysis literature because of its importance for H_2 production. There have been many recent advances in our understanding of the LTS catalysts [6, 7], but HTS catalysts remain poorly understood as will be revealed in the literature review below. Furthermore, little progress has been made in the development of these catalysts during the past three decades.

The industrial water-gas shift catalytic reaction was initially developed in 1914 by Bosch and Wild. An unsupported iron-chromium oxide catalyst was used to remove CO from the H_2 stream for the Haber-Bosch ammonia synthesis process since CO is a poison for the ammonia synthesis Fe-based catalyst [8]. The iron-chromium oxide WGS catalyst technology was subsequently applied to control the H_2/CO ratio of syngas for production of hydrogen from methane steam reforming, methanol synthesis and Fischer-Tropsch synthesis of hydrocarbons [1, 6, 9]. Until the 1980s, the patent and scientific literature focused on improving the synthesis of the existing iron-chromium oxide catalyst [10-17]. Research in the 1980s began to explore, by trial-and-error, the effect of a wide range of promoters to try to stabilize surface area, increase activity and enhance thermal stability of catalysts under the WGS reaction conditions. The additives can be broadly divided into two categories: chemical promoters (Cu, Rh) [18-23] and textural promoters (Cr, Al, Th, Zr, Zn, Mg) [24-29].

Extensive literature reviews of the WGS catalytic reaction have already appeared.

Newsome summarized the catalysis literature up to 1980 [1], Rhodes *et al*. reviewed the literature up to 1995 [9], Ladebeck and Wagner assessed developments up to 2003 with an emphasis on fuel cell applications [30], and Ratnasamy and Wagner reviewed more recent developments up to 2009 [6]. A more recent survey on Cr-free Fe-based HTS catalysts reflects the current strong interest on this topic [31]. Despite extensive study, the functioning of the iron-based HTS catalyst is still not well understood because the prior studies focused on the catalyst bulk properties. Almost no surface information has been provided, especially under *in situ* and reaction conditions. Consequently, the reaction mechanism, the most abundant reactive intermediates (mari) and the rate–determining- step (rds) for the iron –catalyzed HT-WGS reaction remain the subjects of ongoing debate.

This opening chapter reviews the extensive results from the study of iron-based HTS catalysts in the past decades with emphasis on understanding the catalytic active sites, reaction mechanism, reaction kinetics, and the role of different additives.

1.2 Reaction Mechanism, Kinetics and Rate-Determining-Step

The reaction mechanism and kinetics of the high temperature WGS reaction have been extensively studied without reaching a general agreement [32]. Armstrong and Hilditch were the first to propose a reaction mechanism that involves a surface reaction intermediate such as surface formate, HCOO∗, in 1920.[33] This mechanism is referred

to as the associative mechanism. Subsequent experimental and modeling studies of the high temperature WGS reaction have been inconclusive, both supporting and contradicting the presence of a surface formate intermediate.[34, 35]

Although the associative mechanism is widely accepted as the predominant mechanism for the low temperature water-gas shift reaction, the redox mechanism is thought to be dominant for the HT-WGS reaction over iron–based catalysts. The importance of the redox mechanism for these high temperature catalysts has been confirmed by Boreskov *et al.* [36] who studied the reaction dynamically by separately measuring the catalyst oxidation and reduction rates. He showed that a Fe^{2+}/Fe^{3+} redox couple occurred for Cr_2O_3-Fe_2O_3 catalysts, with Fe^{2+} being oxidized to Fe^{3+} by H_2O and Fe^{3+} becoming reduced by CO. Diagne *et al*. [35] studied the WGS reaction mechanism between 250~400°C with a commercial Fe based catalyst by chemical trapping (by using dimethyl sulfate) on activated catalyst, TPD after reaction and HCOOH adsorption. The results showed a decrease in the surface formate coverage as the temperature increased, suggesting that surface formate is not the predominant reaction intermediate under HT-WGS conditions and that the redox mechanism is more plausible. Khan and Smirniotis [37] more recently analyzed a series of promoted ferrites (Cr, Mn, Co, Ni, Cu, Zn and Ce) by comparing their WGS activity and the H_2-TPR results. Incorporation of metal promoters into hematite (Fe_2O_3) was found to

change the reducibility of Fe^{3+} species, which in turn changed the WGS activity. Higher WGS activity was found to be related to easier reduction of Fe^{3+} oxide, which lead to the conclusion that the WGS activity depends on the reducibility of $Fe^{3+}\leftrightarrow Fe^{2+}$ redox couple. Such dependency indicated that the redox mechanism is more likely to taking place during HT-WGS on Fe-based catalysts.

In 1949, Kulkova and Temkin first proposed that the WGS reaction proceeds via alternating reduction and oxidation of the surface of iron oxides, which is known today as the regenerative or redox mechanism, and is shown as reaction steps 3 and 4 below:

$$CO + O* \leftrightarrow CO_2 + * \quad (3)$$

$$H_2O + * \leftrightarrow H_2 + O* \quad (4)$$

with "$*$" representing a catalytic active site [38]. This mechanism involves alternating reduction of the catalyst surface by CO and oxidation of the catalyst surface by H_2O. It is the most popular mechanism in the current catalysis literature for the HT WGS reaction by iron-based catalysts [6, 9, 39-41]. Support of this mechanism came from Boreskov et al. [36] who showed that the rates at which water oxidizes the magnetite surface and carbon monoxide reduces it correspond to the rate of the water-gas shift reaction. Kubsh and Dumesic [39] performed an *in situ* gravimetric study of oxygen removal from and incorporation into Cr_2O_3/Fe_2O_3 catalysts by CO_2/CO and H_2O/H_2 gas mixtures at about 350^{o}C. The equilibrium surface coverage by oxygen was found

to depend on the ratios of $P(CO_2)/P(CO)$ and $P(H_2O)/P(H_2)$. The same surface oxygen coverage was found with CO_2/CO gas mixtures as with H_2O/H_2 mixtures, provided that the ratio of $P(CO_2)/P(CO)$ was equal to that of $P(H_2O)/P(H_2)$. These data further supported the redox mechanism. Note that in this study, the oxygen uptake was considered to only be surface oxygen.

In the Kubsh work, however, there was a discrepancy between the predicted and measured steady-state reaction rates. The discrepancy was concluded to arise from the presence of adsorbed species other than oxygen, which indicated that an adsorption mechanism for HT-WGS may also exist over magnetite based catalysts. Lund and Dumesic [42] concluded that catalysts not active for adsorption of CO and CO_2 are also not active for the WGS reaction. Furthermore, other researchers observed that H_2 is liberated slowly by performing transient reactor studies, which was not consistent with the two-step redox mechanism [43-46]. However, in these studies, the adsorption of H_2O was performed on oxidized catalysts that are expected to retard the dissociative adsorption of moisture and the release of H_2. Because of the conclusion that H_2 release is slow, more detailed mechanisms with adsorptive steps were proposed and investigated. A multistep Langmuir-Hinshelwood mechanism represented by reaction steps 5-9 was proposed by Mezaki and Oki [47-49]. By using the stoichiometric number method developed by Horiuti [50], they simultaneously measured the exchange

rates of various isotopes (deuterium, carbon-13, carbon-14 and oxygen-18) between reactants and products and the free energies of the exchange reactions. They concluded that the rate-determining-step is the evolution of H_2 gas (Eq. 9) at low CO conversion and the adsorption of CO (step 5) at the steady-state, near-equilibrium conditions prevalent in industrial reactors.

$$CO + * \leftrightarrow CO* \quad (5)$$

$$H_2O + 3* \leftrightarrow 2H* + O* \quad (6)$$

$$CO* + O* \leftrightarrow CO_2* + * \quad (7)$$

$$CO_2* \leftrightarrow CO_2 + * \quad (8)$$

$$2H* \leftrightarrow H_2 + 2* \quad (9)$$

Tinkle and Dumesic [51] investigated the adsorption/desorption and the interconversion of CO and CO_2 on chromium promoted magnetite at 565 and 627K with $^{13}CO/^{12}CO_2$ and $^{12}CO/^{13}CO_2$. The rate of interconversion was shown to be limited by the rates of adsorption/desorption, indicating that either adsorbed CO/CO_2 are in equilibrium on the surface or that the adsorption of CO and CO_2 leads to the same surface species. A 5-step mechanism involving both adsorptive and regenerative steps was then proposed as:

$$CO + O* \leftrightarrow CO_2* \quad (10) \quad \text{slow}$$

$$CO_2* \leftrightarrow CO2 + * \quad (11) \quad \text{slow}$$

$$H_2O + * \leftrightarrow H_2O*$$ (12) fast

$$H_2O* + O* \leftrightarrow 2OH*$$ (13) fast

$$2OH* \leftrightarrow 2O* + H_2$$ (14) slow

in which the adsorption and cleavage of water steps are fast.

Salmi *et al*. [43] investigated the WGS reaction over an industrial ferrochrome catalyst by transient experiments in a gradientless spinning basket reactor. The responses of CO, CO_2 and H_2 were measured after step changes at the reactor inlet. The authors concluded that the rate of the water-gas shift over chromium promoted magnetite is controlled by the interconversion rate of CO/CO_2 and desorption rate of hydrogen, whereas the adsorption of H_2O is rapid. Hence, the steady-state kinetics was described with a rate expression that is first order with respect to CO, zero-order in H_2O, first-order in CO_2 and second-order in H_2. A mechanism was then proposed involving two different types of active sites, and both adsorptive and regenerative steps:

$$CO + (O*_2) \leftrightarrow CO_2(*)_2$$ (15) slow

$$CO_2(*)_2 \leftrightarrow CO_2 + (*)_2$$ (16) slow

$$H_2O + (*)_1 \leftrightarrow H_2O(*)_1$$ (17) fast

$$H_2O(*)_1 + (*)_1 + (*)_2 \leftrightarrow 2H(*)_1 + O(*)_2$$ (18) slow

$$2H(*)_1 \leftrightarrow H_2 + 2(*)_1$$ (19) slow

Where $(*)_1$ and $(*)_2$ denote different sites for CO and H_2O adsorption. However, no

supporting evidence for two active sites was provided.

In Salmi *et al*.'s work, delayed H_2 evolution was observed upon switching from inert gas to CO and H_2O feeds over activated catalysts. Pretreatment of the activated catalyst with H_2O, however, was found to retard the response of H_2 while having no effect on the formation of CO_2. This delay was extensively discussed and fitted by the author. Without *in situ* characterization, however, the conclusions are untenable due to the possibility that catalyst surface became partially oxidized during the N_2 flush or H_2O pretreatment. A similar switch of feeds over partially oxidized catalysts will also result a slower response of H_2 compared to CO_2 since the CO will first reduce the catalysts to its working condition and then allow water to decompose to H_2.

Many other reaction mechanisms which involve small modifications to one or two steps of a previously reported mechanism have also been suggested in the catalyst literature. Several researchers have proposed micro-kinetic mechanisms based on a large number of elementary steps [52-56]. However, in these proposals, there is no consensus on the rds, with some authors suggesting that it is CO adsorption [44, 47, 57, 58], CO oxidation [56, 59, 60], CO_2 desorption [44, 45], H_2 formation [44, 45, 47] or a combination of these steps.

Density Functional Theory (DFT) calculation have also been applied to examine the possible reaction pathways of the water-gas shift reaction. Most of the studies,

however, are based on metals (e.g. Pt, Cu) that perform the LTS [61-63]. Studies of Fe-based catalysts are confined to investigation of the adsorption of reactants or the presence of intermediates like formic acid [21, 46, 60] . More recently, Chen *et al.* [64] applied DFT calculations to a Fe_3O_4 (111) surface without surface hydroxyls to investigate both the redox and associative mechanisms. They concluded that the adsorption energy for CO is higher than that for H_2O and that H_2 formation is the rate-determining-step for both reaction mechanisms.

Researchers seeking to model the high temperature WGS have proposed numerous reaction rate equations and more than 20 different kinetic equations have appeared over the past 40 years. Newsome [1] extensively discussed the proposed kinetic equations published prior to 1975. However, disagreement on the precise form of the rate equation and values of the rate constants and activation energies still lingers. This uncertainty has been attributed to the presence of gas phase impurities, to varying degrees of mass-transfer limitation, and to the fact that kinetic measurements have been mostly obtained with integral rather than differential reactors that were often operating around atmospheric pressure. Fott *et al*. [65] stated that the main criterion which enables suitable evaluation of a given kinetic expression is the dependence of pressure on the reaction rate.

Five main classes of reaction models (see Table 1.1) have been proposed for the HT-

WGS reaction over Cr-Fe-O mixed oxide catalysts [66]: (i) Langmuir-Hinshelwood model; (ii) Hulburt -Vasan model; (iii) Kodama model; (iv) Oxidation - reduction model and (v) Power law model. Podolski *et al*. [67] performed experiments in a recycle reactor and concluded that only the Langmuir-Hinshelwood and the empirical power law models (reaction order values are given in Table 1.2) could fit all of the experimental results better.

The steady-state reaction orders (a, b, c, and d for CO, H_2O, CO_2 and H_2, respectively) for the reported power law analyses are listed in Table 1.2. For Fe-Cr catalysts, the dependence on CO partial pressure is ~1.0 and between 0-0.5 for H_2O partial pressure (an average of ~0.25). These reaction orders are consistent with the larger H_2O equilibrium adsorption constant, K_{H2O}, on oxides and the smaller CO equilibrium adsorption constant, K_{CO}, on oxides, [68] which suggests that the working catalyst surface has a much higher concentration of adsorbed H_2O than adsorbed CO. For the reverse reaction by Fe-Cr catalysts, the reaction order is 0 on the H_2 partial pressure dependence and between -0.6-0 on the CO_2 partial pressure dependence (an average of ~-0.3), which suggests that the supply of H_2 and CO_2 to the surface is not limiting and CO_2 even slightly inhibits the forward reaction by undergoing reverse WGS. The almost zero-order dependence on the partial pressures of CO_2 and H_2 suggest that the equilibrium adsorption constants are large for these two gas phase molecules. For the

Fe-Cr-Cu catalyst, the dependence on CO partial pressure remains ~1 and the dependence on H_2O partial pressure is between 0-0.3 with an average value of ~0.1. The dependence on H_2 partial pressure is ~0 and the dependence on CO_2 partial pressure is between -0.16 to -0.36 (an average of -0.26). The kinetic parameters in Table 1.2 indicate that the reaction orders are comparable for the Fe-Cr and Fe-Cr-Cu catalysts suggesting that Cu addition has only a modest, if any effect, on the partial pressure dependence of the reactants and products for the HT-WGS reaction. The activation energy values vary from 95-118 kJ/mol (average of 109 kJ/mol) for Fe-Cr and 75-111 kJ/mol (average of 92 kJ/mol) for Fe-Cr-Cu. The addition of Cu to Fe-Cr catalysts, thus, appears to decrease the activation energy by ~20-40 kJ/mol reflecting the promoting role of Cu for the HT-WGS reaction.

Other researchers extended the above models to industrial scale for reactor design. Chinchen *et al*. [69-71] studied the kinetics of an industrial HT-WGS catalyst from experiments with a semi-technical unit and a micro-reactor system under relevant industrial conditions (up to 30bar) combined to give consistent kinetics parameters. They estimated the activation energy to be 129.4±2.1 kJ/mol, in good agreement with the value of 121.8 kJ /mol deduced from semi-technical experiments with the same catalyst. Zhao *et al*. [72] evaluated 5 kinetic models proposed by others by using a reduced rate method that is based on the fact that the HT-WGS reaction rate decreases

at lower pressures allowing easier differentiation between the proposed kinetic models. The reduced reaction rates were measured experimentally with an internal circulating gradientless reactor. The study concluded that the most appropriate intrinsic kinetic equation for the high temperature WGS reaction was the one suggested by Fott *et al*. [65] derived from the Langmuir–Hinshelwood model with the rate-determining-step being the surface reaction between adsorbed CO and H_2O at pressures up to 10bar. Singh *et al*. [73] extended the kinetics from the laboratory catalyst studies to industrial scale by incorporating factors for diffusion limitation, catalyst aging, pressure correction and effect of exposure to H_2S. Rase [74], based on industrial data, provided a kinetic expression for the HT-WGS reaction, which was later adopted by Elnashaie *et al*. [75] in their modeling of the WGS reaction. Hla *et al*. [76] carried out the HT-WGS reaction for varying catalyst compositions and derived two rate equations (see Table 1.2). Adams *et al*. [77] further improved Hla *et al*.'s model by introducing correction factors for porosity.

The fact that the reaction kinetics are described equally well by several equations hinders determination of a unique reaction mechanism based on kinetic analysis. The similar mathematical fits by multiple kinetic expressions is a recognized dilemma in the kinetics literature which results from the simplifying assumptions made during derivation of kinetic equations. Consequently, it is impossible to discriminate among

the reaction mechanisms solely based on reaction kinetics without supporting *in situ* and *operando* spectroscopy studies.

1.3 Unpromoted Iron Oxide Catalysts

There have been extensive studies on iron oxide catalysts, especially *in situ* IR studies with chemical probe molecules (N_2, H_2, O_2, CO, CO_2, CH_3OH, HCOOH and HCHO), that indicate the type of surface complexes that form on iron oxides [34, 78-88]. Only one *in situ* IR investigation of unpromoted Fe_2O_3 during the WGS reaction at 450^{o}C has been reported; no surface reaction intermediates were observed [79]. The authors concluded that no surface formate or carbonate species can form on iron-based catalyst during WGS, and advanced this observation as proof for the redox mechanism for iron-based catalysts. However, the surface concentration and lifetime of potential surface intermediates at such elevated temperatures would be too small to permit their detection.

Three different bulk iron oxide phases have been reported for Cr-containing iron-based WGS catalysts [89, 90]: hematite (γ-Fe_2O_3 and α-Fe_2O_3) for the fresh, oxidized catalyst and Fe_3O_4 (magnetite) during the reaction. That the Fe_3O_4 phase is the bulk active phase during the HT-WGS reaction has been confirmed by multiple characterization techniques: *in situ* XRD [90, 91], *ex situ* XRD [19, 92-94], *in situ* Mössbauer [95-97], *ex situ* Mössbauer [19, 92-94, 98, 99], *in situ* XAS [90], *in situ*

XPS [18], *ex situ* XPS [92] and *ex situ* Raman [90]. A recent *in situ* XRD-XAS spectroscopy investigation [90] before and during HT-WGS found that the initial γ/α-Fe_2O_3 bulk phases only formed γ-Fe_2O_3 upon heating to 400ºC in an oxidizing environment, transformed to bulk Fe_3O_4 during the WGS reaction, and returned to bulk γ-Fe_2O_3 upon cooling to room temperature. This *in situ* spectroscopy study nicely demonstrates the pronounced dynamics of the bulk iron oxide phases in response to changing environmental conditions and the need to obtain characterization information under relevant reaction conditions. A detailed *in situ* Mössbauer spectroscopy study by Cherkezova-Zheleva and Mitov [96] observed that changing the HT-WGS reaction conditions (temperature and reactant composition) leads to redistribution of the tetrahedeally and octahedrally coordinated cations in the bulk Fe_3O_4 phase. It was observed that among three reaction temperatures tested (573K, 623K and 673K), the Fe^{2+}/Fe^{3+} ratio reached a maximum at 623K. With increasing oxidation potential of the reactants, the Fe^{2+}/Fe^{3+} ratio decreased. It was proposed that the catalytic active sites are probably pairs of Fe^{2+}-Fe^{3+} cations and that the catalytic activity can be explained by combination of the natural thermo-activated and catalytically induced electron exchange that better synchronize the oxidation and reduction steps of the HT-WGS catalyst. Supporting evidence for this hypothesis, however, was not provided. Furthermore, Mössbauer spectroscopy is a bulk technique and does not provide any

information about the surface catalytic active sites

It is important to avoid over-reduction of the bulk Fe_3O_4 to lower oxides, carbides or metallic iron species during catalyst use (reduction, activation and reaction) because the metallic iron and iron-carbide phases are active catalysts for the highly exothermic methanation and Fischer-Tropsch reactions which in turn cause physical damage to the catalyst pellets [9]. One possible cause of over-reduction is the combination of a low concentration of steam and higher than the optimal reaction temperatures. Therefore, the iron-based HTWGS catalyst requires careful reduction before operation by using specific process gas mixtures of hydrogen, nitrogen, carbon monoxide, carbon dioxide and water vapor [66]. Based on plant experience, Lywood and Twigg [100] developed an empirical formula to ensure reliable reduction operation of the iron-based catalysts.

1.4 Promotion of Iron Oxide Catalysts

1.4.1 Chromium

Unpromoted Fe_2O_3 catalysts are easily to sinter under HT-WGS conditions, which will cause a decrease of activity due to reduced surface area. Hence a structural stabilizer, usually Cr_2O_3, is added to industrial HT-WGS catalysts during the co-precipitation synthesis stage. Inclusion of this promoter results in an order of magnitude increase in surface area. Various Cr_2O_3-Fe_2O_3 catalyst compositions have been

examined; incorporation of ~14 wt. % Cr_2O_3 was found to produce the greatest resistance to sintering [101]. The mechanism by which Cr stabilizes the iron oxide surface area is not clear since chromium forms bulk solid solutions with iron oxides ($Fe_{2-x}Cr^{3+}_x O_3$ and $Fe_{3-x}Cr^{3+}_xO_4$). Fresh catalysts initially contain surface Cr^{+6} species that subsequently reduce to Cr^{3+} by the HT-WGS reaction conditions (see Figure 1.1) [26, 89, 92, 102-108]. Despite numerous studies on the structure of Cr_2O_3-Fe_2O_3 catalysts, primarily by bulk analysis, the role of the chromium oxide promoter in stabilizing the iron oxide phase has not been elucidated [31].

The presence of surface Cr and its role in HT-WGS catalyst system has still not been resolved. Some researchers [69-71, 109] proposed that the role of crystalline Cr_2O_3 grains is to physically block the sintering of neighboring Fe_3O_4 particles. Chinchen *et al*. [69-71] evaluated the effect of time-on-stream upon the activity of a variety of Cr_2O_3-Fe_2O_3 catalysts and observed that catalyst sintering does not affect the activation energy for the HT-WGS reaction. It was proposed that catalyst sintering was prevented by discrete Cr_2O_3 crystallites which blocked direct contact between adjacent Fe_3O_4 particles. Such a simple physical barrier model, however, is incompatible with the characterization findings which reveal that crystalline Cr_2O_3 particles are not present for chromium-iron oxide HT-WGS catalysts [19, 25, 27, 89, 90, 92-94, 102, 103, 106-108, 110-116]. Edwards *et al*. [110] found, by high resolution electron

microscopy (HR-TEM) and high spatial resolution energy dispersive X-ray analysis (STEM-EDX), that the activated catalyst is surface enriched in chromia. The stabilization mechanism was proposed to involve a surface region enriched with Cr^{3+}, which is thought to be more thermodynamically stable than an iron oxide rich core. The presence of this Fe-Cr shell would reduce iron diffusion and sintering effects. More recently, it was concluded that Cr^{3+} is also oxidized to Cr^{6+} which in turn would promote the redox cycle of the Fe_3O_4 phase [105]. Currently, chromia is believed to function both as a textural promoter that stabilizes the Fe_3O_4 surface area and as a chemical promoter that enhances the $Fe^{2+} \leftrightarrow Fe^{3+}$ redox cycle.

Only limited information is available in the literature about the surfaces of iron-chromium oxide catalysts; none of it was obtained from studies under relevant HT-WGS reaction conditions. Surface analyses of iron-chromium oxide catalysts with IR [26, 89, 102-104] and XPS [92, 103, 105-108] under ambient air and vacuum conditions, respectively, revealed that both Cr^{3+} and Cr^{6+} are initially present and Cr^{6+} is reduced to Cr^{3+} after exposure to the HT-WGS reaction. The presence of a Cr^{6+}=O band was also detected by IR, but the assignment of this vibration was not made and its origin was not known [117]. In addition, surface carbon was not found to accumulate on the catalyst and thus is not responsible for deactivation. This implies that thermal sintering or surface structural changes are involved. Other studies have proposed that

surface carbonates accumulate on the catalyst; however, no supporting data is provided. Clearly, there is a strong need to obtain surface information under HT-WGS reaction conditions to fully understand the role of Cr in the iron-chromium and copper-iron-chromium oxide catalysts.

A major concern of the HT-WGS catalyst is the presence of hexavalent chromium (Cr^{+6}), a potent carcinogen that threatens human life and the environment [118]. The U.S. EPA has published many guidelines for the identification and assessment of hexavalent chromium [119] and the U.S. Occupational Health and Safety Organization (OSHA) has passed strict guidelines for workplace exposure to hexavalent chromium in several industries [120]. In Europe, hexavalent chromium is already banned from all electronic/electrical equipment [121]. The issue of replacing chromium in catalysts for fatty alcohol production by hydrogenation of fatty esters is already receiving discussion [122, 123]. These concerns have motivated the intensive research over the past decades for new catalysts that have high WGS activity and are less toxic.

1.4.2 Copper

The promotion of commercial Cr_2O_3-Fe_2O_3 HT-WGS catalysts by Cu has received much attention since the 1980s. Mars *et al.* [124] observed the promoting effects of first row transition metal oxide catalyst additives, and especially with Cu, for HT-WGS

catalysts. Similar results were also obtained by Andreev *et al.*[125] and Rhodes *et al.*[57]. Both groups showed that Cu-promoted Cr_2O_3-Fe_2O_3 catalysts have the highest activity over the greatest temperature range. The effect of Cu loading was also investigated in several studies. Idakiev *et al.* [126] compared Cr_2O_3-Fe_2O_3 catalysts promoters with 5 wt.% and 15 wt.% CuO and found that the latter had the highest activity. Subramanian *et al.* [127] compared different Cu loading in Cu-Al-Fe catalyst ranging from 2.5 mol. % to 15 mol. %, the catalyst with 12.5 mol. % Cu loading exhibited the highest WGS activity. Rhodes *el al*. [58] performed kinetic studies to compare the activation energy for both Cr_2O_3-Fe_2O_3 and CuO-Cr_2O_3-Fe_2O_3 catalysts. The addition of CuO to the Cr_2O_3-Fe_2O_3 catalyst was found to significantly decrease the activation energy from 118 to 75-80 kJ/mol. Similar effects were also found by San *et al.* [76]. Recently different preparation methods of Cu-Fe catalysts were compared and discussed. Meshkani and Rezaei[128] synthesized Fe-Cr-Cu catalyst by the pyrolysis method and optimized the catalyst composition for HT-WGS. Among all the catalyst tested, the catalyst with Fe/Cr=10 and Fe/Cu=20 showed even higher activity than commercial catalyst and high thermal stability on stream up to 10h. Lin *et al*. [129] prepared the catalyst by co-precipitation, which was claimed to exhibit the highest activity and stability compared to deposition-precipitation, sol–gel, solid state reaction and mechanical mixing. Meshkani and Rezaei [130-132] further studied the

catalyst synthesis by co-precipitation and analyzed the effect of experimental parameters (precursor concentration, precipitation pH, aging temperature, aging time and calcination temperature) on the catalytic activity to determine the best synthesis condition for maximum catalyst activity. The best preparation conditions were given as: precipitation pH=10, concentration of the precursor solution of 0.06M, aging temperature at 60°C, aging time of 5h and calcination temperature at 400°C.

The chemical state(s) of Cu during HT-WGS as well as its promotion mechanism have not yet been definitively established. Andreev *et al.* [125] suggested that Cu provided new catalytic active sites for the HT-WGS, reacting in the same manner as the metallic copper for the $Cu/ZnO/Al_2O_3$ low temperature WGS catalyst. However, no supporting experimental or simulation evidence was provided. Idakiev *et al.* [126] observed that metallic Cu gradually sintered into larger metallic Cu particles that sharply decreased the catalytic activity during the reaction. Edwards *et al.* [110] analyzed $CuO\text{-}Cr_2O_3\text{-}Fe_2O_3$ catalysts after the HT-WGS reaction using high resolution electron microscopy (HREM) and high spatial resolution energy dispersive X-ray analysis (STEM-EDX) and concluded that Cu exists in solid solution within the iron oxide lattice with preferential segregation into the surface layers of the oxide spinel structure (see Figure 1.2a). Copper easily oxidizes upon exposure to air, however, the Cr substituted magnetite phase is stable upon air exposure [133]. Since the state of the

Cu is sensitive to its environment, understanding the role of the Cu promoter in an iron-based HT-WGS catalyst necessitates characterization of Cu under reaction conditions.

More recent *in situ* characterization studies (XAFS, XRD and XPS) revealed that the initially incorporated Cu^{2+} is reduced to metallic Cu^0 during the HT-WGS reaction. Grunwaldt *et al.*[133-135], for the first time, performed *in situ* transmission XAFS on CuO-Cr_2O_3-Fe_2O_3 and concluded that is Cu present as metallic copper under the conditions of the HT-WGS reaction. These measurements, however, were performed under $H_2/H_2O/N_2$ gas mixtures, which were claimed to have a similar reduction potential as that of the industrial WGS reaction mixture. A more relevant experiment was performed by Estrella *et al.* [136] in 2009 employing *in situ* XRD and XAFS to analyze $CuFe_2O_4$ and Cu/Fe_3O_4 during the HT-WGS. They observed that above 250ºC CuO was reduced to metallic Cu in the CO/H_2O atmosphere. The same findings were obtained by Puig-Molina *et al.* for CuO-Cr_2O_3-Fe_2O_3 catalysts at 380ºC and elevated pressure by using in situ XANES and XAFS. [20] They concluded that metallic Cu exists on the catalyst surface during the reaction (see Figure 1.2b), but experimental evidence about the Cu location was not provided. More recently, Ye *et al.*[18] investigated the role of Cu in CuO-Al_2O_3-Fe_2O_3 catalysts for HT-WGS by *in situ* near ambient pressure X-ray photoelectron spectroscopy. These authors proposed a double-layered structure consisting of a surface layer of Fe_3O_4 and a metallic Cu layer

below it during HTS (see Figure 1.2c).

The effect of Cu promotion upon the iron oxide surface species was also examined with Density Functional Theory (DFT) calculations.[21] The authors simulated the effect of Cu^{2+} on the Fe_3O_4 (111) crystal surface and found a decrease in the bonding energy of the surface intermediates. Unfortunately, this study did not address the effect of metallic Cu particles on the Fe-Cr HT-WGS catalyst system, which would be a more relevant study to perform.

Three Cu promotion mechanisms have been proposed in the literature: (i) Cu provides new catalytic active sites for the WGS reaction, (ii) Cu exists as Cu cations dispersed in solid solution and modifies the electronic or structural properties of the standard Cr_2O_3-Fe_2O_3 catalyst, and (iii) metallic Cu facilitates the cycle of water dissociation and hydrogen production. The *in situ* studies under reaction conditions demonstrate that the solid solution model (ii) is not valid since copper is present as metallic Cu particles. To date, no supporting evidence has been provided for models (i) and (iii).

1.4.3 Cerium

A series of papers published by the Smirniotis group discussed the potential of Ce to be added into hematite as a promoter. A variety of metal ions (Cr, Mn, Co, Ni, Cu, Zn, and Ce) were evaluated by addition to hematite. [137] The Fe/Ce was

considered a promising catalyst system for the HT-WGS during steam-rich conditions with the highest activity. The promotion of Ce was ascribed to (i) potential for Ce to form $Ce^{4+} \leftrightarrow Ce^{3+}$ redox cycle; (ii) promoting the mobility of bulk lattice oxygen by formation of labile oxygen vacancies [138] and (iii) providing high oxygen storage capacity and cooperative effect of Ce.[139] The Fe/Ce catalyst showed high activity and stability at a steam:CO ratio of 3.5. At a low steam to CO ratios of 1.5, however, the catalyst deactivated rapidly by formation of carbon deposition and methane. [140] In addition, XRD revealed rapid sintering of catalyst under low steam to CO ratios. The local structural rearrangements of the iron ions were monitored with Mössbauer spectroscopy. It was also found that addition of Cr or Co improved the stability of the Fe-Ce oxide catalyst at low steam to CO ratios, which inhibited both carbonate formation and methanation. [140, 141] It was concluded that both Cr and Co occupy the octahedral sites of the magnetite phase during the activation process from Mössbauer spectroscopy analysis.

Interestingly, copper was found to behave very differently for Fe/Cr when compared to the Fe/Ce catalyst by acting as a promoter for Fe/Cr and as an inhibitor for Fe/Ce catalyst. [19, 92-94] By performing *ex situ* Mossbauer measurements, they observed distortions in the cubic lattice of magnetite due to the incorporation of copper and ceria in the lattice. In conjunction with an XRD and XPS study, it was concluded

that both Ce and Cu substitutionally enter the iron oxide bulk lattice upon activation and the FeO phase forms along with the magnetite phase. In turn, formation of FeO is proposed to be responsible for the decreased WGS activity upon Cu co-doping of Fe/Ce catalyst.

1.4.4 Cr-Free Fe-Based Catalysts

Early in 1982, Chinchen [142] was the first to study Ca, Ce and Zr oxides that form spinel structures with Fe oxide. Rethwisch and Dumesic [143] tested the activity of magnetite by adding Zn and Mg, but these catalysts showed lower activity compared to commercial catalysts. Basifiska and Domka [144] investigated Fe-Ru catalysts prepared by impregnation of calcination products of α-, β-, γ- and δ-iron oxide-hydroxides with either ruthenium chloride or ruthenium red. The sequence of activity for the WGS reaction was found to decrease as follows: δ>α>>β>γ. The activity of the Fe-Ru catalysts was further improved when the $Ru_3(CO)_{12}$ precursor was used. [145] Gadolinium was also investigated as a substitute for Cr [146, 147]. The Fe-Gd catalysts exhibited remarkable catalytic activity that was attributed to its p-type semi-conductivity. The authors claimed that the Fe-Gd catalysts can even, in many cases, exceed the activity of some industrial catalysts used for WGS reaction. Costa *et al.* [24] studied Th as a replacement for Cr and found that Th prevents sintering and over reduction of iron oxide during the HT-WGS reaction. The Fe-Cr-Th catalyst was

claimed to be more active than conventional Fe-Cr-Cu catalysts.

Junior *et al.* [148] investigated vanadium as a replacement for Cr. Ammonium metavanadate and iron nitrate were used as precursors. The Fe and V catalyst was synthesized by heating vanadium-doped iron (III) hydroxo-acetate (IHA) under nitrogen. Vanadium was found to be a promising dopant leading to active and stable catalysts comparable to commercial Cr containing catalysts. Vanadium was found to increase the specific surface area of the catalysts and retarding sintering. Pereira *at al.* [149] reported about Fe-Co catalysts for HT-WGS reaction. At high Co concentrations (Co/Fe (molar) = 1.0), cobalt increased the surface area and formed cobalt ferrite and Co_3Fe_7 alloy, and was more active and resistant against reduction than magnetite. Martos *et al.* [115] replaced chromium with molybdenum in the iron-based catalysts prepared by the oxidation–precipitation and wet impregnation method. Molybdenum was shown to increase the thermal stability of the magnetite active phase and prevent metallic iron formation during the HT-WGS reaction.

Lee *at al*. published a few papers discussing Ni as a possible replacement for Cr [108, 150, 151]. The incorporation of Ni increased the CO conversion until the Ni content reached 40 wt. % by increasing the surface area of the catalysts, but low selectivity was found due to the methanation side reaction. Subsequent studies added cesium and zinc as promoters to inhibit the methanation reaction and to increase the

selectivity of HT-WGS reaction. Similar work has also been reported by some other groups showing high activity for Cu-Ni-Fe catalysts [152, 153]. The high activity was mainly ascribed to increase in lattice strain, decreased lattice oxygen binding energy, higher BET area and easier reducibility of Fe oxide. The Cu-Ni alloy was also observed by XPS and was believed to inhibit the methanation side reaction [152].

Among the Cr-free Fe-based catalysts that have been studied, Al has received the most attention in the literature. In 1995, Ladebeck and Kochloefl [154] tried to replace Cr_2O_3 by the combination of Al_2O_3 and oxides of ZrO_2, MnO_2, La_2O_3 and CeO_2. The iron catalyst containing Al_2O_3 and CeO_2 showed sufficient thermal resistance and highest activity that was claimed to be superior in activity to a commercial HT-WGS catalyst. Most of the reported findings were trial-and-error studies and only discussed the activity and thermal-stability under different reaction conditions [28, 29, 137, 155-158]. Araujo and Rangel [155] synthesized Fe-Al, Fe-Cu and Fe-Al-Cu catalysts by co-precipitation and claimed the Fe-Al-Cu catalyst has similar HT-WGS activity compared to a commercial Cr-containing catalyst. Liu *et al.* [159] synthesized Fe-Al-Ce catalysts by wet precipitation that exhibited high activity and thermal-stability even after pretreatment at 530^{o}C, which was claimed to be comparable to those of commercial Cr-Fe catalysts. More recently, Meshkani and Rezaei [160, 161] examined the Fe-Al-Cu catalyst system by testing the promotion of a series of elements (Ba, Ca,

Mg, Sr, Ce, La, Zn, Y, and Mn) with Ba and Mn showing higher performance. The promotion of alkali metal oxides to Fe_2O_3-Al_2O_3-NiO catalyst, [162] especially Na, was found to suppress methanation and increase the HT-WGS activity by increasing the number of weakly basic sites. Upon further evaluation of the Na content, it was found that 3 wt.% Na exhibited the highest activity and stability under stream for up to 50h.

The effect of preparation method and condition on the activity of Al-Fe based catalysts were examined by several groups. Natesakhawat *et al.* [105] evaluated the effects of Fe/promoter ratio, pH of precipitation medium and calcination and reduction temperature on the performance of Al-Fe and Al-Fe-Cu catalysts. The HT-WGS activity of Fe-Al catalysts is highest when Fe/Al molar ratio reaches 10. Further addition of Al causes a significant drop in the HT-WGS activity. The optimum pH of the precipitation was 9 and a calcination temperature of 450^{o}C resulted in the highest HT-WGS activity. It was concluded from H_2-TPR that the addition of aluminum stabilizes Fe_3O_4 by retarding its further reduction to FeO or metallic iron, making it a promising chromium replacement by acting as a textural promoter for iron-based HT-WGS catalyst. Zhang *et al*. [163] investigated the effects of preparation methods on catalyst activity by comparing a Fe-Al-Cu catalyst synthesized by the sol-gel method with catalysts prepared by a 1-step precipitation or a 2-step precipitation-impregnation

method. The catalyst prepared by sol-gel method showed much higher activity compared to the other two preparation methods and was even claimed to surpass the activity of commercial catalysts over a wide temperature range. Such improved performance was attributed to better dispersed Cu and more oxygen vacancies which facilitate the redox cycle of HT-WGS reaction. However, Na *et al*. [164] investigated impregnated, sol–gel prepared and co-precipitated Fe/Al/Cu catalysts, and found that the co-precipitated catalyst was stable, possesses a high surface area and highly active for HT-WGS. Jeong *et al.* [165] prepared Fe-Al-Cu catalysts with varying Fe/Cu ratio and fixed Al content and the catalysts were found to exhibit higher and more stable activity compared to commercial catalysts. Similar work has also been reported by Meshkani and Rezaei,[166] who proposed that a catalyst with Fe/Al=10 and Fe/Cu=5 weight ratios exhibit highest activity. Both authors proposed that the improved properties were easier to reduce and the synergistic interaction between copper and aluminum was responsible for the stability of the active phase. The absence of characterization studies prevented the needed supporting data that would allow for firm conclusions about the different reported activities for HT-WGS that may just be related to higher catalyst surface areas.

1.4.5 Supported Fe-based catalysts

Given that iron oxide easily sinters and loses surface area during the HT-WGS

reaction, researchers have also been trying to disperse iron oxide on a support to increase the surface area of the iron-based active phase. In 1985, Rethwisch *et al*. [99] were the first to report supported iron oxide by dispersing Fe_3O_4 on a graphite support. The supported catalyst initially showed high activity, but the activity sharply decreased during the first few hours of reaction. The agglomeration of smaller magnetite particles during WGS reaction was also monitored from Electron Microscopy. Correia *et al*. [167] synthesized supported Fe/MCM-41 catalysts with different iron contents by impregnation. Due to the presence of the hematite nanoparticles in the pores, the specific surface areas decreased with the increase of iron oxide in MCM-41. The HT-WGS activity increased with the amount of iron and the sample with the highest amount of iron showed the highest activity and all samples were more active than unsupported hematite. The authors proposed that the supported hematite nanoparticles were more easily reduced than large hematite particles and, thus, more easily formed the magnetite active phase. However, the magnetite phase always forms during HT-WGS and the higher activity was most likely related to the greater number of exposed active sites for the supported Fe/MCM-41. A very active char-supported nano iron catalyst, prepared from the pyrolysis and gasification of iron-loaded Victorian brown coal, was more recently reported by Yu *et al*. [168] , which was found to be active for the HT-WGS reaction at temperatures as low as 300°C. Boudjemaa *et al*. [34] examined the effect of

support on the activity of Cr- free Fe based catalysts (Fe_2O_3/MgO, Fe_2O_3/TiO_2, Fe_2O_3 and Fe_2O_3/SiO_2). A correlation between catalytic activity and acid/base properties (measured by the activity of isopropanol dehydrogenation) of the supported catalysts was found: Fe_2O_3/MgO >> Fe_2O_3/TiO_2> unsupported Fe_2O_3 >> Fe_2O_3/SiO_2. Kharaji *et al*. [169] investigated supported Mo/Al_2O_3, Fe/Al_2O_3 and Fe-Mo/Al_2O_3 catalysts prepared by impregnation for HT-WGS in a batch reactor. The supported Fe-Mo/Al_2O_3 catalyst was found to enhance the HT-RWGS reaction, which was proposed to result from better dispersion of the Fe oxide phase. The absence of characterization of the different reported supported iron oxide catalysts prevents determining the origin of the observed variation in catalytic activity (e.g., smaller particles, greater number of exposed active sites, iron oxide-support interactions, etc.)

1.5 Conclusions

Extensive efforts have been made in the past 100 years to develop and understand bulk iron-based HT-WGS catalysts. Especially since 1980s, researchers have been more focused on the design of catalysts with either higher activity or more environmental friendly materials.

1) The HT-WGS reaction follows either a regenerative or redox mechanism with the redox mechanism more widely accepted as the predominant mechanism on Fe-based catalysts. This conclusion is mainly due to lack of observed reactive

intermediates as well as the well-known redox property of iron oxide. There is no consensus on the rds, with some authors suggesting that it is CO adsorption, CO oxidation, CO_2 desorption, H_2 formation or a combination of these steps. There are no discussions about the most abundant reactive intermediate for iron-based catalyst due to lack of reported *in situ* characterization of the catalyst surface during the HT-WGS reaction.

2) The bulk phase of iron-based HT-WGS catalysts during reaction is Fe_3O_4 and $Fe^{3+} \leftrightarrow Fe^{2+}$ pairs,[66] as well as their ratio, are thought to be dynamically dependent on the reaction conditions.[96] It is important to avoid over-reduction of the Fe_3O_4 active materials to lower oxides, carbides or metallic iron species that are not thought to be the active phases for HT-WGS.

3) Cr functions as a textural promoter that stabilizes magnetite from sintering. Mössbauer studies showed the Cr^{3+} ions replaced Fe^{3+} ions at the octahedral sites of the inverse spinel bulk lattice of magnetite during the HT-WGS reaction. Some research groups also propose Cr promotes the redox cycle of the Fe_3O_4 phase by $Cr^{6+} \leftrightarrow Cr^{3+}$ pairs. No direct supporting evidence for the Cr redox cycle, however, has been provided.

4) Cu is an important promoter for the iron-chromium oxide HT-WGS catalyst. Copper promotion has been shown to decrease the WGS activation energy by ~40

kJ/mole [57, 58], lower the reaction temperature and retard the $Fe_2O_3 \rightarrow Fe_3O_4$ phase transition during catalyst activation [19, 94]. There is no consensus about the chemical state, location, morphology and promotion mechanism of Cu during the HT-WGS.

5) Great effort has been made to find replacement elements for Cr due to environmental and health concerns of hexavalent Cr. A promising candidate is Al and has received much focus in recent years. The Fe/Al/Cu and Fe/Al/Ce/Cu catalysts already showed similar or superior performance compared to commercial Cr/Fe/Cu catalysts. These investigations have been trial-and-error studies without providing fundamental understanding of the reaction mechanism and catalytic roles of Cu and Cr in commercial Cu/Cr/Fe catalysts.

1.6 Outline of Research

The importance of the HT-WGS reaction is increasing due to recent emphasis on a hydrogen economy [4]. The high activity, durability and relatively low manufacturing costs of iron-based catalysts still make them the preferred industrial catalysts for HT-WGS. The very different HT-WGS experimental reaction conditions employed by researchers, makes it difficult to compare the relative performance of the investigated catalysts. The focus of the HT-WGS literature has been on bulk structures and the absence of any critical surface information about Cr-free catalysts hampers

development of a fundamental model that could guide the rational design of a Cr-free catalyst. Thus, the main research objectives of this study are (i) establishing the reaction mechanism, rate-determining-steps and reactive intermediates of HT-WGS on Fe-based catalysts; (ii) understanding the role of the Cr promoter at a molecular level and (iii) understanding the interaction mechanism between Cu and Fe oxide which is still not fully known because of the absence of *in situ* and *operando* spectroscopy studies on catalyst surface during HT-WGS reaction in the literature. In accomplishing these objectives, Cr-free environmentally friendly Fe-based HT-WGS catalysts can be rationally designed based on aforementioned fundamental understanding of the existing CuO-Cr_2O_3-Fe_2O_3 catalyst system. The general scheme for the present research is outlined as follows:

Chapter 1: Overview of Iron-Based Catalysts for the High Temperature Water-Gas Shift (HT-WGS) Reaction

This chapter reviews the literature on iron-based catalysts for the High Temperature Water-Gas Shift (HT-WGS) reaction. The reaction mechanism, reaction intermediates, rate-determining-step, kinetics, active site and promoters are covered.

Chapter 2: Resolving the Reaction Mechanism for High-Temperature Water-Gas Shift Reaction on Iron Oxide Catalysts

This chapter resolves the reaction mechanism of the high temperature water-gas

shift (HT-WGS) reaction catalyzed by chromium-iron oxide catalysts which has been studied for 100 years with two reaction mechanisms proposed and debated: redox and associative.

Chapter 3: Determining Number of Active Sites and TOF for the High-Temperature Water Gas Shift Reaction by Iron Oxide-Based Catalysts

This chapter further demonstrated the mechanism and the role of surface oxygen of high temperature water-gas shift (HT-WGS) reaction. Number of active site(Ns) and Turnover frequency (TOF) of Iron based WGS catalysts are, *for the first time*, calculated by isotope switch experiments.

Chapter 4: Promotion Mechanisms of Iron Oxide-Based High Temperature-Water Gas Shift (HT-WGS) Catalysts by Chromium and Copper

This chapter critically investigated the structure of CuO-Cr_2O_3-Fe_2O_3 catalyst under working condition and the promotion mechanism of Copper and Chromium. The state-of-the art *in situ*/*operando* characterization techniques employed have provided new insights and clarity to these unsolved problems.

Chapter 5: Rational Design of Chromium-Free Iron-Based Catalysts for High Temperature Water-Gas Shift Reaction

This chapter rationally designed chromium-free catalysts by evaluating three candidate elements (Aluminum, Silicon and Magnesium) based on two criteria: 1)

Turnover frequency, 2) Thermostability. Based on which, the best chromium-free iron-based catalysts have been proposed.

Chapter 6: Conclusions and Future Studies

This chapter summarized the most important conclusions of the research in this dissertation. The outlook in terms of development of chromium-free iron-based HT-WGS catalysts will be discussed.

References

[1] D.S. Newsome, Catal. Rev.: Sci. Eng. 21 (1980) 275-318.

[2] P. Law, One Hundred Ninth Congress of the United States of America Energy Policy Act of 2005 109.

[3] P. Law, One Hundred Tenth Congress of the United States of America Energy Independence and Security Act of 2007 110-140.

[4] DOE The Department of Energy Hydrogen and Fuel Cells Program Plan DOE/EE-0651 (2011).

[5] M.M. Bomgardner, Chem. Eng. News (2014) 15.

[6] C. Ratnasamy, J.P. Wagner, Catal. Rev.: Sci. Eng. 51 (2009) 325-440.

[7] J.A. Rodriguez, J.C. Hanson, D. Stacchiola, S.D. Senanayake, PCCP 15 (2013) 12004-12025.

[8] C. Bosch, W. Wild, United States Patent 1914.

[9] C. Rhodes, G.J. Hutchings, A.M. Ward, Catal. Today 23 (1995) 43-58.

[10] C. Bosch, A. Mittasch, C. Beck, United States Patent 1920.

[11] A.T. Larson, United States Patent 1,908,484 (1933).

[12] O.W. Moak, W.E. Spicer, United States Patent 2,631,086 (1953).

[13] C. Sciallano, R. Carles, United States Patent 2,968,636 (1961).

[14] M.H. Jorgensen, United States Patent 3,711,426 (1973).

[15] F. Domka, M. Laniecki, Z. Anorg. Allg. Chem. 435 (1977) 273-283.

[16] J.R. Jennings, United States Patent 4,305,846 (1981).

[17] F. Domka, A. Basinska, R. Fiedorow, Surface Technology 18 (1983) 275-282.

[18] Y.C. Ye, L. Wang, S.R. Zhang, Y. Zhu, J.J. Shan, F. Tao, Chem. Commun. 49 (2013) 4385-4387.

[19] G.K. Reddy, P.G. Smirniotis, Catal. Lett. 141 (2011) 27-32.

[20] A. Puig-Molina, F.M. Cano, T.V.W. Janssens, J. Phys. Chem. C 114 (2010) 15410-15416.

[21] R.M. Van Natter, J.S. Coleman, C.R.F. Lund, J. Mol. Catal. A: Chem. 311 (2009) 17-22.

[22] Y. Lei, N.W. Cant, D.L. Trimm, J. Catal. 239 (2006) 227-236.

[23] Y. Lei, N.W. Cant, D.L. Trimm, Chem. Eng. J. 114 (2005) 81-85.

[24] J.L.R. Costa, G.S. Marchetti, M.D.C. Rangel, Catal. Today 77 (2002) 205-213.

[25] L.S. Chen, G.L. Lu, J. Mater. Sci. 34 (1999) 4193-4197.

[26] F. Domka, A. Basinska, W. Przystajko, R. Fiedorow, Surface Technology 21 (1984) 101-108.

[27] J. Koy, J. Ladebeck, J.R. Hill, Natural Gas Conversion V 119 (1998) 479-484.

[28] A.O. de Souza, M.D. Rangel, React. Kinet. Catal. Lett. 79 (2003) 175-180.

[29] J.M.T. de Souza, M.D. Rangel, React. Kinet. Catal. Lett. 77 (2002) 29-34.

[30] J.R. Ladebeck, J.P. Wagner, Catalyst development for water–gas shift, Handbook of Fuel Cells, John Wiley & Sons, Ltd, Chichester, 2003, pp. 190-201.

[31] D.-W. Lee, M.S. Lee, J.Y. Lee, S. Kim, H.-J. Eom, D.J. Moon, K.-Y. Lee, Catal Today 210 (2013) 2-9.

[32] R.J.B. Smith, M. Loganathan, M.S. Shantha, Int. J. Chem. React. Eng. 8 (2010) 1-32.

[33] E.F. Armstrong, T.P. Hilditch, Proc. R. Soc. London, Ser. A 97 (1920) 265-273.

[34] A. Boudjemaa, C. Daniel, C. Mirodatos, M. Trari, A. Auroux, R. Bouarab, C. R. Chim. 14 (2011) 534-538.

[35] C. Diagne, P.J. Vos, A. Kiennemann, M.J. Perrez, M.F. Portela, React. Kinet. Catal. Lett. 42 (1990) 25-31.

[36] G.K. Boreskov, T.M. Yurieva, A.S. Sergeeva, Kinet. Catal. 11 (1970) 374-381.

[37] A. Khan, P.G. Smirniotis, J Mol Catal a-Chem 280 (2008) 43-51.

[38] N.V. Kulkova, M.I. Temkin, Zh. Fiz. Khim. 23 (1949) 695-698.

[39] J.E. Kubsh, J.A. Dumesic, AlChE J. 28 (1982) 793-800.

[40] M.I. Temkin, Adv. Catal. 28 (1979) 173-291.

[41] M.I. Temkin, M.L. Nakhmanovich, N.M. Morozov, Kinet. Catal. 2 (1961) 722-726.

[42] C.R.F. Lund, J.A. Dumesic, J. Catal. 76 (1982) 93-100.

[43] T. Salmi, S. Bostrom, L.E. Lindfors, J. Catal. 112 (1988) 345-356.

[44] R.L. Keiski, T. Salmi, P. Niemistö, J. Ainassaari, V.J. Pohjola, Appl. Catal., A 137 (1996) 349-370.

[45] R. Hakkarainen, T. Salmi, R.L. Keiski, Catal. Today 20 (1994) 395-408.

[46] M.E. Grillo, M.W. Finnis, W. Ranke, Physical Review B 77 (2008).

[47] R. Mezaki, S. Oki, J. Catal. 30 (1973) 488-489.

[48] S. Oki, R. Mezaki, J. Phys. Chem. 77 (1973) 1601-1605.

[49] S. Oki, R. Mezaki, Ind. Eng. Chem. Res. 27 (1988) 15-21.

[50] A. Matsuda, J. Horiuti, J. Res. Inst. Catalysis, Hokkaido Univ. 10 (1962) 14-23.

[51] M. Tinkle, J.A. Dumesic, J. Catal. 103 (1987) 65-78.

[52] C.V. Ovesen, P. Stoltze, J.K. Norskov, C.T. Campbell, J. Catal. 134 (1992) 445-468.

[53] C.V. Ovesen, B.S. Clausen, B.S. Hammershoi, G. Steffensen, T. Askgaard, I. Chorkendorff, J.K. Norskov, P.B. Rasmussen, P. Stoltze, P. Taylor, J. Catal. 158 (1996) 170-180.

[54] E. Tserpe, K.C. Waugh, Dynamics of Surfaces and Reaction Kinetics in Heterogeneous Catalysis 109 (1997) 401-416.

[55] K.C. Waugh, Catal. Today 53 (1999) 161-176.

[56] C. Callaghan, I. Fishtik, R. Datta, M. Carpenter, M. Chmielewski, A. Lugo, Surf. Sci. 541 (2003) 21-30.

[57] C. Rhodes, B.P. Williams, F. King, G.J. Hutchings, Catal. Commun. 3 (2002) 381-384.

[58] C. Rhodes, G.J. Hutchings, PCCP 5 (2003) 2719-2723.

[59] H.M. Hulburt, C.D.S. Vasan, A. I. Ch. E. Journal 7 (1961) 143-147.

[60] D.M. Huang, D.B. Cao, Y.W. Li, H.J. Jiao, J. Phys. Chem. B 110 (2006) 13920-13925.

[61] L.C. Grabow, A.A. Gokhale, S.T. Evans, J.A. Dumesic, M. Mavrikakis, J Phys Chem C 112 (2008) 4608-4617.

[62] A.A. Gokhale, J.A. Dumesic, M. Mavrikakis, J. Am. Chem. Soc. 130 (2008) 1402-1414.

[63] Q.L. Tang, Z.X. Chen, X. He, Surf Sci 603 (2009) 2138-2144.

[64] L. Chen, G. Ni, B. Han, C.G. Zhou, J.P. Wu, Acta Chim. Sin. 69 (2011) 393-398.

[65] P. Fott, J. Vosolsobe, V. Glaser, Collect. Czech. Chem. Commun. 44 (1979) 652-659.

[66] V. Twigg, Catalyst handbook, Wolfe1989.

[67] W.F. Podolski, Y.G. Kim, Industrial & Engineering Chemistry Process Design and Development 13 (1974) 415-421.

[68] M. Tinkle, J.A. Dumesic, J. Phys. Chem. 88 (1984) 4127-4130.

[69] G.C. Chinchen, R.H. Logan, M.S. Spencer, Appl. Catal. 12 (1984) 89-96.

[70] G.C. Chinchen, R.H. Logan, M.S. Spencer, Appl. Catal. 12 (1984) 69-88.

[71] G.C. Chinchen, R.H. Logan, M.S. Spencer, Appl. Catal. 12 (1984) 97-103.

[72] H.Q. Zhao, Y.Q. Hu, J.J. Li, J. Mol. Catal. A: Chem. 149 (1999) 141-146.

[73] C.P.P. Singh, D.N. Saraf, Ind. Eng. Chem. Process Des. Dev. 16 (1977) Medium: X; Size: Pages: 313-319.

[74] H.F. Rase, Chemical Reactor Design for Process Plants: Principles and techniques, Wiley1977.

[75] S.S.E.H. Elnashaie, S.S. Elshishini, Modelling, Simulation, and Optimization of Industrial Fixed Bed Catalytic Reactors, Gordon and Breach Science1993.

[76] S.S. Hla, D. Park, G.J. Duffy, J.H. Edwards, D.G. Roberts, A. Ilyushechkin, L.D. Morpeth, T. Nguyen, Chem. Eng. J. 146 (2009) 148-154.

[77] T.A. Adams Ii, P.I. Barton, Int. J. Hydrogen Energy 34 (2009) 8877-8891.

[78] F. Almashta, N. Sheppard, V. Lorenzelli, G. Busca, J Chem Soc Farad T 1 78 (1982) 979-989.

[79] J. Baltrusaitis, J.H. Jensen, V.H. Grassian, J. Phys. Chem. B 110 (2006) 12005-12016.

[80] G. Busca, V. Lorenzelli, J. Catal. 66 (1980) 155-161.

[81] G. Busca, V. Lorenzelli, React. Kinet. Catal. Lett. 15 (1980) 273-278.

[82] G. Busca, V. Lorenzelli, Mater Chem 5 (1980) 213-224.

[83] G. Busca, V. Lorenzelli, Mater Chem 7 (1982) 89-126.

[84] G. Busca, V. Lorenzelli, J Chem Soc Farad T 1 78 (1982) 2911-2919.

[85] G. Busca, V. Lorenzelli, G. Ramis, R.J. Willey, Langmuir 9 (1993) 1492-1499.

[86] V. Lorenzelli, G. Busca, N. Sheppard, J. Catal. 66 (1980) 28-35.

[87] V. Lorenzelli, G. Busca, N. Sheppard, F. Almashta, J. Mol. Struct. 80 (1982) 181-186.

[88] G. Ramis, G. Busca, V. Lorenzelli, Mater. Chem. Phys. 29 (1991) 425-435.

[89] M.L. Kundu, A.C. Sengupta, G.C. Maiti, B. Sen, S.K. Ghosh, V.I. Kuznetsov, G.N. Kustova, E.N. Yurchenko, J. Catal. 112 (1988) 375-383.

[90] A. Patlolla, E.V. Carino, S.N. Ehrlich, E. Stavitski, A.I. Frenkel, ACS Catal. 2 (2012) 2216-2223.

[91] D. Zanchet, C.B. Rodella, L.J.S. Lopes, M.A. Logli, V.P. Vicentini, W. Wen, J.C. Hanson, J.A. Rodriguez, AIP Conf. Proc. (2009) 25-28.

[92] G.K. Reddy, P. Boolchand, P.G. Smirniotis, J. Phys. Chem. C 116 (2012) 11019-11031.

[93] G.K. Reddy, K. Gunasekara, P. Boolchand, P.G. Smirniotis, J. Phys. Chem. C 115 (2011) 920-930.

[94] G.K. Reddy, K. Gunasekera, P. Boolchand, J.H. Dong, P.G. Smirniotis, J. Phys. Chem. C 115 (2011) 7586-7595.

[95] A. Andreev, I. Mitov, V. Idakiev, T. Tomov, S. Asenov, In Situ Investigation of The Water-Gas Shift Reaction Over Magnetite by Mössbauer Spectroscopy, in: F.S. L. Guczi, T. P (Eds.) Stud. Surf. Sci. Catal., Elsevier1993, pp. 1523-1526.

[96] Z. Cherkezova-Zheleva, I. Mitov, Journal of Physics: Conference Series 217 (2010) 012044.

[97] H. Topsoe, M. Boudart, J. Catal. 31 (1973) 346-359.

[98] G. Doppler, A.X. Trautwein, H.M. Ziethen, E. Ambach, R. Lehnert, M.J. Sprague, U. Gonser, Appl. Catal. 40 (1988) 119-130.

[99] D.G. Rethwisch, J. Phillips, Y. Chen, T.F. Hayden, J.A. Dumesic, J. Catal. 91 (1985) 167-180.

[100] W.J. Lywood, M.V. Twigg, Hydrogen production including a shift reaction process, Google Patents, 1990.

[101] M.I. Markina, G.K. Boreskov, F.P. Ivanovskii, B.G. Lyudkovskaya, Kinet. Catal. 2 (1961) 867-871.

[102] M.D. Rangel, R.M. Sassaki, F. Galembeck, Catal. Lett. 33 (1995) 237-254.

[103] A.L.C. Pereira, G.J.P. Berrocal, S.G. Marchetti, A. Albomoz, A.O. de Souza, M.D. Rangel, J. Mol. Catal. A: Chem. 281 (2008) 66-72.

[104] P. Tsokov, V. Blaskov, D. Klissurski, I. Tsolovski, J. Mater. Sci. 28 (1993) 184-188.

[105] S. Natesakhawat, X.Q. Wang, L.Z. Zhang, U.S. Ozkan, J. Mol. Catal. A: Chem. 260 (2006) 82-94.

[106] V. Martis, R. Oldman, R. Anderson, M. Fowles, T. Hyde, R. Smith, S. Nikitenko, W. Bras, G. Sankar, PCCP 15 (2013) 168-175.

[107] R.L. Keiski, T. Salmi, Appl. Catal., A 87 (1992) 185-203.

[108] J.Y. Lee, D.W. Lee, Y.K. Hong, K.Y. Lee, Int. J. Hydrogen Energy 36 (2011) 8173-8180.

[109] J.C. Gonzalez, M.G. Gonzalez, M.A. Laborde, N. Moreno, Appl. Catal. 20 (1986) 3-13.

[110] M.A. Edwards, D.M. Whittle, C. Rhodes, A.M. Ward, D. Rohan, M.D. Shannon, G.J. Hutchings, C.J. Kiely, PCCP 4 (2002) 3902-3908.

[111] E.B. Quadro, M.D.L.R. Dias, A.M.M. Amorim, M.D.C. Rangel, Journal of the Brazilian Chemical Society 10 (1999) 51-59.

[112] P. Kumar, R. Idem, Energy & Fuels 21 (2007) 522-529.

[113] M. Scariot, M.S.P. Francisco, M.H. Jordao, D. Zanchet, M.A. Logli, V.P. Vicentini, Catal. Today 133 (2008) 174-180.

[114] A. Boudjemaa, A. Auroux, S. Boumaza, M. Trari, O. Cherifi, R. Bouarab, React. Kinet. Catal. Lett. 98 (2009) 319-325.

[115] C. Martos, J. Dufour, A. Ruiz, Int. J. Hydrogen Energy 34 (2009) 4475-4481.

[116] A. Khaleel, I. Shehadi, M. Al-Shamisi, Colloid Surface A 355 (2010) 75-82.

[117] G. Busca, V. Lorenzelli, J Chem Soc Farad T 1 88 (1992) 2783-2789.

[118] C. Pellerin, S.M. Booker, Environ. Health Perspect. 108 (2000) A402-A407.

[119] P.C. Grevatt, U.S. Environmental Protection Agency (1998).

[120] U.S.D.o. Labor, OSHA (2009) 3373-3310.

[121] Official Journal of the European Union 46 (2003) 19-37.

[122] Y. Hattori, K. Yamamoto, J. Kaita, M. Matsuda, S. Yamada, J. Am. Oil Chem. Soc. 77 (2000) 1283-1287.

[123] J. Ladebeck, T. Regula, Stud. Surf. Sci. Catal. 121 (1999) 215-220.

[124] c. Congrès international de, Actes du deuxième Congrès international de catalyse Paris, 1960, Éditions Technip, Paris, 1961.

[125] A. Andreev, V. Idakiev, D. Mihajlova, D. Shopov, Appl. Catal. 22 (1986) 385-387.

[126] V. Idakiev, D. Mihajlova, B. Kunev, A. Andreev, React. Kinet. Catal. Lett. 33 (1987) 119-124.

[127] V. Subramanian, D.W. Jeong, W.B. Han, W.J. Jang, J.O. Shim, J.W. Bae, H.S. Roh, New J Chem 38 (2014) 4872-4878.

[128] F. Meshkani, M. Rezaei, Chem. Eng. Res. Des. 95 (2015) 288-297.

[129] X. Lin, R. Li, Y. Zhang, Y. Zhan, C. Chen, Q. Zheng, J. Ma, Int. J. Hydrogen Energy 40 (2015) 1735-1741.

[130] F. Meshkani, M. Rezaei, Korean J. Chem. Eng. 32 (2015) 1278-1288.

[131] F. Meshkani, M. Rezaei, Ind. Eng. Chem. Res. 54 (2015) 1236-1242.

[132] F. Meshkani, M. Rezaei, Chem. Eng. J. 260 (2015) 107-116.

[133] P. Kappen, J.D. Grunwaldt, B.S. Hammershoi, L. Troger, B.S. Clausen, J. Catal. 198 (2001) 56-65.

[134] J.D. Grunwaldt, B.S. Clausen, Top. Catal. 18 (2002) 37-43.

[135] J.D. Grunwaldt, P. Kappen, B.S. Hammershoi, L. Troger, B.S. Clausen, J. Synchrotron Radiat. 8 (2001) 572-574.

[136] M. Estrella, L. Barrio, G. Zhou, X.Q. Wang, Q. Wang, W. Wen, J.C. Hanson, A.I. Frenkel, J.A. Rodriguez, J. Phys. Chem. C 113 (2009) 14411-14417.

[137] A. Khan, P. Chen, P. Boolchand, P.G. Smirniotis, J. Catal. 253 (2008) 91-104.

[138] B.M. Reddy, K.N. Rao, G.K. Reddy, A. Khan, S.E. Park, J Phys Chem C 111 (2007) 18751-18758.

[139] C. Zerva, C.J. Philippopoulos, Appl Catal B-Environ 67 (2006) 105-112.

[140] G.K. Reddy, S.J. Kim, J.H. Dong, P.G. Smirniotis, J.B. Jasinski, Appl Catal a-Gen 415 (2012) 101-110.

[141] G.K. Reddy, P. Boolchand, P.G. Smirniotis, J. Catal. 282 (2011) 258-269.

[142] G.C. Chinchen, in: E.B. Catalytic preparation of hydrogen from carbon monoxide and water (Ed.), 1982.

[143] D.G. Rethwisch, J.A. Dumesic, Appl. Catal. 21 (1986) 97-109.

[144] A. Basinska, F. Domka, Catal. Lett. 17 (1993) 327-332.

[145] A. Basinska, F. Domka, Catal. Lett. 22 (1993) 327-331.

[146] C.L.S. Silva, S.G. Marchetti, A.D. Faro, T.D. Silva, J.M. Assaf, M.D. Rangel, Catal. Today 213 (2013) 127-134.

[147] J. Tsagaroyannis, K.J. Haralambous, Z. Loizos, G. Petroutsos, N. Spyrellis, Mater. Lett. 28 (1996) 393-400.

[148] I.L. Junior, J.M.M. Millet, M. Aouine, M. do Carmo Rangel, Appl. Catal., A 283 (2005) 91-98.

[149] A. L.C. Pereira, N. A. dos Santos, M. L.O. Ferreira, A. Albornoz, M. do Carmo Rangel, Effect of cobalt on the activity of iron-based catalysts in water gas shift reaction, in: M.S. Fábio Bellot Noronha, S.-A. Eduardo Falabella (Eds.) Stud. Surf. Sci. Catal., Elsevier2007, pp. 225-230.

[150] J.Y. Lee, D.W. Lee, K.Y. Lee, Y. Wang, Catal. Today 146 (2009) 260-264.

[151] J.Y. Lee, D.W. Lee, M.S. Lee, K.Y. Lee, Catal. Commun. 15 (2011) 37-40.

[152] A. Jha, D.W. Jeong, J.O. Shim, W.J. Jang, Y.L. Lee, C.V. Rode, H.S. Roh, Catal. Sci. Technol. 5 (2015) 2752-2760.

[153] D.W. Jeong, W.J. Jang, A. Jha, W.B. Han, K.W. Jeon, S.H. Kim, H.S. Roh, Journal of Nanoelectronics and Optoelectronics 10 (2015) 530-534.

[154] J. Ladebeck, K. Kochloefl, Preparation of Catalysts Vi 91 (1995) 1079-1083.

[155] G.C. de Araujo, M.D. Rangel, Catal. Today 62 (2000) 201-207.

[156] Q.S. Liu, W.P. Ma, R.X. He, Z.J. Mu, Catal Today 106 (2005) 52-56.

[157] J.M.T. de Souza, M.D. Rangel, React. Kinet. Catal. Lett. 83 (2004) 93-98.

[158] F. Meshkani, M. Rezaei, M. Jafarbegloo, Mater. Res. Bull. 70 (2015) 229-235.

[159] Q. Liu, W. Ma, R. He, Z. Mu, Catal. Today 106 (2005) 52-56.

[160] F. Meshkani, M. Rezaei, Journal of Industrial and Engineering Chemistry 30 (2015) 353-358.

[161] F. Meshkani, M. Rezaei, Chem. Eng. Technol. 38 (2015) 1380-1386.

[162] F. Meshkani, M. Rezaei, Rsc Adv 5 (2015) 9955-9964.

[163] L.Z. Zhang, X.Q. Wang, J.M.M. Millet, P.H. Matter, U.S. Ozkan, Appl. Catal., A 351 (2008) 1-8.

[164] H.-S. Na, D.-W. Jeong, W.-J. Jang, J.-O. Shim, H.-S. Roh, Int. J. Hydrogen Energy 40 (2015) 12268-12274.

[165] D.W. Jeong, V. Subramanian, J.O. Shim, W.J. Jang, Y.C. Seo, H.S. Roh, J.H. Gu, Y.T. Lim, Catal. Lett. 143 (2013) 438-444.

[166] F. Meshkani, M. Rezaei, Renew Energ 74 (2015) 588-598.

[167] D. Correia dos Santos, A.C. Oliveira, P.C. Morais, V.K. Garg, A.C. de Oliveira, M.L. Santos Correa, M. do Carmo Rangel, Evaluation of Fe/MCM-41 catalysts in the water gas shift reaction, in: M.C. E. van Steen, L.H. Callanan (Eds.) Stud. Surf. Sci. Catal., Elsevier2004, pp. 2417-2424.

[168] J. Yu, F.J. Tian, L.J. McKenzie, C.Z. Li, Process Safety and Environmental Protection 84 (2006) 125-130.

[169] A.G. Kharaji, A. Shariati, M.A. Takassi, Chinese Journal of Chemical Engineering 21 (2013) 1007-1014.

[170] S. Kodama, K. Fukui, T. Tame, M. Kinoshita, Shokubi 8 (1952) 50.

[171] V. Glavachek, M. Morek, M. Korzhinkova, Kinet. Katal. 9 (1968) 1107.

[172] H. Bohlbro, E. Mogensen, An Investigation on the Kinetics of the Conversion of Carbon Monoxide with Water Vapour Over Iron Oxide Based Catalysts, Gjellerup1969.

[173] H. Bohlbro, Chem. Eng. World 46 (1970) 5-8.

FIGURES

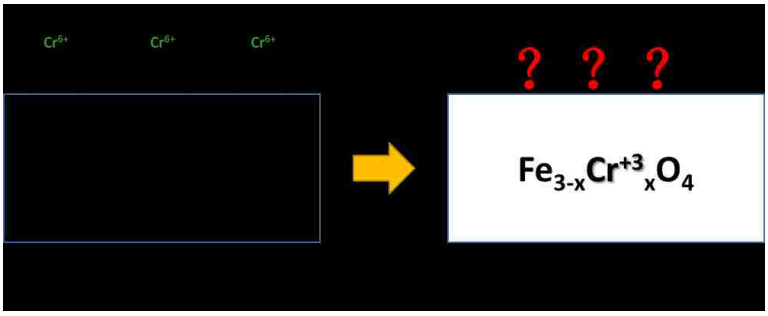

Figure 1.1 Proposed molecular structures of the Cr_2O_3-Fe_2O_3 catalyst before and during the WGS reaction.

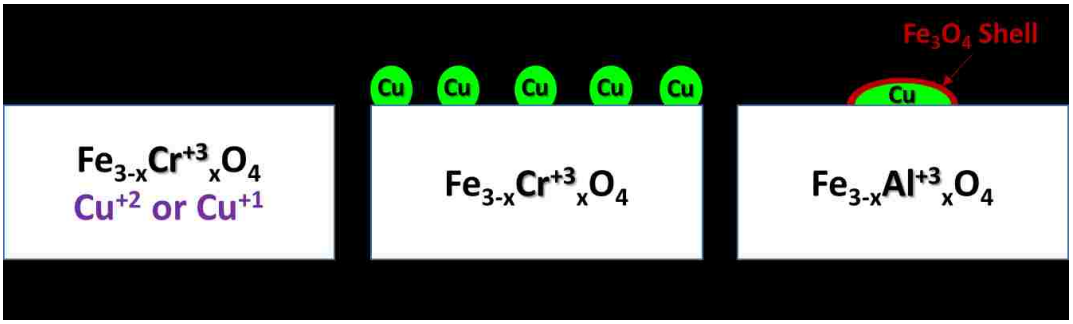

Figure 1.2 Different proposed molecular structures of copper promoted iron-based catalysts during the HT-WGS reaction

TABLES

Model	Kinetic Expression
Langmuir-Hinshelwood Model [65, 67, 69-71]	$r = \frac{kK_{CO}K_{H_2O}([CO][H_2O] - \frac{[CO_2][H_2]}{K})}{(1 + K_{CO}[CO] + K_{H_2O}[H_2O] + K_{CO_2}[CO_2] + K_{H_2}[H_2])^2}$
Hulburt -Vasan Model [59]	$r = \frac{k[H_2O]}{1 + K[H_2O]/[H_2]}$
Kodama Model [170]	$r = \frac{k([CO][H_2O] - \frac{[CO_2][H_2]}{K})}{(1 + K_{CO}[CO] + K_{H_2O}[H_2O] + K_{CO_2}[CO_2] + K_{H_2}[H_2])}$
Oxidation - reduction model [38, 171]	$r = \frac{k_1k_2([CO][H_2O] - [CO_2][H_2]/K)}{k_1[CO] + k_2[H_2O] + k_{-1}[CO_2] + k_{-2}[H_2]}$
Power law model [67, 171, 172]	$r = kP_{CO}^{a}P_{H_2O}^{b}P_{CO_2}^{c}P_{H_2}^{d}$

Table 1.1 Proposed Kinetic Expression for HT-WGS Reaction over Iron-based Catalysts

Catalyst	Reaction orders				E	Reference
	a (CO)	b (H_2O)	c (CO_2)	d (H_2)	(kJ/mol)	
Fe-Cr	0.9	0.25	-0.6	0	114	Bohlbro (1970) [173]
Fe-Cr	1.1	0.53	0	0	95	Keiski *et al*. (1996) [44]
Fe-Cr	1	0	-	-	118	Rhodes *et al*. (2003) [58]
Fe-Cr-Cu	1	0	-	-	75-80	Rhodes *et al*. (2003) [58]
Fe-Cr-Cu	1	0	-0.36	-0.09	111	Hla *et al*. (2009) [76]
Fe-Cr-Cu	0.9	0.31	-0.16	-0.05	88	Hla *et al*. (2009) [76]

Table 1.2 Kinetic parameters of Power Law kinetic expressions for Iron-based HT-WGS catalysts

CHAPTER 2

Resolving the Reaction Mechanism for High-Temperature Water-Gas Shift Reaction on Iron Oxide Catalysts

Abstract

The reaction mechanism of the high temperature water-gas shift (HT-WGS) reaction catalyzed by chromium-iron oxide catalysts for H_2 production has been studied for 100 years with two reaction mechanisms proposed: redox and associative (involving surface HCOO*). Direct experimental support for either mechanism, however, is still lacking, which hinders a thorough understanding of catalytic roles of each elements and the rational design of Cr-free catalysts. The current study demonstrates, with temperature programmed surface reaction (TPSR) spectroscopy (CO-TPSR, CO+H_2O-TPSR and HCOOH-TPSR), *for the first time* that the HT-WGS reaction follows the redox mechanism and that the associative mechanism does not take place.

2.1 Introduction

Most industrial H_2 is currently produced by methane steaming reforming (MSR) followed by the water-gas shift (WGS) reaction to increase or control the H_2/CO ratio and is employed in numerous applications (ammonia synthesis (from H_2/N_2), methanol

synthesis (from $H_2/CO/CO_2$), synthetic fuels (from H_2/CO), etc.). Ammonia synthesis alone is responsible for more than 2% of the world's daily energy use and produces the synthetic fertilizer required to feed the world's growing population.[1] While there is much interest in developing sustainable H_2 production from photo catalytic splitting of H_2O [2-4] and biomass reforming,[5, 6] production of H_2 from fossil fuels (CH_4 >> hydrocarbons >> coal) will be around for quite some time given its established technology and cost competitiveness. For example, H_2 fueling stations for fuel cell powered automobiles currently being set up in America and Germany rely on MSR and WGS because of the availability of abundant and inexpensive natural gas.[7]

$$CO + H_2O \leftrightarrow CO_2 + H_2 \qquad \Delta H = -40.6 KJ/mol \quad (1)$$

The WGS reaction involves carbon monoxide reacting with steam to produce carbon dioxide and hydrogen and was first applied by Bosch and Wild in 1914 with a Cr_2O_3-Fe_2O_3 catalyst to provide H_2 for the synthesis of ammonia.[8] Currently, the WGS reaction is commercially performed in several stages with different catalysts to optimize the greater CO equilibrium conversion attained at lower temperatures since the reaction is exothermic and reversible.[9, 10] The low temperature WGS (LT-WGS) reaction is performed at ~190-250^oC with a $Cu/ZnO/Al_2O_3$ catalyst and the high temperature WGS (HT-WGS) reaction is performed at ~350-450^oC with a Cu-promoted chromium-iron mixed oxide catalyst.

The reaction mechanism and kinetics of the HT-WGS reaction by Cr_2O_3-Fe_2O_3 catalysts have been extensively studied for 100 years, yet no consensus has been reached.[9-13] The "regenerative" or redox mechanism is the most accepted reaction mechanism involving alternate reduction of the catalyst surface oxygen site (O*), with "*" representing an empty surface site, by gas phase CO (eq. 2) and oxidation of the reduced catalyst surface empty site by H_2O vapor (eq. 3).[14-18] The reversible nature of the WGS reaction also allows reaction steps 2 and 3 to take place from the right to the left whereby the catalyst is oxidized by CO_2 and reduced by H_2.

$$CO + O^* \leftrightarrow CO_2 + * \qquad (2)$$

$$H_2O + * \leftrightarrow H_2 + O^* \qquad (3)$$

The existing evidence for the redox mechanism is the observation of the bulk $Fe^{2+}\leftrightarrow Fe^{3+}$ redox couple with Mössbauer spectroscopy with bulk Fe^{2+} oxidized to Fe^{3+} by H_2O and bulk Fe^{3+} reduced to Fe^{+2} by CO.[18, 19] *In situ* gravimetric analysis (GA) demonstrated that the catalyst oxygen content is dependent on the oxyreduction potential of the reaction gases (H_2/H_2O and CO/CO_2).[17] It was concluded that the oxygen changes measured with the GA as a function of the oxyreduction environments correspond to that of surface oxygen on the catalyst, but GA measures the total weight of the catalysts and is not able to distinguish between the bulk and surface oxygen content. The redox mechanism has become widely accepted because of these reported

studies which, however, are not able to distinguish between changes taking place in the bulk lattice and surface of the iron oxide catalysts since they monitor the entire volume of the catalyst. The dynamic nature of the iron oxide catalyst bulk phases upon gas oxyreduction potential further complicates the above conclusions.[20]

The alternative mechanism is referred to as the "associative" mechanism that involves surface reaction intermediates formed by reaction between CO and H_2O that subsequently decompose to CO_2 and H_2 (eq. 4). The most commonly proposed reaction intermediate is surface formate (HCOO*).[21-24] The associative mechanism has been criticized mainly by not detecting surface formate species or any other surface intermediates during the HT-WGS reaction [25, 26], which neglects the possibility of low concentrations and/or transient formation of surface formate species duirng HT-WGS. Such complexity has intrigued many computational studies which, however, both support and refute the associative mechanism.[27-29]

$$CO + H_2O \leftrightarrow (\text{Intermediate}) \leftrightarrow CO_2 + H_2 \qquad (4)$$

The focus of this opening chapter is to resolve the reaction mechanism for H_2 production during HT-WGS by the Cr_2O_3-Fe_2O_3 mixed oxide catalyst. We will show how employing transient kinetic studies, temperature programmed surface reaction (TPSR) spectroscopy, allows *for the first time* to finally provide solid experimental evidence that demonstrates the HT-WGS reaction by chromium-iron oxide catalysts

only proceeds via the redox mechanism.

2.2 Experimental

2.2.1 Catalyst Synthesis and Preparation

The Cr_2O_3-Fe_2O_3 catalyst used in this study was synthesized using ammonia assisted co-precipitation method. Iron nitrate (Sigma Aldrich, ≥99.999% trace metals basis) and chromium nitrate (Sigma Aldrich, ≥99.99% trace metals basis) were chosen as precursors. Calculated amounts of metal nitrates were mixed and dissolved in deionized water. Dilute aqueous ammonia was added to the solution drop wise until the pH reached 8.5. The dark brown precipitate formed was further aged overnight and filtered off. The filtered precipitate was then oven-dried at 80°C for 12 h and calcined at 400°C for 3 h in static air. The final catalyst contains 8 wt.% Cr_2O_3 and 92 wt.% Fe_2O_3.

2.2.2 Temperature Programmed Surface Reaction (TPSR) Spectroscopy

The TPSR studies were carried out using an Altamira Instruments system (AMI-200) connected to Dymaxion Dycor mass spectrometer (DME200MS). Approximately 30 mg of catalyst was loaded into a glass U-tube fixed-bed reactor and held in place by quartz wool. For all the experiments described below, the catalyst was first dehydrated under 10% O_2/Ar (Airgas, certified, 9.99% O_2/Ar balance) at 350°C for 1 hour followed by catalyst equilibration by the HT-WGS reaction at 350°C for 1

hour. The WGS reactant gas consisted of 10 ml/min 10% CO/Ar (Airgas, UHP certifies gas) and 30ml/min He (Airgas, UHP certifies gas) flowing through a water bubbler at room temperature to carry approximately 2.5 vol. % water vapor. The catalyst was then cooled in flowing Ar before introducing the reactant gases at ~110^{o}C for 15min. Finally, the fixed-bed reactor was heated at ~10^{o}C/min in the flowing reactant gases and the evolution of the products was monitored with the online mass spectrometer. The H_2O and CO reactants were supplied as indicated above and the HCOOH reactant was introduced by bubbling He through a bubbler containing formic acid (Sigma-Aldrich, reagent grade, ≥95%) at room temperature (~5 vol. %).

2.3 Results

2.3.1 CO-TPSR

The CO-TPSR spectra presented in Figure 2.1 were collected from an equilibrated catalyst after a 15-min water vapor treatment at 110°C to enhance the surface hydroxyl concentration. Water does not desorb during the TPSR experiment reflecting the absence of residual molecular water on the initial catalyst surface. Evolution of CO_2 initiates at ~135^{o}C (Tp=215^{o}C) and H_2 formation initiates at ~240^{o}C (Tp=285^{o}C). The CO-TPSR spectra reveal that the formation of CO_2 and H_2 occurs at different temperatures. This indicates that the formation of CO_2 proceeds by reaction between CO and a surface O* and the formation of H_2O involves reaction of two

surface *OH species. TPSR in flowing He, however, does not produce H_2 (see Figure 2.2). This suggests that the surface oxygen vacancies created by CO oxidation may be required for activation of the surface hydroxyls for H_2 formation. The independent formation of CO_2 and H_2 demonstrates that these two products are not formed by a common reaction intermediate. Above ~285^{o}C, CO is more extensively oxidized to CO_2 with additional oxygen from the catalyst. Although the CO-TPSR environment is not the actual WGS reaction conditions because of the absence of H_2O, the findings reveal that the redox reaction pathway can take place during WGS reaction conditions.

2.3.2 CO+H2O-TPSR

The evolution of H_2O, CO, CO_2 and H_2 during CO+H_2O-TPSR are shown in Figure 2.3(a) and the normalized CO_2 and H_2 signals are exhibited in Figure 2.3(b). For the normalized spectra, the MS signals were rescaled to the same maximum and minimum intensity to better compare their transient behavior. The slight increase in H_2O evolution may be related to water desorption from the catalyst surface at these low temperatures. Formation of CO_2 initiates at ~125^{o}C, but the appearance of H_2 is significantly delayed to ~240^{o}C indicating that the CO_2 production between 125-240^{o}C involves CO oxidation by surface O*. This behavior was already observed above during CO-TPSR. Even when both CO_2 and H_2 are simultaneously formed above 240^{o}C, the evolution of H_2 is retarded relative to CO_2 and the H_2/CO_2 ratio is less than

1, which finally reaches 1 as equilibrium is achieved at ~500°C. The initial delay in H_2 formation relative to CO_2 evolution has also been previously observed in constant temperature transient partial pressure experiments.[30, 31] The different kinetic responses of CO_2 and H_2 during CO+H_2O-TPSR reveal that these two products are not generated by a common surface reaction intermediate undergoing the same elementary reaction step.

2.3.3 HCOOH-TPSR

Formic acid (HCOOH) is known to decompose to CO_2 and H_2 from HCOO* which is the most proposed reaction intermediate of associative mechanism. [21, 32] The evolution of CO_2 and H_2 from formic acid decomposition during HCOOH-TPSR on the equilibrated Cr_2O_3-Fe_2O_3 catalyst is presented in Figure 2.4. The modest increase in HCOOH evolution at lower temperatures may be related to formic acid desorption from the catalyst surface. The production of the CO_2 and H_2 decomposition products initiates at ~225°C. The evolution of CO_2 and H_2 from HCOOH decomposition follows the exact same kinetics between 225-300°C as would be expected for their origin from the same surface reaction intermediate.

2.4 Discussion

2.4.1 Associative Mechanism vs. Redox Mechanism

The evolution of CO_2 and H_2 from CO+H_2-TPSR and HCOOH-TPSR are

compared in Figure 2.5. As indicated above, evolution of CO_2 and H_2 from HCOOH decomposition initiates at the same temperature and follows the exact same kinetics as expected for decomposition of a common surface reaction intermediate (HCOO*), which is the rate-determining-step.[33] In contrast, the production of CO_2/($CO+H_2O$) begins at a much lower temperature than H_2/($CO+H_2O$) formation because of CO oxidation by surface O*. The kinetics for evolution of CO_2/($CO+H_2O$) and H_2/($CO+H_2O$) above 250^oC are not the same with more CO_2 being initially formed than H_2. Furthermore, the kinetics for CO_2 and H_2 evolution from $CO+H_2O$-TPSR are also different than found for the kinetics for CO_2 and H_2O production from the decomposition of formic acid. The TPSR findings demonstrate that (i) an associated mechanism through a common surface intermediate, especially formic acid or formate, is not supported by the current findings and (ii) the current findings are only consistent with a redox or regenerative mechanism.

2.4.2 Reaction Pathways

The new insights suggest the following redox reaction mechanism for the HT-WGS reaction by chromium-iron mixed oxide catalysts.

$$CO + O^* \leftrightarrow CO_2^* \quad (5)$$

$$CO_2^* \leftrightarrow CO_2 + * \quad (6)$$

$$H_2O + * \leftrightarrow H_2O^* \quad (7)$$

$$H_2O^* + * \leftrightarrow OH^* + H^* \quad (8)$$

$$OH^* + * \leftrightarrow O^* + H^* \quad (9)$$

$$H^* + H^* \leftrightarrow H_2 + 2\,* \quad (10)$$

The oxidation of CO by surface O* appears rather straightforward, but isotopic oxygen studies showed rapid oxygen scrambling that also implicates the presence of surface carbonates (CO_3*) during the HT-WGS.[34] The surface carbonates may just be formed by complexation of the CO_2 product with surface O* and not directly involved in the HT-WGS reaction.[35] The details of the elementary steps involved in water decomposition during HT-WGS are not completely clear at present since formation of H_2 must involve several reaction steps such as reactions 8-10. The current findings also suggest that activation of surface hydroxyls to yield H_2 involves formation of surface vacant sites by CO oxidation. It appears that the HT-WGS shift reaction is much more complex involving multiple elementary steps than originally conceived as reflected by equations 2 and 3.

2.5 Conclusions

In conclusion, the evolution of CO_2 and H_2 from CO+H_2O-TPSR with equilibrated Cr_2O_3-Fe_2O_3 catalysts has, *for the first time*, been able to provide experimental evidence that the HT-WGS reaction follows a redox mechanism where the catalyst surface is alternatively reduced by CO and re-oxidized by H_2O. The

alternatively proposed associative reaction mechanism for CO_2 and H_2 formation proceeding through a common surface reaction intermediate and elementary decomposition step is disproved by the current findings. The new mechanistic insight will contribute towards the discovery of a non-toxic Cr-free HT-WGS catalyst for manufacture of clean H_2 fuel.

Acknowledgement

The authors gratefully acknowledge the financial support by the NSF CBET Grant 1511689.

References

[1] S. Licht, B.C. Cui, B.H. Wang, F.F. Li, J. Lau, S.Z. Liu, Science 345 (2014) 637-640.

[2] A. Kudo, Y. Miseki, Chem. Soc. Rev. 38 (2009) 253-278.

[3] M.G. Walter, E.L. Warren, J.R. McKone, S.W. Boettcher, Q.X. Mi, E.A. Santori, N.S. Lewis, Chem. Rev. 110 (2010) 6446-6473.

[4] A.J. Bard, M.A. Fox, Acc. Chem. Res. 28 (1995) 141-145.

[5] R.M. Navarro, M.A. Peña, J.L.G. Fierro, Chem. Rev. 107 (2007) 3952-3991.

[6] R.M. Navarro, M.C. Sanchez-Sanchez, M.C. Alvarez-Galvan, F. del Valle, J.L.G. Fierro, Energ Environ Sci 2 (2009) 35-54.

[7] E. Calo, A. Giannini, G. Monteleone, Int. J. Hydrogen Energy 35 (2010) 9828-9835.

[8] C. Bosch, W. Wild, United States Patent 1914.

[9] D.S. Newsome, Catal. Rev.: Sci. Eng. 21 (1980) 275-318.

[10] C. Ratnasamy, J.P. Wagner, Catal. Rev.: Sci. Eng. 51 (2009) 325-440.

[11] M. Zhu, I.E. Wachs, ACS Catal. 6 (2016) 722-732.

[12] D.W. Lee, M.S. Lee, J.Y. Lee, S. Kim, H.J. Eom, D.J. Moon, K.Y. Lee, Catal. Today 210 (2013) 2-9.

[13] R.J.B. Smith, M. Loganathan, M.S. Shantha, Int. J. Chem. React. Eng. 8 (2010) 1-32.

[14] N.V. Kulkova, M.I. Temkin, Zh. Fiz. Khim. 23 (1949) 695-698.

[15] G.G. Shchibrya, N.M. Morozov, M.I. Temkin, Kinet. Catal. 6 (1965) 1057-1059.

[16] M.I. Temkin, Adv. Catal. 28 (1979) 173-291.

[17] J.E. Kubsh, J.A. Dumesic, AlChE J. 28 (1982) 793-800.

[18] G.K. Boreskov, T.M. Yurieva, A.S. Sergeeva, Kinet. Catal. 11 (1970) 374-381.

[19] H. Topsoe, M. Boudart, J. Catal. 31 (1973) 346-359.

[20] Z. Cherkezova-Zheleva, I. Mitov, Journal of Physics: Conference Series 217 (2010) 012044.

[21] E.F. Armstrong, T.P. Hilditch, Proc. R. Soc. London, Ser. A 97 (1920) 265-273.

[22] S. Oki, R. Mezaki, J. Phys. Chem. 77 (1973) 1601-1605.

[23] F.G. Botes, Appl. Catal., A 328 (2007) 237-242.

[24] G.P. Van der Laan, A.A.C.M. Beenackers, Appl. Catal., A 193 (2000) 39-53.

[25] A. Boudjemaa, C. Daniel, C. Mirodatos, M. Trari, A. Auroux, R. Bouarab, C. R. Chim. 14 (2011) 534-538.

[26] C. Diagne, P.J. Vos, A. Kiennemann, M.J. Perrez, M.F. Portela, React. Kinet. Catal. Lett. 42 (1990) 25-31.

[27] L. Chen, G. Ni, B. Han, C.G. Zhou, J.P. Wu, Acta Chim. Sin. 69 (2011) 393-398.

[28] L. Huang, B. Han, Q. Zhang, M. Fan, H. Cheng, J. Phys. Chem. C 119 (2015) 28934-28945.

[29] R.M. Van Natter, J.S. Coleman, C.R.F. Lund, J. Mol. Catal. A: Chem. 311 (2009) 17-22.

[30] T. Salmi, L.E. Lindfors, S. Bostrom, Chem. Eng. Sci. 41 (1986) 929-936.

[31] T. Salmi, S. Bostrom, L.E. Lindfors, J. Catal. 112 (1988) 345-356.

[32] C. Rhodes, G.J. Hutchings, A.M. Ward, Catal. Today 23 (1995) 43-58.

[33] S. Poulston, E. Rowbotham, P. Stone, P. Parlett, M. Bowker, Catal. Lett. 52 (1998) 63-67.

[34] M. Zhu, I.E. Wachs, ACS Catal. 6 (2016) 1764-1767.

[35] C.M. Kalamaras, G.G. Olympiou, A.M. Efstathiou, Catal. Today 138 (2008) 228-234.

FIGURES

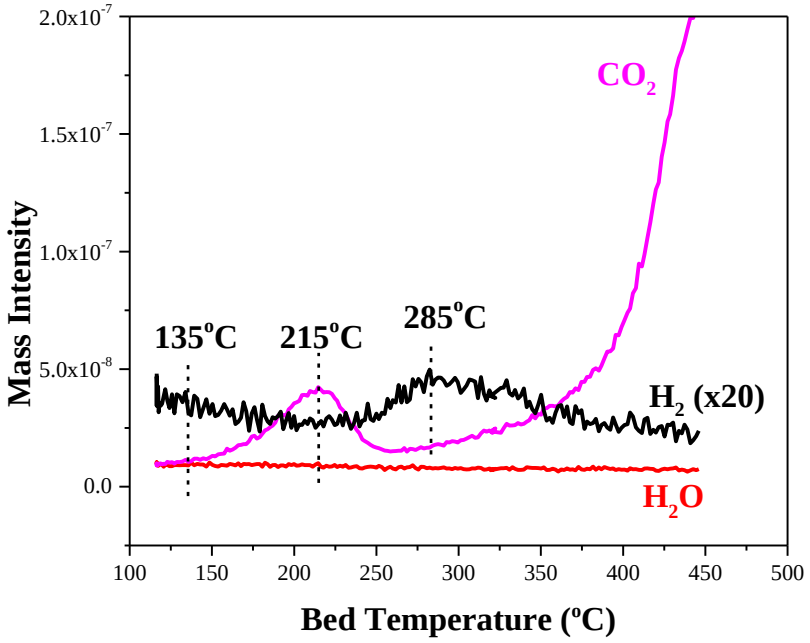

Figure 2.1 MS signals for CO_2, H_2 and H_2O during CO-TPSR.

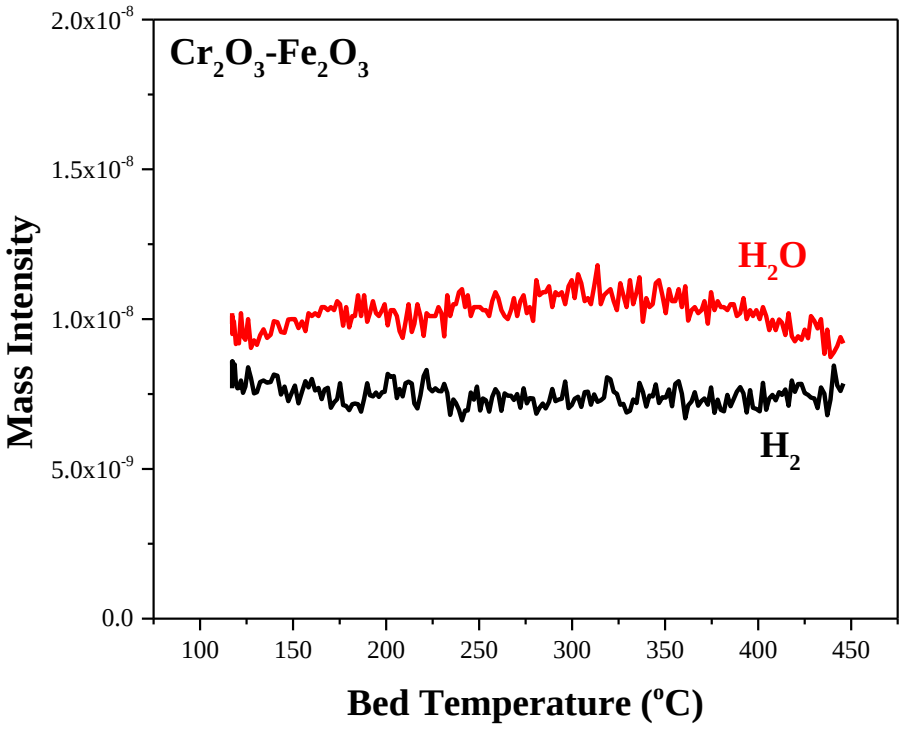

Figure 2.2 MS signals during He-TPSR for equilibrated Cr_2O_3-Fe_2O_3 catalyst. The spectra were collected from an equilibrated catalyst after a 15-min water vapor treatment at 110°C to hydroxylate the surface.

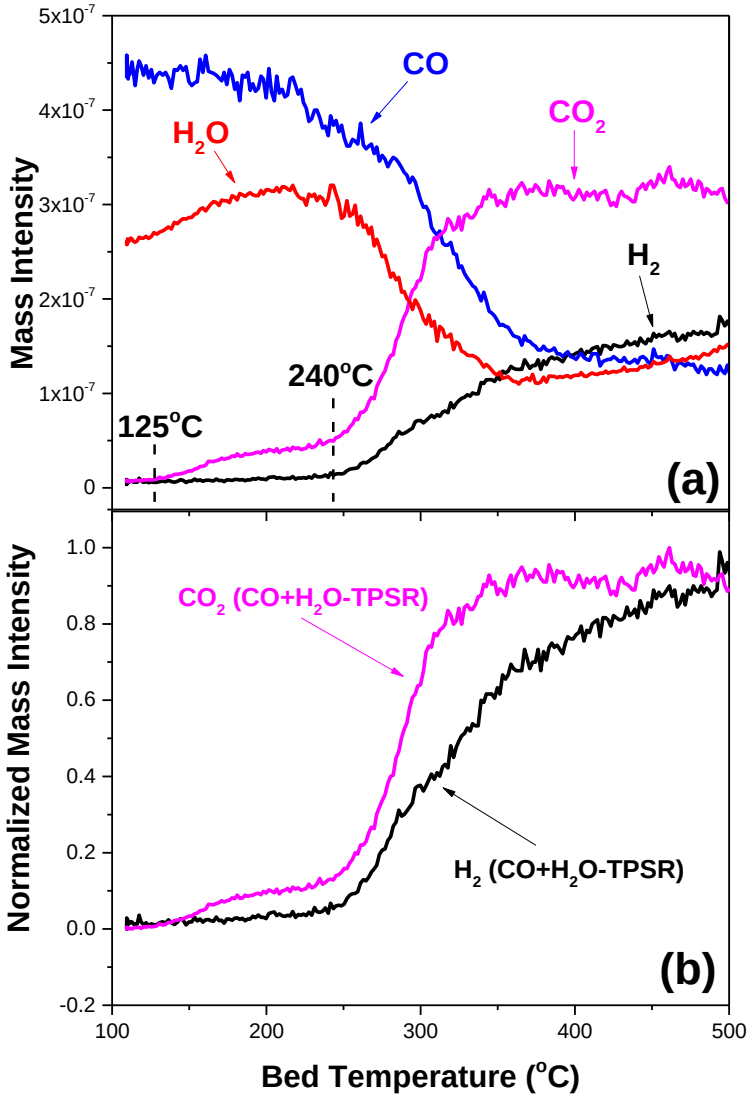

Figure 2.3 (a) MS signals for evolution of H_2O, CO, CO_2 and H_2 during $CO+H_2O$-TPSR from the equilibrated Cr_2O_3-Fe_2O_3 catalyst and (b) the normalized CO_2 and H_2 MS signals (CO: H_2O=1:1).

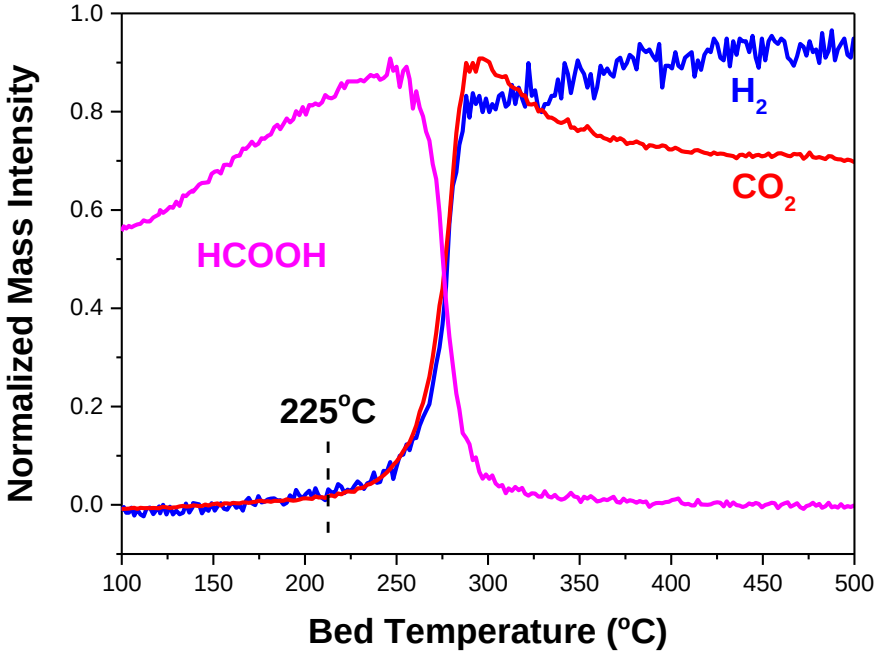

Figure 2.4 Normalized MS signals for HCOOH, CO_2 and H_2 during HCOOH-TPSR on equilibrated Cr_2O_3-Fe_2O_3 catalyst.

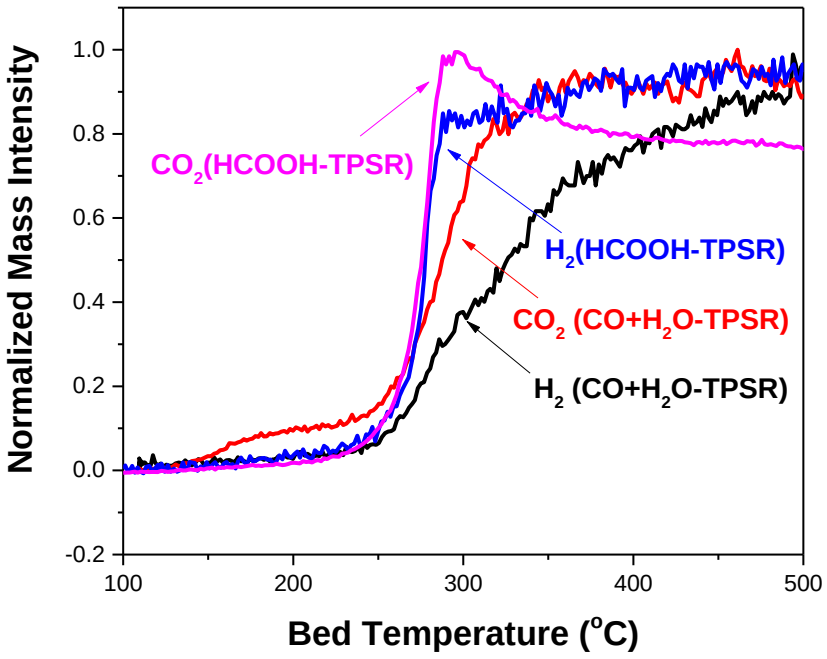

Figure 2.5 Normalized MS signals for CO_2 and H_2 evolution during HCOOH-TPSR and CO+H_2O-TPSR on equilibrated Cr_2O_3-Fe_2O_3 catalyst.

CHAPTER 3

Determining Number of Active Sites and TOF for the High-Temperature Water Gas Shift Reaction by Iron Oxide-Based Catalysts

ABSTRACT

This chapter demonstrates, with $C^{16}O_2/C^{18}O_2$ isotope switch and H_2-TPR experiments, *for the first time* that (*i*) the high temperature water-gas shift (HT-WGS) reaction by copper-chromium-iron oxide catalysts follows a redox mechanism dominated by the surface layer, (*ii*) the number of catalytic active sites can be quantified by the isotopic switch, and (*iii*) the turnover frequency (TOF) can be determined from knowledge of the number of sites. The quantitative TOF values reveal that chromium is only a textural promoter while copper is a chemical promoter.

3.1 Introduction

Industrial H_2 is currently primarily produced by methane steaming reforming (MSR) followed by the water-gas shift (WGS) reaction to increase or control the H_2/CO ratio and is employed in numerous applications like ammonia synthesis (from H_2/N_2), methanol synthesis (from $H_2/CO/CO_2$), synthetic fuels (from H_2/CO), etc. The WGS

reaction involves reaction of carbon monoxide with steam to produce H_2 and CO_2 and is commercially performed in several temperature stages with different catalysts to optimize the greater CO equilibrium conversion attained at lower temperatures since the reaction is exothermic and reversible[1, 2].

$$CO + H_2O \leftrightarrow CO_2 + H_2 \qquad \Delta H = -40.6 kJ/mol \qquad (1)$$

The high temperature water-gas shift (HT-WGS) reaction is commercially performed at ~350-450°C with iron-based catalysts and the low temperature water-gas shift (LT-WGS) reaction is performed at ~190-250°C with copper-based catalysts.

The reaction mechanism of the HT-WGS reaction catalyzed by iron-chromium oxide based catalyst has been extensively studied without reaching general agreement[3]. Armstrong and Hilditch were the first to propose a mechanism that involves a surface reaction intermediate such as surface formate ($HCOO*$) which is referred to as the associative mechanism.[4] Subsequent experimental and modeling studies of the high temperature WGS reaction have been inconclusive, both supporting and contradicting the presence of a surface formate intermediate.[5, 6] The most accepted mechanism, however, is the "regenerative" or redox mechanism involving alternate reduction of the oxidized catalyst by CO and oxidation of the reduced catalyst by H_2O[2, 5, 7-9]. The importance of the redox mechanism for this HT-WGS catalyst has been confirmed by the observation of the bulk Fe^{2+}/Fe^{3+} redox couple, with bulk

Fe^{2+} being oxidized to bulk Fe^{3+} by H_2O and bulk Fe^{3+} becoming reduced to bulk Fe^{+2} by CO.[10, 11] While numerous detailed redox mechanisms were proposed,[12-20] direct experimental proof is still lacking and no information has been provided about the catalyst surface during HT-WGS reaction conditions.

During the HT-WGS reaction, the equilibrated bulk iron oxide phase is present as magnetite (Fe_3O_4), which is produced by the partial reduction of the starting hematite (Fe_2O_3) phase.[21, 22] Chromium oxide is added as a textural promoter to inhibit sintering and stabilize the surface area of the magnetite. The chemical promotion of magnetite by chromia during the HTS reaction has been proposed and several models have been given.[12-14, 23, 24] Copper is also added as a promoter in commercial iron-chromium oxide catalyst to increase the activity over a wider temperature range.[25, 26] The promotion mechanism of copper during HT-WGS has received extensive discussion without reaching a consensus.[23, 25-31]

This opening chapter provides direct experimental evidence about fundamental aspects of the HT-WGS reaction by Fe-based catalysts: (*i*) reaction mechanism of the HT-WGS catalytic reaction by the Cr_2O_3-Fe_2O_3 mixed oxide catalyst (*ii*) number of catalytic active sites, (*iii*) nature of the most abundant reaction intermediate (mari), (*iv*)specific reaction rates (TOF = turnover frequency), and (*v*) promotion mechanisms of Cr and Cu. The specific catalytic activity allows *for the first time* quantitative

comparison of HT-WGS iron oxide-based catalysts and determining the promotion of Cr and Cu. Such fundamental information establishes the foundation for the rational design of Cr-free iron-based HT-WGS catalysts.

3.2 Experimental

3.2.1 Catalyst Synthesis and Preparation

The Fe_2O_3, Cr_2O_3-Fe_2O_3 and CuO-Cr_2O_3-Fe_2O_3 catalysts used in this study were synthesized using ammonia assisted co-precipitation method. Iron nitrate (Sigma Aldrich, 99.999% trace metals basis), chromium nitrate (Sigma Aldrich, 99.99% trace metals basis) and copper(II) nitrate (Sigma Aldrich, 99.99% trace metals basis) were chosen as precursors. Calculated amounts of metal nitrates were mixed and dissolved in deionized water. Dilute aqueous ammonia was added to the solution dropwise until the pH reaches 8.5. The dark brown precipitate formed was further aged overnight and filtered off. The filtered precipitate was then oven-dried at 80°C for 12 h and calcined at 400°C for 3 h in static air. The composition of all catalysts were listed in Table 3.1.

3.2.2 Flow BET Surface Area

The BET surface areas of both fresh and used catalysts were measured by a 3-point flow BET method with an Altamira Instruments system (AMI 200) equipped with a TCD detector. The N_2 adsorption/desorption amount were measured at three different partial pressures (P/P_0=0.14, 0.22 and 0.30) for the calculation of surface areas. The

activated catalysts after WGS reaction were directly measured without exposing the pyrophoric catalysts to air. The measured surface areas are listed in Table 3.2.

3.2.3 Isotope Switch Experiments

The $C^{16}O_2/C^{18}O_2$ isotope switch experiments were carried out with an Altamira Instruments system (AMI 200) connected to Dymaxion Dycor mass spectrometer (DME200MS). Approximately 20mg of catalyst was loaded into a quartz U-tube and initially dehydrated with 10% O_2/Ar at 400ºC to remove any residual carbonaceous residue and moisture. After dehydration, the catalyst was first equilibrated under rWGS reaction conditions (10 ml/min $C^{16}O_2$, 10 ml/min H_2) for 1 hour, subsequently, two different experiments were performed. In the "steady-state isotope switch" experiment, the $C^{16}O_2/H_2$ flow was switched to the isotopic labelled $C^{18}O_2/H_2$ at 400°C for 30min. Afterwards the catalyst was flushed by He, cooled down to 100°C and then heated up to 850°C under 10% H_2/He (30 ml/min) at a rate of 10°C/min. In the "isotope switch after inert flush", the catalyst was first equilibrated in the flowing $C^{16}O_2/H_2$ rWGS reaction conditions at 330°C, then flushed with inert He (20 ml/min He) for 10 min to remove residual $C^{16}O_2/H_2$ reactants from the system, and lastly exposed to a flow of isotopic labelled $C^{18}O_2/H_2$ reaction mixture (10ml/min $C^{18}O_2$, 10 ml/min H_2). The time-resolved reaction products were monitored every 0.5 seconds with the online mass spectrometer (MS).

3.2.4 Activity Measurement

The HT forward WGS ($CO + H_2O \rightarrow CO_2 + H_2$) reaction activity was measured with a mixture of 10% CO/Ar (10 ml/min), He (30 ml/min) and water vapor (H_2O/CO ~1) introduced by flowing gas through water bubbler at 25°C. The WGS reaction was performed at 330°C to ensure low conversions (<10%) and the steady-state data were collected after 90 minutes.

3.3 Results and Discussion

3.3.1 Reaction Mechanism

The steady-state isotope switch experiment was performed with the iron-chromium oxide catalyst and the time-resolved MS signals are presented in Figure 3.1 (the experimental details are given in the Supporting Information section). Upon isotope switch ($C^{16}O_2/H_2 \rightarrow C^{18}O_2/H_2$), the H_2 signal remains constant while the $C^{16}O_2$ signal sharply decreases and the $C^{18}O_2$ signal increases. The increase in $C^{18}O_2$ is slightly slower than the decrease in $C^{16}O_2$ because of the transient production of $C^{16}O^{18}O$ during the isotope switch. The production of $C^{16}O^{18}O$ also shows that oxygen exchange is taking place between the reactants and the oxygen from the catalyst. The decrease of the $H_2{}^{16}O$ signal is slightly slower than the decrease of the $C^{16}O_2$ signal reflecting the longer holdup of moisture than carbon dioxide in the catalyst bed. The entire isotope switch response takes place in ~2 min, which demonstrates that only a

finite amount of oxygen is involved. To gain insight into the oxygen isotopes remaining in the catalyst after the isotope switch, H_2-TPR was performed afterwards to monitor the population of ^{18}O and ^{16}O in the catalyst by formation of the corresponding isotopic water and presented in Figure 3.2. The production of water between ~200-300°C corresponds to the reduction of surface oxygen from the catalyst and yields comparable amounts of $H_2{}^{18}O/H_2{}^{16}O$~1. The presence of the doublet in the H_2-TPR spectra suggests that two distinct oxygen sites may be participating in the reduction process, but the identity of the participating oxygen sites are not known. The production of water above 350°C corresponds to the reduction of bulk lattice oxygen from the catalyst and the $H_2{}^{18}O/H_2{}^{16}O$ <<1. Some surface ^{16}O and bulk ^{18}O was observed which reveals that oxygen exchange is also taking place between the surface and bulk phases, which may be facilitated by the reduction process, but the exchange is mostly confined to the surface region. By integrating the H_2-TPR isotopic water peaks, only ~8% of the total oxygen in the equilibrated catalyst is involved in the steady-state isotope switch experiment. These isotopic oxygen exchange studies prove *for the first time* that the HT-WGS reaction by chromium-iron oxide catalysts follows a redox reaction mechanism and not an associative reaction mechanism involving a surface reaction intermediates (e.g. surface HCOO*). The redox process is dominated by a *surface* Mars-van Krevelen (MVK) reaction mechanism, where only the catalyst surface layer

is rapidly exchanging oxygen with the reactants, and the catalyst bulk lattice MVK mechanism also contributes to the oxygen exchange by slower diffusion over an extended period of reaction time.

3.3.2 Most Abundant Reactive Intermediates (mari) and Number of Active Sites (Ns)

The total oxygen participating in the HT-WGS redox process with the chromium-iron oxide catalyst was quantified by the isotope switch after inert flush experiment ($C^{16}O_2/H_2 \rightarrow He \rightarrow C^{18}O_2/H_2$) and the time-resolved evolution of the products is shown in Figure 3.3. The isotope switch experiment was performed at 330^{o}C because this reaction temperature provides differential reaction conditions (conversions < 10%) and this temperature will be used below to measure the steady-state reaction rates.

Exposure of the equilibrated iron-chromium oxide catalyst to flowing $C^{18}O_2/H_2$ yielded all the possible isotopes of carbon dioxide, carbon monoxide and water. The decay of the He signal indicates the hold-up time of an inert gas in the catalyst fixed-bed (~1 minute) and the H_2 reactant breaks through the catalyst bed in ~0.5 minutes. The first two carbon dioxide isotopes to appear were $C^{16}O_2$ and $C^{16}O^{18}O$ with the former appearing slightly faster. The final carbon dioxide isotope to appear was the unexchanged $C^{18}O_2$ and indicates that the catalyst surface is dominated by $^{18}O^*$ sites. The $C^{16}O$ and $C^{18}O$ transients follow that of the $C^{16}O_2$ and $C^{18}O_2$, respectively, and

may reflect the difficulty of accurately correcting for the CO_2 cracking to CO in the MS. The entire CO_2 and CO oxygen isotope exchange transients occur in less than 2 minutes indicating that only a finite amount of oxygen from the catalyst is involved in the exchange process. The distribution of the carbon oxide isotopes reflects the oxygen isotope population on the catalyst surface during the HT-WGS reaction. The first water isotope to form was $H_2{}^{16}O$ followed by appearance of $H_2{}^{18}O$. The appearance of the water isotopes ($H_2{}^{16}O/H_2{}^{18}O$) lags the corresponding carbon dioxide isotopes ($C^{16}O_2/C^{18}O_2$ and $C^{16}O/C^{18}O$), respectively, reflecting the longer holdup of water than carbon oxides in the catalyst bed and walls of the capillary to the MS. The longer evolution of $H_2{}^{16}O$ is mostly related to the holdup of moisture in the reactor system (catalyst and walls of the capillary to the MS) and possibly also a second slower oxygen exchange process related to slow diffusion of bulk lattice oxygen to the surface of the catalyst. The isotopic switch findings also demonstrate that the most abundant reactive intermediate (mari) for the HT-WGS reaction by chromium-iron oxide catalysts is the reactive O*.

The isotope switch experiment after the inert flush also provides for quantification of the number of oxygen sites participating in the HT-reverse WGS, as well as HT-forward WGS because of well-known concept of microscopic reversibility,[32] over the chromium-iron oxide catalyst by counting the number of ^{16}O atoms in the reaction

products ($C^{16}O_2$, $C^{16}O^{18}O$, $C^{16}O$ and $H_2{}^{16}O$). The number of oxygen sites per gram of each catalyst is given in Table 3.3. Both Cr-promoted catalysts have almost twice as many active sites per gram as the unprompted iron oxide catalyst that is primarily related to the higher surface area of the Cr-promoted catalysts (Table 3.2). The density of the active sites was calculated by dividing the Ns by specific surface area of activated catalysts and shown in Table 3.3. The BET surface area of the catalysts after reaction was measured in the catalyst bed after reaction without removing and exposing the pyrophoric catalyst to ambient air. Within the experimental error, the surface density of Ns for all three catalysts is essentially the same (~16-19 ^{16}O atoms/nm^2), indicating the Ns value is proportional to surface area. The Fe_3O_4 (111) surface contains ¾ ML of oxygen atoms (14.2 atoms/nm^2)[33] and ¼ ML of iron atoms that can be saturated by hydroxyl species [34] (4.7 atoms/nm^2) in a moist environment, which results in an overall surface oxygen atom density of 18.9 atoms/nm^2. The experimentally determined ~16-19 ^{16}O atoms/nm^2 corresponds to the theoretical value of 18.9 O atoms/nm^2 suggesting that only the catalyst surface layer is primarily participating in the HT-WGS reaction by iron oxide-based catalysts.

3.3.3 Turnover Frequency (TOF)

The HT-WGS activity and TOF values for the forward reaction ($H_2O + CO \rightarrow H_2 + CO_2$) are presented for the unpromoted iron oxide, chromium-iron oxide and copper-

chromium oxide catalysts in Table 3.3. The catalyst activity values show that both Cr and Cu promoters have a positive effect on the HT-WGS reaction rate (CuO-Cr_2O_3-Fe_2O_3 > Cr_2O_3-Fe_2O_3 > Fe_2O_3) with Cr enhancing the reaction rate per gram by ~2x and Cu by an additional ~3x. The double Cr-Cu promoted iron oxide catalyst is ~5x more active than unpromoted iron oxide per gram of catalyst.

The corresponding TOF values (TOF=activity/Ns) indicate that the specific TOF value for HT-WGS by the chromium-iron oxide catalyst is essentially the same as the unpromoted iron oxide catalyst. Thus, Cr is a textural promoter that increases the number of catalytic active sites by stabilizing higher surface area iron oxide, but Cr does not chemically promote the HT-WGS reaction by iron oxide. In contrast, Cu is a chemical promoter increasing the TOF value by ~3x compared to the TOF values for Cr_2O_3-Fe_2O_3 and unpromoted Fe_2O_3 catalysts.

3.4 Conclusions

In conclusion, the HT-WGS reaction by iron-based catalysts follows a redox mechanism primarily involving oxygen atoms from the surface layer and the participating oxygen atoms represent the most abundant reactive intermediate (mari). The isotopic switch experiments allow *for the first time* determination of the number of catalytic active sites and specific catalytic reactivity (TOF). The Cr is a textural promoter that increases the number of participating oxygen sites by stabilizing iron

oxides with higher surface areas. The Cu is a chemical promoter that increases the specific reaction rate (TOF) of the HT-WGS reaction by iron-based catalysts. The dual promotion of iron oxide by Cr and Cu yields a HT-WGS catalyst that has a specific reaction rate (TOF) that is ~3x greater and a catalyst activity per gram that is ~5x greater than an unpromoted iron oxide catalyst.

Acknowledgment

The authors acknowledge financial support from National Science Foundation Grant CBET - 1511689.

References

[1] D.S. Newsome, Catal. Rev.: Sci. Eng. 21 (1980) 275-318.

[2] C. Ratnasamy, J.P. Wagner, Catal. Rev.: Sci. Eng. 51 (2009) 325-440.

[3] R.J.B. Smith, M. Loganathan, M.S. Shantha, Int. J. Chem. React. Eng. 8 (2010) 1-32.

[4] E.F. Armstrong, T.P. Hilditch, Proc. R. Soc. London, Ser. A 97 (1920) 265-273.

[5] A. Boudjemaa, C. Daniel, C. Mirodatos, M. Trari, A. Auroux, R. Bouarab, C. R. Chim. 14 (2011) 534-538.

[6] C. Diagne, P.J. Vos, A. Kiennemann, M.J. Perrez, M.F. Portela, React. Kinet. Catal. Lett. 42 (1990) 25-31.

[7] C. Rhodes, G.J. Hutchings, A.M. Ward, Catal. Today 23 (1995) 43-58.

[8] J.R. Ladebeck, J.P. Wagner, Catalyst development for water–gas shift, Handbook of Fuel Cells, John Wiley & Sons, Ltd, Chichester, 2003, pp. 190-201.

[9] J.E. Kubsh, J.A. Dumesic, AlChE J. 28 (1982) 793-800.

[10] G.K. Boreskov, T.M. Yurieva, A.S. Sergeeva, Kinet. Catal. 11 (1970) 374-381.

[11] A. Khan, P. Chen, P. Boolchand, P.G. Smirniotis, J. Catal. 253 (2008) 91-104.

[12] G.C. Chinchen, R.H. Logan, M.S. Spencer, Appl. Catal. 12 (1984) 89-96.

[13] G.C. Chinchen, R.H. Logan, M.S. Spencer, Appl. Catal. 12 (1984) 69-88.

[14] G.C. Chinchen, R.H. Logan, M.S. Spencer, Appl. Catal. 12 (1984) 97-103.

[15] R.L. Keiski, T. Salmi, P. Niemistö, J. Ainassaari, V.J. Pohjola, Appl. Catal., A 137 (1996) 349-370.

[16] T. Salmi, L.E. Lindfors, S. Bostrom, Chem. Eng. Sci. 41 (1986) 929-936.

[17] S. Oki, R. Mezaki, Ind. Eng. Chem. Res. 27 (1988) 15-21.

[18] R. Mezaki, S. Oki, J. Catal. 30 (1973) 488-489.

[19] M. Tinkle, J.A. Dumesic, J. Catal. 103 (1987) 65-78.

[20] M. Tinkle, J.A. Dumesic, J. Phys. Chem. 88 (1984) 4127-4130.

[21] M.L. Kundu, A.C. Sengupta, G.C. Maiti, B. Sen, S.K. Ghosh, V.I. Kuznetsov, G.N. Kustova, E.N. Yurchenko, J. Catal. 112 (1988) 375-383.

[22] A. Patlolla, E.V. Carino, S.N. Ehrlich, E. Stavitski, A.I. Frenkel, ACS Catal. 2 (2012) 2216-2223.

[23] M.A. Edwards, D.M. Whittle, C. Rhodes, A.M. Ward, D. Rohan, M.D. Shannon, G.J. Hutchings, C.J. Kiely, PCCP 4 (2002) 3902-3908.

[24] S. Natesakhawat, X.Q. Wang, L.Z. Zhang, U.S. Ozkan, J. Mol. Catal. A: Chem. 260 (2006) 82-94.

[25] A. Andreev, V. Idakiev, D. Mihajlova, D. Shopov, Appl. Catal. 22 (1986) 385-387.

[26] V. Idakiev, D. Mihajlova, B. Kunev, A. Andreev, React. Kinet. Catal. Lett. 33 (1987) 119-124.

[27] J.D. Grunwaldt, P. Kappen, B.S. Hammershoi, L. Troger, B.S. Clausen, J. Synchrotron Radiat. 8 (2001) 572-574.

[28] P. Kappen, J.D. Grunwaldt, B.S. Hammershoi, L. Troger, B.S. Clausen, J. Catal. 198 (2001) 56-65.

[29] C. Rhodes, B.P. Williams, F. King, G.J. Hutchings, Catal. Commun. 3 (2002) 381-384.

[30] M. Estrella, L. Barrio, G. Zhou, X.Q. Wang, Q. Wang, W. Wen, J.C. Hanson, A.I. Frenkel, J.A. Rodriguez, J. Phys. Chem. C 113 (2009) 14411-14417.

[31] A. Puig-Molina, F.M. Cano, T.V.W. Janssens, J. Phys. Chem. C 114 (2010) 15410-15416.

[32] M. Boudart, G. Djéga-Mariadassou, Kinetics of Heterogeneous Catalytic Reactions, Princeton University Press, Princeton, 1984.

[33] J.C. Sharp, Y.X. Yao, C.T. Campbell, J. Phys. Chem. C 117 (2013) 24932-24936.

[34] Y. Joseph, C. Kuhrs, W. Ranke, M. Ritter, W. Weiss, Chem. Phys. Lett. 314 (1999) 195-202.

FIGURES

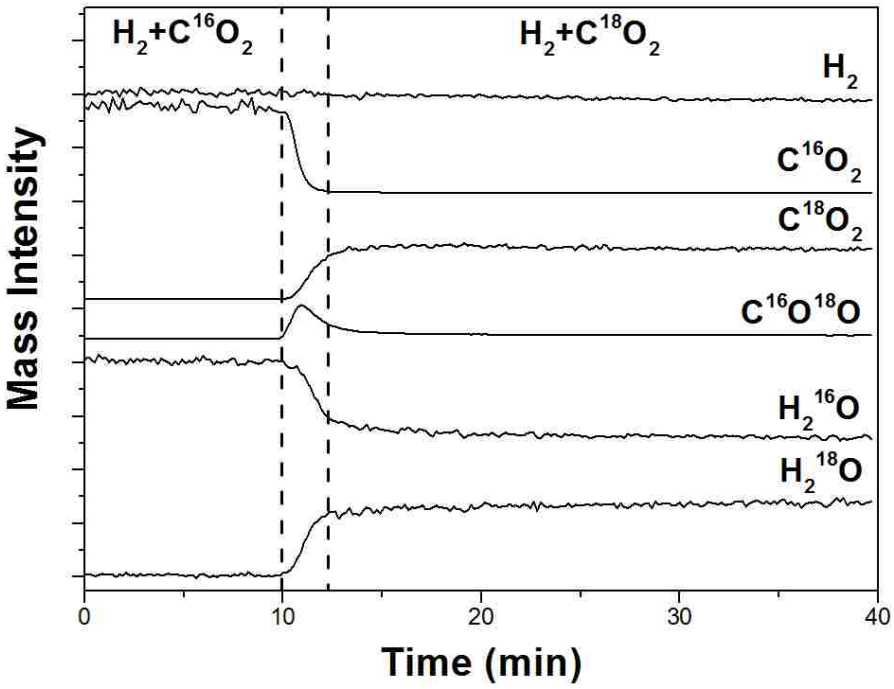

Figure 3.1 Transient response of H_2, $C^{16}O_2$, $C^{16}O^{18}O$, $C^{18}O_2$, $H_2{}^{16}O$ and $H_2{}^{18}O$ during steady-state isotope switch from $C^{16}O_2$+H_2 to $C^{18}O_2$+H_2 on Cr_2O_3-Fe_2O_3 catalyst (T=400°C)

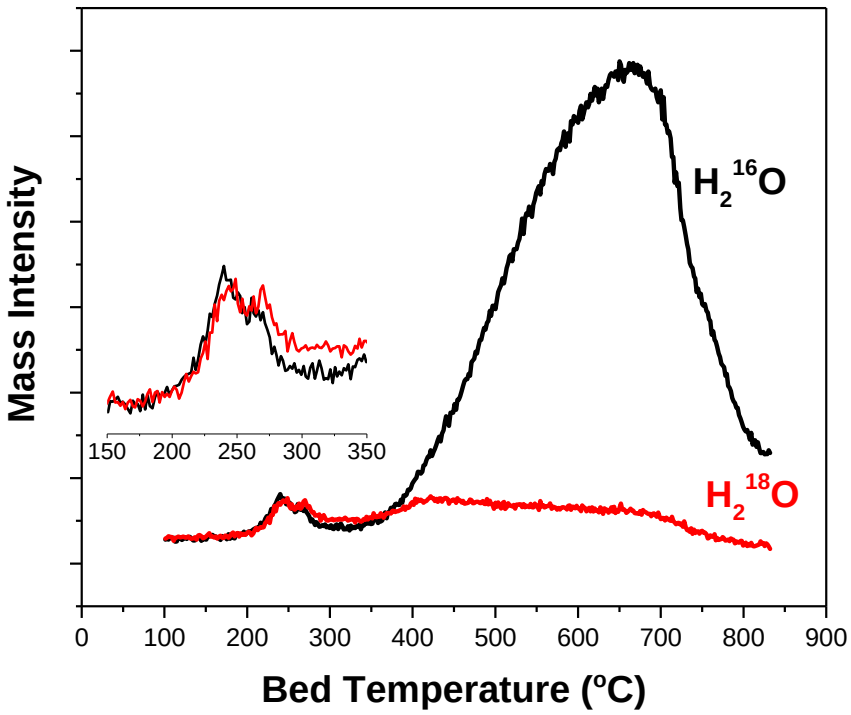

Figure 3.2 H_2-TPR profile of Cr_2O_3-Fe_2O_3 catalyst after the steady-state isotope switch experiment. Catalyst was cooled down in flowing He and then heated at 10ºC/min of flowing 10% H_2/He (30 ml/min).

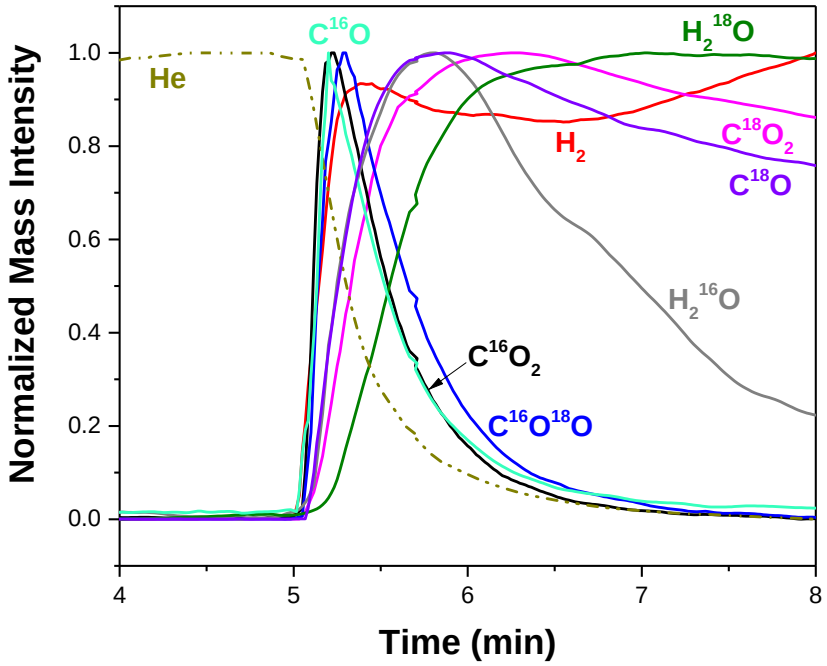

Figure 3.3 Transient response of He, H_2, $C^{16}O_2$, $C^{16}O^{18}O$, $C^{18}O_2$, $C^{16}O$, $C^{18}O$, $H_2{}^{16}O$ and $H_2{}^{18}O$ during isotope switch after inert flush on Cr_2O_3-Fe_2O_3 (T=330°C). The MS signals for all products were normalized to the same maximum and minimum intensity for better comparison of their transient behavior. The CO isotope signals are corrected for contribution of CO_2 cracking in the MS since cracking of the dominant CO_2 isotopes in the mass spectrometer significantly contribute to the CO MS signals.

TABLES

Catalyst	Composition
Fe_2O_3	100 wt.% Fe_2O_3
Cr_2O_3-Fe_2O_3	8 wt.% Cr_2O_3; 92 wt.% Fe_2O_3
CuO-Cr_2O_3-Fe_2O_3	3 wt.% CuO; 8 wt.% Cr_2O_3; 89 wt.% Fe_2O_3

Table 3.1 Composition of all prepared catalysts

Catalyst	Surface Area of Fresh Sample (m^2/g)	Surface Area after WGS Reaction (330°C) (m^2/g)
Fe_2O_3	40	29
Cr_2O_3-Fe_2O_3	101	63
CuO-Cr_2O_3-Fe_2O_3	93	60

Table 3.2 BET surface areas of fresh and activated Fe_2O_3, Cr_2O_3-Fe_2O_3 and CuO-Cr_2O_3-Fe_2O_3 catalysts

Catalyst	WGS Activity- H_2O conversion ($\times 10^{-6}$ mol/s·g)	Ns: n(^{16}O) ($\times 10^{-3}$ mol/ g)	Density of Ns (^{16}O atoms/nm^2)	TOF ($\times 10^{-3}$ s^{-1})
Fe_2O_3	1.2 ± 0.1	0.9 ± 0.1	19 ± 2	1.3 ± 0.2
Cr_2O_3-Fe_2O_3	2.0 ± 0.1	1.7 ± 0.2	16 ± 2	1.2 ± 0.2
CuO-Cr_2O_3-Fe_2O_3	5.7 ± 0.3	1.6 ± 0.2	16 ± 2	3.5 ± 0.4

Table 3.3 WGS activity, number of sites [n(^{16}O)], and turnover frequencies (TOFs).

(10% CO/Ar (10 ml/min), He (30 ml/min) and water vapor (H_2O/CO ~1); T=330°C)

CHAPTER 4

Promotion Mechanisms of Iron Oxide-Based High Temperature-Water Gas Shift (HT-WGS) Catalysts by Chromium and Copper

ABSTRACT

The Cr and Cu promotion mechanisms of high temperature water-gas shift (HT-WGS) iron oxide catalysts, synthesized by co-precipitation, were investigated as a function of reaction conditions. XRD and *in situ* Raman characterization showed that the initial calcined catalysts consisted of the Fe_2O_3 (hematite) bulk phase and transformed to the Fe_3O_4 (magnetite) phase during the HT-WGS reactions. *In situ* NAP-XPS and HS-LEIS surface analysis revealed that Cr was surface enriched as Cr^{+6} for the initial catalyst and reduced to Cr^{+3} during the HT-WGS reactions, with the Cr^{+3} dissolving into the bulk iron oxide lattice forming a solid solution. *In situ* NAP-XPS, XANES and HS-LEIS characterization indicated that Cu was initially present as Cu^{+2} cations dissolved in the Fe_2O_3 bulk lattice and reduced to metallic Cu^0 nanoparticles (~3 nm) on the external surface of the iron oxide support during the HT-WGS reactions. *In situ* HS-LEIS surface analysis also suggests that ~1/3 of the surface of the Cu nanoparticles was

covered by a FeO_x overlayer. The CO-TPR probe demonstrated that Cr does not chemically promote the iron oxide catalyst and that only Cu is a chemical promoter for the iron oxide HT-WGS catalysts. The Cu promoter introduces new catalytic active sites that enhance the reaction rates of the WGS reactions.

4.1 Introduction

Industrial H_2 is currently primarily produced by methane steam reforming (MSR) followed by the water-gas shift (WGS) reaction to increase or control the H_2/CO ratio and is employed in numerous applications (such as ammonia synthesis (from H_2/N_2), methanol synthesis (from $H_2/CO/CO_2$), synthetic fuels (from H_2/CO), etc.). The WGS reaction involves reaction of carbon monoxide with steam to produce H_2 and CO_2. The high temperature water-gas shift (HT-WGS) reaction is performed at ~350-450°C with iron-based catalysts and the low temperature water-gas shift (LT-WGS) reaction is performed at ~190-250°C with copper-based catalysts.[1, 2] The different temperatures are performed in industrial practice to optimize the greater CO equilibrium conversion attained at lower temperatures since the reaction is exothermic and reversible[1, 2].

$$CO + H_2O \leftrightarrow CO_2 + H_2 \qquad \Delta H = -40.6 kJ/mol \qquad (1)$$

The reaction mechanism of the HT-WGS reaction catalyzed by the unsupported iron-chromium oxide catalyst has been extensively studied without reaching a general agreement.[3, 4] Armstrong and Hilditch were the first to propose a mechanism that

involves a surface reaction intermediate such as surface formate ($HCOO*$) and is referred to as the associative mechanism.[5] Subsequent experimental and modeling studies of the HT-WGS reaction have been inconclusive, both supporting and contradicting the presence of a surface formate intermediate.[6, 7] The most accepted reaction mechanism, however, is the "regenerative" or redox mechanism involving alternative reduction of the oxidized catalyst by CO and oxidation of the reduced catalyst by H_2O.[2, 6, 8-10] Support for the redox mechanism for the HT-WGS catalytic reaction comes from the observation of the bulk Fe^{2+}/Fe^{3+} redox couple, with bulk Fe^{2+} being oxidized to bulk Fe^{3+} by H_2O and bulk Fe^{3+} becoming reduced to bulk Fe^{+2} by CO.[11, 12] While numerous detailed redox mechanisms for the HT-WGS reaction have been proposed,[13-21] direct experimental proof is still lacking and no information has been provided about the catalyst surface during HT-WGS reaction conditions with Fe-based catalysts.

During the HT-WGS reaction, the equilibrated bulk iron oxide phase is present as magnetite (Fe_3O_4), which is produced by the partial reduction of the starting hematite (Fe_2O_3) phase.[22, 23] The chromium oxide is added as a textural promoter to inhibit sintering and stabilize the surface area of the magnetite phase. The nature and distribution of Cr species during the reaction were proposed and several models have appeared in the literature: (i) formation of crystalline Cr_2O_3 to physically block the

direct contact and sintering of neighboring Fe_3O_4 particles,[13-15] (ii) formation of a surface region enriched with Cr^{3+} which is more thermodynamically stable than iron oxide[24] and (iii) Cr^{3+} enter into the magnetite lattice and occupy the octahedral sites with the displaced Fe^{2+} and Fe^{3+} transferred to tetrahedral sites[25, 26]. Many researchers believe that chromium can also enhance the HT-WGS activity by the formation of the $Cr^{3+}\leftrightarrow Cr^{6+}$ redox cycle.[27-29] Copper is also added as a promoter in commercial iron-chromium oxide catalyst and is claimed to increase the catalytic activity over a wider temperature range.[30-36] Three promotion mechanisms of copper were proposed in the literature: (i) Cu acts as a co-catalyst to promote the HT-WGS activity at lower temperature (<340°C),[30, 31] (ii) Cu exists as Cu cations dispersed in solid solution with iron oxide and modifies the electronic or structural properties of the Cr_2O_3-Fe_2O_3 catalyst,[24] and (iii) metallic Cu facilitates the cycle of water dissociation and hydrogen production.[37] The lack of fundamental understanding of how the HT-WGS catalyst functions, however, hampers the fundamental understanding of the Cr and Cu promotion mechanisms for iron oxide-based HT-WGS catalysts.

In Chapter 3, the turnover frequency (TOF) values of the HT-WGS reaction for iron oxide, chromium-iron oxide and copper promoted chromium-iron oxide catalysts were calculated and discussed. The number of catalytic active surface sites was

quantitatively determined by $C^{16}O_2/C^{18}O_2$ isotopic switch experiments, which revealed that only the outermost surface iron oxide layer is involved in the HT-WGS/RWGS redox reactions. The TOF values for HT-WGS by the chromium-iron oxide and unpromoted iron oxide catalyst are essentially the same (1.2×10^{-3} s^{-1} and 1.3×10^{-3} s^{-1}, respectively). The addition of copper, however, increases TOF value by ~3x (3.5×10^{-3} s^{-1}), indicating that Cu is a chemical promoter for the HT-WGS reaction.[38] In this opening chapter, iron oxide, chromium-iron oxide and copper promoted chromium-iron oxide were prepared and extensively studied with modern characterization techniques. The catalyst bulk and surface structures both before and during the reaction were analyzed with *operando* NAP-XPS (Near Ambient Pressure X-ray Photoelectron Spectroscopy)-MS, *in situ* Raman, *in situ* XANES (X-ray Absorption Near Edge Spectroscopy), XRD, TEM/EDX and HS-LEIS (High Sensitivity-Low Energy Ion Scattering). The nature of the catalytic active sites and the redox characteristics of the catalyst bulk and surface components during WGS were examined by *in situ* XANES and NAP-XPS-MS. The promotion mechanisms of chromium and copper upon the redox behavior of the iron oxide catalysts were also examined by CO-TPR on catalysts activated under the HT-WGS reaction conditions. The new fundamental insights *for the first time* provide direct experimental evidence of the promotion mechanisms of chromium and copper upon iron oxide-based HT-WGS catalysts.

4.2 Experimental

4.2.1 Catalyst Synthesis and Preparation

The Fe_2O_3, Cr_2O_3-Fe_2O_3 and CuO-Cr_2O_3-Fe_2O_3 catalysts used in this study were synthesized using ammonia assisted co-precipitation method. Iron nitrate (Sigma Aldrich, 99.999% trace metals basis), chromium nitrate (Sigma Aldrich, 99.99% trace metals basis) and copper nitrate (Sigma Aldrich, 99.99% trace metals basis) were chosen as precursors. Calculated amounts of metal nitrates were mixed and dissolved in deionized water. Dilute aqueous ammonia was added to the solution dropwise until the pH reaches 8.5. The dark brown precipitate formed was further aged overnight and filtered off. The filtered precipitate was then oven-dried at 80°C for 12 h and calcined at 400°C for 3 h in static air. The Cr_2O_3-Fe_2O_3 catalyst contains 8 wt.% Cr_2O_3 and 92 wt.% Fe_2O_3. And the CuO-Cr_2O_3-Fe_2O_3 catalyst contains 3 wt.% CuO, 8 wt.% Cr_2O_3 and 89 wt.% Fe_2O_3.

4.2.2 X-ray Diffraction (XRD) Spectroscopy

Powder X-ray diffraction (XRD) patterns of fresh WGS catalysts were measured with a Rigaku Miniflex II diffractometer using Cu K-α radiation (1.5418 Å). Full scans of 10-80 degrees (2-theta) were performed with a scan rate of 1 deg/min. Additionally, the major Fe_2O_3 peak at 34.5-37.5 degrees was scanned with a rate of 0.1 deg/min to examine for possible formation of Cr-Fe-O and Cu-Cr-O solid solutions. The XRD

patterns of activated catalysts were recorded on a Bruker D8 Advance in Bragg-Brentano geometry. Sample was first activated under RWGS condition (1:1 CO_2:H_2 in N_2) at 400°C, then transferred via an X-ray transparent hemispherical plastic cap from the glove box to the diffractometer.

4.2.3 *In Situ* Raman Spectroscopy

The *in situ* Raman spectra were collected with a Horiba-Jobin Yvon LabRam-HR spectrometer equipped with a confocal microscope, 2400/900 grooves/mm gratings, and a notch filter. The visible laser excitation at 442 nm (violet) was generated by a He-Cd laser. The lasers were focused on the samples with a confocal microscope equipped with a 50X long working distance objective (Olympus BX-30- LWD). And the scattered photons were directed and focused onto a single-stage monochromator and measured with a UV-sensitive LN2-cppled CCD detector (Horiba CCD-3000V). The catalyst samples were placed in an environmentally controlled high-temperature cell reactor (Linkam CCR1000) with the temperature controlled by a temperature controller (Linkam TMS94). The spectrum of the dehydrated sample was collect after catalysts treated by 10% O_2/Ar (Airgas, certified, 9.99% O_2/Ar balance) at 400°C for 1 hour to remove any possible adsorbed organic impurities and adsorbed moisture. For spectra of the activated catalysts during RWGS reaction, the catalysts were first dehydrated with 10% O_2/Ar at 400°C for 1 hour followed by switching to the RWGS

reaction conditions (10 ml/min CO_2 (Airgas, UHP certified gas), 10 ml/min H_2 (Airgas, UHP certified gas), 10 ml/min Ar (Airgas, UHP certified gas)). The *in situ* Raman spectra were then collected after the catalysts were equilibrated under the RWGS reaction conditions for 1 hour.

4.2.4 Near Ambient Pressure X-ray Photoelectron Spectroscopy (NAP-XPS)

The synchrotron-based NAP-XPS experiments were performed in the NAP-XPS setup at the ISISS beamline of the Fritz-Haber-Institute located at the BESSY II synchrotron radiation facility in Berlin, Germany. The setup consists of a stainless steel NAP-XPS chamber[39, 40] attached to a set of differentially pumped electrostatic lenses and a separately pumped analyzer (Phoibos 150 Plus, SPECS GmbH). The NAP-XPS spectra were collected at a temperature of 400°C and a pressure of 0.3 mbar. The catalyst (50mg) was first dehydrated under O_2 (6 ml/min) at 400°C for 2h, followed by HT-WGS reaction under H_2O (6 ml/min) and CO (0.6 ml/min) for 1h. The spectra were collected after each experimental step and also the first 15min of the HT-WGS reaction.

4.2.5 High-Sensitivity Low-Energy Ion Scattering (HS-LEIS) Spectroscopy

The outermost surface layer was analyzed by Qtac^{100} HS-LEIS spectrometer (ION-TOF) equipped with a highly sensitive double toroidal analyzer. The equipment provides 3000-fold higher sensitivity than conventional LEIS spectrometers, allowing for quantitative static depth profiling. Prior to the measurements, the sample was

dehydrated in static O_2 feed by a balloon at 400°C for 1 hour in a preparation chamber connected to the spectrometer to remove any possible adsorbed organic impurities and adsorbed moisture. After dehydration, the preparation chamber was evacuated and the sample was directly transferred to the main UHV chamber for the measurements. To collect the surface information of activated catalysts after RWGS reaction, the dehydrated catalyst was further treated under a static reaction mixture (~100 mbar CO_2 (Airgas, UHP certified gas) and ~100 mbar H_2 (Airgas, UHP certified gas)) at 400°C. The design of the preparation chamber on HS-LEIS prevents the pretreated catalyst from contacting air when transferred into the measurement chamber. The HS-LEIS depth profiling spectrum were collected using 5 KeV Ne^+ as ion sources. For deeper depth profiling, the surface was sputtered with 0.5 KeV Ar^+, each sputter and measurement cycle yields a total of 1×10^{15} ions/cm^2, which corresponds to ~1 atomic layer.[41]

4.2.6 *In Situ* X-ray Absorption Spectroscopy

The X-ray Absorption Spectroscopy (XAS) experiments were performed at Brookhaven National Laboratory (BNL) National Synchrotron Light Source (NSLS) beamline X18A and X18B. The "O_2→RWGS→CO_2" redox cycle was performed in a Nasner-Adler (NA) reactor. Catalyst was first dehydrated under 10% O_2/He (Airgas, certified) at 350°C for 1 hour followed by activation under RWGS mixture

(CO_2:H_2=1:1) for 1 hour. After activation, the catalyst was treated by 33% CO_2/He for 30 min at 350°C to test the re-oxidation ability. The "O_2→WGS→H_2O" redox cycle was performed using a Clausen cell equipped with a 1.0 mm o.d. (0.9 mm i.d.) quartz capillary. The catalyst was dehydrated by 10% O_2/He and activated under WGS mixtures (CO: H_2O≈1:1) at 350°C with the water vapor introduced by flowing gas through a water bubbler. Then the catalyst was treated by 2.5% H_2O/He at 350°C for 30min. The Cu, Cr and Fe K-edge XAS data were obtained after each experimental step in fluorescence mode with a PIPS detector.

4.2.7 TEM

Transmission electron microscopy (TEM) was performed on a JEM-ARM200F with a CEOS CESCOR and a CEOS CETCOR hexapole aberration correctors for probe and image forming lenses, respectively, a cold field emission gun (CFEG) and an energy dispersive X-ray detector (EDX). Scanning TEM (STEM) images were recorded with a JEOL high angle annular dark-field (HAADF) Samples were grained and placed on a lacey carbon coated Au TEM grid. After RWGS reaction (1:1 CO_2:H_2 in N_2 at 400°C) samples were transferred without exposure to air and stored in a glove box under Ar atmosphere. Subsequently, the sample was inserted into the TEM via a secure transfer using a GATAN VTST 4006 vacuum transfer holder. Samples were prepared dry to avoid carbon contamination.

4.2.8 CO-TPR

The CO-TPR experiments were carried out using an Altamira Instruments system (AMI-200). Approximately 30 mg of catalyst was loaded into a U-tube sample holder for analysis. To perform CO-TPR on fresh catalysts, samples were first dehydrated under 10% O_2/Ar (Airgas, certified, 9.99% O_2/Ar balance) at 350°C for 1 hour then flushed by He (Airgas, UHP certified gas) and cooled down to room temperature. The CO-TPR experiments were then performed by ramping up the temperature under 10% CO/Ar (Airgas, UHP certified gas, 30 ml/min) at a rate of 10°C/min. To perform CO-TPR on activated catalysts, samples were first dehydrated under 10% O_2/Ar at 350°C for 1 hour followed by activation of WGS reaction (10ml/min 10% CO/Ar, 30ml/min He flowing through bubbler at room temperature to carry 2.5 % water vapor) at 350°C for 90min. After the catalyst was activated, the reactor was flushed by He and then cooled down to 80°C. A flow of 30 ml/min 10% CO/Ar was then introduced and the temperature was ramped up to 450°C at a rate of 10°C/min. The gases flowing out of the reactor were analyzed by an online quadrupole mass spectrometer (Dycor Dymaxion DME200MS).

4.2.9 Steady-State WGS Reaction

The steady-state forward WGS reaction was perform on an Altamira AMI-200 spectroscope equipped with a Dycor Dymaxion DME200MS online quadrupole mass

spectrometer. Approximately 10 mg of catalyst was loaded into a U-type quartz tube for the reaction and the catalyst was held in place by quartz wool. Initially the catalyst was treated with 10% O_2/Ar (Airgas, certified, 9.99% O_2/Ar balance) at 400°C for 1 hour to remove any possible adsorbed organics by combustion. Then the system was flushed with He for 10 min, after which the reaction mixture was introduced (10% CO/Ar (Airgas, UHP certified gas, 10 ml/min), He (Airgas, UHP certified gas, 30 ml/min) and water vapor introduced by flowing the gas through a water bubbler at 25°C). The WGS reaction was performed at different temperatures each for 90 min to ensure the steady-state reaction conditions. The gases exiting the quartz tube reactor were analyzed with the online mass spectrometer. The following *m/e* ratios were employed for the identification of reaction gases and products: H_2, *m/e* = 2; H_2O, *m/e* = 18; CO, *m/e* = 28; CO_2, *m/e* = 44.

4.3 Results

4.3.1 XRD

The XRD diffractograms of fresh Fe_2O_3, Cr_2O_3-Fe_2O_3 and CuO-Cr_2O_3-Fe_2O_3 catalysts calcined at 400°C are presented in Figure 4.1. The bulk phase of all three catalysts is identical and identified as the crystalline Fe_2O_3 (hematite) phase.[42] The XRD patterns of the Cr_2O_3-Fe_2O_3 and CuO-Cr_2O_3-Fe_2O_3 catalysts do not show any separate Cr_2O_3, CuO or Cu_2O crystalline phases. The Cr oxide forms a solid solution

with Fe_2O_3 as indicated by the slight shift in the XRD for the Cr_2O_3-Fe_2O_3 and CuO-Cr_2O_3-Fe_2O_3 catalysts (Figure 4.2). It is not apparent from XRD if CuO-Fe_2O_3 also forms a solid solution since the amount of CuO is small and a shift in the XRD peak is not observed.

After RWGS reaction, the bulk phase of CuO-Cr_2O_3-Fe_2O_3 catalyst transforms from hematite phase to magnetite phase as shown in Figure 4.1. The hill at around 20° can be assigned to the plastic dome of the XRD sample holder and does not originated from the catalyst. Again, the absence of any separate Cr_2O_3, CuO or Cu_2O crystalline phases indicates that Cr and Cu dissolves into bulk lattice of Fe_3O_4 during WGS/RWGS reaction.

4.3.2 *in Situ* Raman Spectroscopy

The *in situ* Raman spectra of the iron oxide and promoted iron oxide catalysts are presented in Figure 4.3 as a function of environmental conditions. Figure 4.3a is from spectra collected under dehydrated conditions (10% O_2/Ar) and Figure 4.3b is under RWGS reaction conditions (10 ml/min CO_2, 10 ml/min H_2 and 10 ml/min Ar). The dehydrated iron oxide catalyst exhibits Raman bands at 612, 498, 410, 290 and 223 cm^{-1} that are characteristic of the bulk α-Fe_2O_3 phase[43]. The dehydrated Cr_2O_3-Fe_2O_3 and CuO-Cr_2O_3-Fe_2O_3 catalysts also possess the Raman bands of α-Fe_2O_3 and three new bands at 664 (bulk $Fe_{2-x}Cr_xO_3$ solid solution with Cr^{+3})[44], 844 (bridging Cr-O-

Fe) and 1003 cm^{-1} (symmetric O=Cr=O stretch of a Cr^{+6} surface dioxo $(O=)_2CrO_2$ sites)[45]. Discrete Cr_2O_3 nanoparticles (sharp peak at 550 cm^{-1})[45] are not present under dehydrated conditions. Under the reverse water gas shift (RWGS) reaction conditions, the bulk $Fe_{2-x}Cr_xO_3$ phase reduces to the bulk $Fe_{3-x}Cr_xO_4$ solid solution magnetite phase (characteristic bands at 289, 517 and 652 cm^{-1})[44]. The initially fully oxidized surface Cr^{6+} species are reduced in the RWGS reaction environment and dissolve into the bulk iron oxide lattice to form additional $Fe_{3-x}Cr_xO_4$ as indicated by the absence of vibrations from surface Cr-O-Fe and O=Cr=O functionalities. Raman bands from Cu are not observed under both dehydrated and reaction conditions, and is related to the lower concentration and Raman cross-section of Cu relative to the higher amounts and Raman cross-sections of iron and chromium oxide[46]. Discrete Cr_2O_3 nanoparticles (sharp peak at 550 cm^{-1})[45] are also not present under the RWGS reaction conditions. The *in situ* Raman analyses were able to provide information about both the bulk (Fe_2O_3, $Fe_{2-x}Cr_xO_3$, Fe_3O_4, $Fe_{3-x}Cr_xO_4$ as well as absence of Cr_2O_3 nanoparticles) and surface (presence and absence of surface CrO_x sites) phases of the catalysts as a function of environmental conditions, but no information could be obtained about the Cu promoter.

4.3.3 Near Ambient Pressure X-ray Photoelectron Spectroscopy (NAP-XPS)

NAP-XPS measurements were performed on the copper-chromium-iron oxide

catalyst to obtain additional surface information during the HT WGS reaction, which is absent from the literature. Typically, XPS with conventional X-ray sources probes 1-3nm of the surface region of a solid, but using synchrotron radiation with tunable energy the probed depth can be reduced to the first few atomic layers[40, 47]. Figure 4.4a-c shows the NAP-XPS Fe 2p, Cr 2p and Cu 2p regions measured *in situ* at different reaction conditions. Under dehydrated conditions, the catalyst is exposed to an oxidizing environment and the surface iron oxide is present as Fe_2O_3 indicated by the $2p_{3/2}$ peak at 711 eV and characteristic satellite peak at 719 eV.[48] The chromium oxide surface signal is dominated by Cr^{6+} (588 eV and 579 eV) with a small amount of Cr^{3+} (587 eV and 577 eV) also present. The observation of surface Cr^{6+} is consistent with the *in situ* Raman findings above for the corresponding dehydrated catalyst. The sharp Cu 2p peaks at 934 eV and the satellite structure at 940-945 eV indicate that Cu^{2+} is dominant at the surface of the dehydrated catalyst. [49]

During the HT-WGS reaction, both CO_2 and H_2 form and the catalyst surface undergoes dramatic changes as shown in Figure 4.4. In the first few minutes, the catalyst surface becomes activated by CO removal of oxygen to form CO_2 and the CO_2 formation subsequently levels off (see Figure 4.4d). Simultaneously, the H_2 production increases monotonically during the catalyst activation stage as shown in Figure 4.4d. The Fe 2p satellite peak vanishes and peak broadening is observed at ~708 eV,

indicating that the surface iron oxides have been transformed to a partially reduced iron oxide phase (consistent with a mixture of Fe^{+2} and Fe^{+3}). The intensity of the Cr^{6+} peaks (588 eV and 579 eV) significantly diminish and are accompanied by an increase of Cr^{3+} peaks (587 eV and 577 eV), indicating that the surface Cr^{6+} species have been reduced to Cr^{3+} during the reaction. A residual amount of Cr^{+6} still remains under the current sub-ambient pressure experimental conditions. The copper component is initially present as Cu^{2+} (Cu2p peaks at ~943 and 934 eV) and becomes reduced to metallic Cu^0 (2p peak at 933 eV) and the intensity of the copper peak sharply decreases within 5 min of reaction (see the time-resolved Cu 2p spectra in Figure 4.5). The sharp decrease is related to both sintering of metallic Cu^0 NPs and possible presence of metal oxides wetting the surface of the Cu^0 NPs (SMSI effect[59]).

4.3.4 High-Sensitivity Low-Energy Ion Scattering (HS-LEIS) Spectroscopy

A more surface sensitive technique than XPS (~1-3nm) is High Sensitivity-Low Energy Ion Scattering (LS-LEIS) that can sample the topmost surface layer of a solid, ~0.3nm, and also performs depth profiling with surface sputtering by the interrogating Ne^+ gas ions. HS-LEIS analyses of fresh and activated CuO-Cr_2O_3-Fe_2O_3 catalysts are shown in Figure 4.6 using Ne^+ ions as the probe. The sputter yield with the 5 KeV Ne^+ ions is 3 atoms/ion.[50, 51] Considering the surface atom density of iron oxide, an ion dose of 5×10^{14} Ne^+/cm^2 corresponds to the removal of approximately one atomic

layer.[52]

In the fresh dehydrated and oxidized catalyst (Figure 4.6a), the Cr promoter is surface enriched since the Cr HS-LEIS signal strongly decreases as the first catalyst layer is sputtered away and is almost 3 times greater than in the bulk (above 5×10^{14} Ne^{+}/cm^{2} dose). The Cu promoter, however, is not surface enriched since its HS-LEIS signal remains constant during the Ne^{+} sputtering indicating its concentration is homogeneous in the catalyst surface region during depth profiling. The depth profiles of Cr and Cu for the activated catalyst are quite different than the fresh catalyst as shown in Figure 4.6b. The intensity of the Cr signal in the topmost surface layer is now much lower than for the dehydrated catalyst, by a factor of ~1/5, and below the signal in the bulk (Ne^{+} dose > $5\times10^{14}/cm^{2}$), by a factor of ~1/3. This trend is consistent with lack of surface enrichment and surface Cr migrating into the bulk lattice of iron oxide (solid solution of $Fe_{3-x}Cr_xO_4$). The depth profile of Cu is quite different, the Cu signal initially increasing by ~30%, to ~2x that in the dehydrated fresh catalyst, in the topmost layer and then decreases upon further sputtering (Ne^{+} dose > $5\times10^{14}/cm^{2}$). The initial increase in the intensity of the Cu signal in the topmost layer suggests that the metallic Cu (as shown by XPS above), most probably present as nanoparticles, are covered by ~1/3 monolayer of either Cr or Fe oxides after exposure to the HT-WGS reaction. The decreasing intensity of the Cu signal with further sputtering (Ne^{+} ion dose > $5\times10^{14}/cm^{2}$)

suggests that the dimension of Cu particle on the surface is small. This was confirmed by Ne^+ dose depth profile with Ar sputtering, which allows accessing deeper into the catalyst and the HS-LEIS depth profile is presented in Figure 4.7. Again, the intensity of the Cu signal initially increases for the first atomic layer and then decreases to a constant value after ~10 atomic layers have been sputtered. This indicates that the thickness of surface metallic Cu particles during the reaction is ~10 atomic layers, corresponding to a thickness of approximately 3.6nm.[53]

4.3.5 *in Situ* X-ray Absorption Spectroscopy

The influence of different gas environments on the Cu, Cr and Fe cations of the CuO-Cr_2O_3-Fe_2O_3 catalyst was examined with *in situ* XANES (Figure 4.8). The CuO-Cr_2O_3-Fe_2O_3 catalyst was initially dehydrated with 10% O_2/Ar at 350ºC and then activated for 60 minutes with either WGS or RWGS reaction conditions. The activated catalyst was then exposed to either CO_2 or H_2O to examine the oxidization ability of these two oxygenates upon each of the elements present in the activated catalyst. The findings reveal that the three elements in the HT-WGS catalyst respond differently to the varying gas environments.

The iron cation is initially present as Fe^{+3} in Fe_2O_3 (confirmed with XANES of Fe_2O_3 reference in Figure 4.9). Activation in WGS and RWGS reaction conditions shifts the edge position to lower energy, which is consistent with partial reduction to

Fe^{+2}/Fe^{+3} in Fe_3O_4 (confirmed with XANES of Fe_3O_4 reference in Figure 4.9). Subsequent exposure to either CO_2 or H_2O only partially oxidizes the Fe^{+2} back towards Fe^{+3} without full oxidation to the initial Fe_2O_3 phase in the dehydrated catalyst. This indicates that only a small fraction of iron in the catalyst is able to undergo a redox process.

The chromium cation initially contains a significant amount of Cr^{+6} (confirmed with XANES of CrO_3 reference in Figure 4.10). From the intensity of XANES pre-edge, it is estimated by linear fitting with CrO_3 and Cr_2O_3 standards that ~41% of the Cr is present as Cr^{+6} in the dehydrated catalyst. Activation of the catalyst in either WGS or RWGS reaction conditions shifts the Cr edge to lower energy and also completely removes the Cr^{+6} XANES pre-edge feature reflecting the presence of only Cr^{+3} sites are formed (confirmed with Cr_2O_3 reference containing Cr^{+3} units). Subsequent exposure to either CO_2 or H_2O, however, does not oxidize the Cr^{+3} back to Cr^{+6} sites revealing that these two oxygenates are not sufficiently oxidizing under the employed WGS and RWGS experimental conditions. This demonstrates that the Cr cation is not able to undergo the redox process during the WGS and RWGS reactions since these are the only oxidizing agents during the WGS reaction. Only exposure to strongly oxidizing molecular O_2 is able to restore some of the surface Cr^{6+} species (see Figures 4.8c and 4.8d).

The Cu cation is initially present as Cu^{+2} and forms solid solution with Fe_2O_3 (confirmed with XANES of $CuFe_2O4$ reference in Figure 4.11). Activation of the catalyst in either WGS or RWGS reaction conditions shifts the edge position to lower energy consistent with metallic Cu^0 (confirmed with XANES of metallic Cu). Subsequent exposure to either CO_2 or H_2O completely oxidizes the Cu^0 back to Cu^{+2} (CuO). This reveals that Cu is able to undergo the $Cu^0 \leftrightarrow Cu^{+2}$ redox cycle.

4.3.6 TEM

The EDX mapping of fresh $CuO\text{-}Cr_2O_3\text{-}Fe_2O_3$ catalyst is shown in Figure 4.12. The EDX map shows that Cu and Cr are homogeneously distributed within the fresh catalyst. After activation of the catalyst under RWGS reaction conditions, a modulation of the elemental distribution can be observed in the EDX map presented in Figure 4.13. The Cr was still homogeneously distributed within the sample. The Cu, however, appears to segregate, which is consistent with the conclusion that Cu^{2+} becomes reduced and condenses to larger metallic Cu^0 clusters during the WGS/RWGS reactions.

4.3.7 CO-TPR

The redox properties of the activated Fe_2O_3, $Cr_2O_3\text{-}Fe_2O_3$ and $CuO\text{-}Cr_2O_3\text{-}Fe_2O_3$ catalysts were chemically probed with CO-TPR and the resulting spectra are shown in Figure 4.14. The reduction of the iron oxide catalyst occurs in two stages: a weak and broad peak from ~100-250°C (Tp=176°C) and a strong peak above ~275°C. The low

temperature evolution of CO_2 is assigned to removal of oxygen from the surface region of the catalyst and the high temperature CO_2 formation is associated with reaction of oxygen from the bulk lattice. The addition of the Cr promoter does not affect the low temperature CO_2 peak involving surface region oxygen, but retards the onset of the removal of oxygen from the bulk lattice of the catalyst. The introduction of Cu to the catalyst significantly shifts the low temperature peak to ~137ºC and also accelerates the start of the oxygen removal from the bulk lattice relative to the Cr_2O_3-Fe_2O_3 catalyst. The CO-TPR measurements indicate that the Cr promoter does not affect the surface redox reaction while the Cu promoter facilitates surface reduction.

4.3.8 Steady-State HT-WGS Reaction Rates

The steady-state Arrhenius plots and the activation energy values of the HT-WGS reaction on the iron oxide-based catalysts are presented in Figure 4.15. The Cu-Cr-Fe catalyst is the most active and the Cr-Fe and catalysts exhibit comparable surface area normalized activity ($mol/m^2 \cdot s$). The activation energy of the unpromoted Fe_2O_3 catalyst is ~85 kJ/mol and addition of the Cr promoter increases the activation energy to ~105 kJ/mol, while addition of the Cu promoter decreases the activation energy to ~67 kJ/mol. These values for the HT-WGS by iron oxide-based catalysts are consistent with the values reported by other researchers.[54-56]

4.4 Discussion

4.4.1 Catalyst Bulk Structure and Surface Compositions

Bulk. All the dehydrated iron oxide-based catalysts before WGS/RWGS contain the bulk α-Fe_2O_3 phase that transforms to the Fe_3O_4 phase during reaction conditions (see Figures 4.1 and 4.3). For the Cr-promoted catalysts, Cr^{+3} is incorporated into the iron oxide bulk lattices forming $Fe_{2-x}Cr_xO_3$ and $Fe_{3-x}Cr_xO_4$ mixed oxide solid solution phases for the fresh and activated catalysts, respectively (see Figures 4.1, 4.3 and 4.6b). The copper promoter is present as Cu^{+2} in the initial dehydrated catalyst and depth profiling suggests that it is homogeneously distributed in the Fe_2O_3 bulk lattice before WGS/RWGS reactions (see Figure 4.6a). During the WGS/RWGS reactions, the Cu^{+2} reduces to Cu^0 and forms metallic copper nanoparticles on the iron oxide support. These bulk structural changes are depicted in the schematic shown in Figure 4.16.

Surface. The initial dehydrated unpromoted Fe_2O_3 catalyst has a surface consisting of Fe^{+3} cations, O^{-2} anions and surface Fe-OH hydroxyls[57]. The activated Fe_3O_4 catalyst has the same surface functional groups and also reduced Fe^{+2} sites.[58] The initial dehydrated Cr-promoted Fe_2O_3 catalyst is surface enriched with CrO_4 (dioxo $(O=)_2Cr^{+6}O_2$) sites (see Figures 4.3a, 4.4b and 4.8c-d) since $Cr^{+6}O_4$ is only present on the surface and cannot be incorporated into the Fe_2O_3 bulk lattice. Activation of the Cr-promoted catalyst in the WGS/RWGS reaction environment reduces the surface $Cr^{+6}O_4$

sites to $Cr^{+3}O_6$ sites that dissolve into the Fe_3O_4 bulk lattice (see Figures 4.4b, 4.6 and 4.8c-d). The initial dehydrated Cu-promoted Fe_2O_3 catalyst is not surface enriched with Cu^{+2} (see Figure 4.6a), but the WGS/RWGS reaction reduces Cu^{+2} to Cu^0 that enriches the activated Fe_3O_4 surface with metallic Cu nanoparticles of ~3.6nm (see Figures 4.4c and 4.6b). The supported metallic Cu nanoparticles, however, appear to be decorated with ~1/3 monolayer of an oxide overlayer (most probably FeO_x since Cr^{+3} has a driving force to form a solid solution with the Fe_3O_4 lattice and the irreducible Cr^{+3} is less likely to undergo such a strong-metal-support-interaction (SMSI))[59]. These surface structural and chemical changes are depicted in the schematic of Figure 4.16.

4.4.2 HT-WGS by Iron Oxide

The *in situ* XANES studies directly demonstrate that the $Fe^{+3} \leftrightarrow Fe^{+2}$ redox cycle operates during the WGS/RWGS reactions (see Figure 4.8a-b). During WGS/RWGS, some of the Fe^{+3} sites reduce to Fe^{+2} and oxidize back to Fe^{+3} by exposure to CO_2 and H_2O and is accompanied by some minor formation Fe_2O_3. Furthermore, the ability of CO_2 and H_2O to only oxidize a fraction of the Fe^{+2} sites suggests that the Fe redox sites reside in a thin surface layer of the iron oxide catalyst with the deeper bulk Fe sites not undergoing redox. Consequently, the catalytic active sites for HT-WGS by iron oxide catalyst are redox surface FeO_x sites.

4.4.3 Chromium Promotion Mechanism

Although Cr is generally thought of as a structural stabilizer that retards sintering of iron oxide,[60, 61] the ability of Cr to shuttle between Cr^{+6} and Cr^{+3} valence states was considered as proof that Cr can facilitate the HT-WGS redox cycle.[27] The present *in situ* XANES redox study demonstrates that the initial Cr^{+6} is indeed reduced to Cr^{+3} during WGS/RWGS reaction conditions, but neither CO_2 or H_2O possess enough oxidizing potential to oxidize Cr^{3+} back to Cr^{6+}. Only molecular O_2, which is a much stronger oxidizing reagent, has the oxidizing potential to convert Cr^{+3} to Cr^{+6}. In addition, it is difficult to oxidize Cr^{+3} while it is present in solid solution of the $Fe_{3-x}Cr_xO_4$ bulk lattice where Cr^{+3} is quite stable. To the best of our knowledge, this is *the first direct evidence* that Cr does not function as a chemical promoter for iron oxide-based catalysts and the $Cr^{6+} \rightarrow Cr^{3+}$ redox couple is a "dead end" for the HT-WGS reaction mechanism.

The lack of influence of the Cr sites upon the surface $Fe^{+3} \leftrightarrow Fe^{+2}$ redox cycle is demonstrated by the same CO-TPR peak for reduction of surface FeO_x by both the activated Fe_3O_4 and $Fe_{3-x}Cr_xO_4$ catalysts (see Figure 4.14). The same CO-TPR T_p value for both activated Fe_3O_4 and $Fe_{3-x}Cr_xO_4$ catalysts further indicates that Cr is not able to perform the WGS reaction and demonstrates that the catalytic active sites are surface FeO_x sites.

4.4.4 Copper Promotion Mechanism

The *in situ* XANES redox study demonstrates that the initial Cu^{+2} is reduced to Cu^0 during WGS/RWGS reaction conditions and that both CO_2 and H_2O can oxidize metallic copper back to Cu^{+2} (see Figure 4.8e-f). Under steady-state WGS/RWGS reaction conditions, the copper promoter is present as metallic Cu nanoparticles that are partially covered by metal oxide (see Figure 4.6), which is thought to be FeO_x since there is a driving force for dissolution of Cr^{+3} into the iron oxide bulk lattice. The CO-TPR of the activated Cu-Cr-Fe catalyst demonstrates that the presence of the metallic copper nanoparticles facilitates the surface redox of iron oxide-based catalysts (see Figure 4.14). This directly demonstrates the chemical promotion of iron oxide-based catalysts by copper. These new insights also allow revisiting the proposed promotional roles of copper in iron oxide-based catalysts for WGS/RWGS reaction previously put forth.

The proposed model that copper acts as co-catalyst is correct since it can perform the HT-WGS reaction, but does not account for the details of the promotion mechanism.[30, 31] The *in situ* XANES redox study demonstrates that the initial Cu^{+2} is reduced to Cu^0 during WGS/RWGS reaction conditions and that CO_2 and H_2O can oxidize metallic copper back to Cu^{+2} (see Figure 4.8e-f). Besides copper is a well-known LT-WGS catalyst and its direct participation in WGS/RWGS via $Cu^0 \leftrightarrow Cu^{+1}$

or $Cu^0 \leftrightarrow Cu^{+2}$ redox cycles is well documented.[8, 62] The co-catalyst model, however, neglects the importance of synergistic interactions between copper and iron oxide as reported by other researchers showing that a mixture of copper and iron oxide is more active than each individually.[63, 64] It also does not consider the possibility of a surface FeO_x overlayer on the metallic Cu^0 nanoparticles found in the present study.

The proposal that copper is present as Cu^{+n} cations as a solid solution in the iron oxide bulk lattice that affects the electronic and structural properties is without merit.[24] This conclusion is based on HR-TEM and STEM studies on activated catalysts while exposing them to the air, which causes re-oxidation of the catalyst surface.[65] By the multiple *in situ* characterization measurements reported in the present study it is shown that copper is present as metallic Cu^0 nanoparticles on the $Fe_{3-x}Cr_xO_4$ support during WGS/RWGS reaction and there is no evidence for the presence of Cu^{+n} cations.

The final proposed promotion mechanism is that metallic copper facilitates the cycle of water dissociation and hydrogen production, but supporting evidence was not provided.[37] This model has some validity since based on DFT calculations, H_2 formation on the copper surface is kinetically more favorable compared than on the Fe_3O_4 surface.[58, 66] The water dissociation ($H_2O^* \leftrightarrow HO^* + H^*$), however, is not the rate-determining-step for HT-WGS according to the reported kinetics in the

literature and it is not clear that facilitating water dissociation will accelerate the WGS/RWGS reaction.[4]

According to recent DFT calculations, the dissociation of water on the Cu surface is kinetically unfavorable and is the rate-determining-step of the WGS reaction on Cu-based catalysts.[66] The relatively less active Fe_3O_4 catalyst, however, can easily dissociate adsorbed water species with its oxygen vacancies.[58] This allows for proposal of a new copper promotion mechanism that emphasizes the synergistic interaction between metallic copper and iron oxide during the HT-WGS reaction. In this new mechanism, carbon monoxide would adsorb on metallic Cu and water would adsorbed and dissociate on oxygen vacancies of Fe_3O_4 with the subsequent reactions taking place at the metal-oxide interfaces.[58, 67] The proposed FeO_x overlayer on the metallic Cu nanoparticles during HT-WGS would further provide a large number of such metal-oxide interfacial sites.

4.5 Conclusions

The fresh Cr_2O_3-Fe_2O_3 and CuO-Cr_2O_3-Fe_2O_3 catalysts contain the α-Fe_2O_3 (hematite) bulk phase and surface Cr^{6+} species with Cu^{2+} and some Cr^{3+} migrated into the iron oxide bulk lattice. During reaction the α-Fe_2O_3 phase becomes partially reduced to Fe_3O_4 (magnetite) and surface Cr^{6+} reduces to Cr^{3+} that dissolves into the bulk lattice to form the $Fe_{3-x}Cr_xO_4$ solid solution. The initially dispersed Cu^{2+} is reduced

to Cu^0 and migrates onto the external catalyst surface and to become metallic Cu^0 nanoparticles with average thickness of ~3nm. About 30% of the Cu surface is also covered by a FeO_x overlayer due to strong metal support interaction (SMSI). The Cr promoter does not function as a chemical promoter and only acts as structural stabilizer (textural promoter) that retards sintering of the working catalyst as well as over-reduction of the bulk iron oxide phase during the HT-WGS reaction. The Cu promoter, however, functions as a chemical promoter by providing highly active new catalytic active metallic Cu^0 sites and Cu - iron oxide interfacial sites.

Acknowledgment

The authors acknowledge financial support from National Science Foundation Grant CBET- 1511689. The authors thank Prof. Anatoly Frenkel from Yeshiva University for offering the beamline accessibility in BNL. Dr. Henry Luftman of Lehigh University is thanked for assisting with the collection of the HS-LEIS data. The authors thank the Alexander von Humboldt Foundation (Germany), for the Humboldt Research Award. The Helmholtz-Zentrum Berlin is gratefully acknowledged for the provision of synchrotron radiation to the ISISS beamline.

References

[1] D.S. Newsome, Catal. Rev.: Sci. Eng. 21 (1980) 275-318.

[2] C. Ratnasamy, J.P. Wagner, Catal. Rev.: Sci. Eng. 51 (2009) 325-440.

[3] R.J.B. Smith, M. Loganathan, M.S. Shantha, Int. J. Chem. React. Eng. 8 (2010) 1-32.

[4] M. Zhu, I.E. Wachs, ACS Catal. 6 (2016) 722-732.

[5] E.F. Armstrong, T.P. Hilditch, Proc. R. Soc. London, Ser. A 97 (1920) 265-273.

[6] A. Boudjemaa, C. Daniel, C. Mirodatos, M. Trari, A. Auroux, R. Bouarab, C. R. Chim. 14 (2011) 534-538.

[7] C. Diagne, P.J. Vos, A. Kiennemann, M.J. Perrez, M.F. Portela, React. Kinet. Catal. Lett. 42 (1990) 25-31.

[8] C. Rhodes, G.J. Hutchings, A.M. Ward, Catal. Today 23 (1995) 43-58.

[9] J.R. Ladebeck, J.P. Wagner, Catalyst development for water–gas shift, Handbook of Fuel Cells, John Wiley & Sons, Ltd, Chichester, 2003, pp. 190-201.

[10] J.E. Kubsh, J.A. Dumesic, AlChE J. 28 (1982) 793-800.

[11] G.K. Boreskov, T.M. Yurieva, A.S. Sergeeva, Kinet. Catal. 11 (1970) 374-381.

[12] A. Khan, P. Chen, P. Boolchand, P.G. Smirniotis, J. Catal. 253 (2008) 91-104.

[13] G.C. Chinchen, R.H. Logan, M.S. Spencer, Appl. Catal. 12 (1984) 89-96.

[14] G.C. Chinchen, R.H. Logan, M.S. Spencer, Appl. Catal. 12 (1984) 69-88.

[15] G.C. Chinchen, R.H. Logan, M.S. Spencer, Appl. Catal. 12 (1984) 97-103.

[16] R.L. Keiski, T. Salmi, P. Niemistö, J. Ainassaari, V.J. Pohjola, Appl. Catal., A 137 (1996) 349-370.

[17] T. Salmi, L.E. Lindfors, S. Bostrom, Chem. Eng. Sci. 41 (1986) 929-936.

[18] S. Oki, R. Mezaki, Ind. Eng. Chem. Res. 27 (1988) 15-21.

[19] R. Mezaki, S. Oki, J. Catal. 30 (1973) 488-489.

[20] M. Tinkle, J.A. Dumesic, J. Catal. 103 (1987) 65-78.

[21] M. Tinkle, J.A. Dumesic, J. Phys. Chem. 88 (1984) 4127-4130.

[22] M.L. Kundu, A.C. Sengupta, G.C. Maiti, B. Sen, S.K. Ghosh, V.I. Kuznetsov, G.N. Kustova, E.N. Yurchenko, J. Catal. 112 (1988) 375-383.

[23] A. Patlolla, E.V. Carino, S.N. Ehrlich, E. Stavitski, A.I. Frenkel, ACS Catal. 2 (2012) 2216-2223.

[24] M.A. Edwards, D.M. Whittle, C. Rhodes, A.M. Ward, D. Rohan, M.D. Shannon, G.J. Hutchings, C.J. Kiely, PCCP 4 (2002) 3902-3908.

[25] M. Robbins, G.K. Wertheim, R.C. Sherwood, D.N. Buchanan, J. Phys. Chem. Solids 32 (1971) 717-729.

[26] G.K. Reddy, K. Gunasekara, P. Boolchand, P.G. Smirniotis, J. Phys. Chem. C 115 (2011) 920-930.

[27] S. Natesakhawat, X.Q. Wang, L.Z. Zhang, U.S. Ozkan, J. Mol. Catal. A: Chem. 260 (2006) 82-94.

[28] D.W. Lee, M.S. Lee, J.Y. Lee, S. Kim, H.J. Eom, D.J. Moon, K.Y. Lee, Catal. Today 210 (2013) 2-9.

[29] D.C. Kim, S.K. Ihm, Environ. Sci. Technol. 35 (2001) 222-226.

[30] A. Andreev, V. Idakiev, D. Mihajlova, D. Shopov, Appl. Catal. 22 (1986) 385-387.

[31] V. Idakiev, D. Mihajlova, B. Kunev, A. Andreev, React. Kinet. Catal. Lett. 33 (1987) 119-124.

[32] G.K. Reddy, K. Gunasekera, P. Boolchand, J.H. Dong, P.G. Smirniotis, J. Phys. Chem. C 115 (2011) 7586-7595.

[33] G.K. Reddy, P. Boolchand, P.G. Smirniotis, J. Phys. Chem. C 116 (2012) 11019-11031.

[34] F. Meshkani, M. Rezaei, Korean J. Chem. Eng. 32 (2015) 1278-1288.

[35] F. Meshkani, M. Rezaei, Chem. Eng. J. 260 (2015) 107-116.

[36] S.M. Latifi, A. Salehirad, Korean J. Chem. Eng. 33 (2016) 473-480.

[37] A. Puig-Molina, F.M. Cano, T.V.W. Janssens, J. Phys. Chem. C 114 (2010) 15410-15416.

[38] M. Zhu, I.E. Wachs, ACS Catal. 6 (2016) 1764-1767.

[39] H. Bluhm, M. Havecker, A. Knop-Gericke, E. Kleimenov, R. Schlogl, D. Teschner, V.I. Bukhtiyarov, D.F. Ogletree, M. Salmeron, J. Phys. Chem. B 108 (2004) 14340-14347.

[40] A. Knop‐Gericke, E. Kleimenov, M. Hävecker, R. Blume, D. Teschner, S. Zafeiratos, R. Schlögl, V.I. Bukhtiyarov, V.V. Kaichev, I.P. Prosvirin, A.I. Nizovskii, H. Bluhm, A. Barinov, P. Dudin, M. Kiskinova, Chapter 4 X‐Ray Photoelectron Spectroscopy for Investigation of Heterogeneous Catalytic Processes, Adv. Catal., Academic Press2009, pp. 213-272.

[41] S.P. Phivilay, A.A. Puretzky, K. Domen, I.E. Wachs, ACS Catal. 3 (2013) 2920-2929.

[42] I.S. Lyubutin, C.R. Lin, Y.V. Korzhetskiy, T.V. Dmitrieva, R.K. Chiang, J. Appl. Phys. 106 (2009) 034311.

[43] J.M. Jehng, I.E. Wachs, F.T. Clark, M.C. Springman, J. Mol. Catal. 81 (1993) 63-75.

[44] K.F. Mccarty, D.R. Boehme, J. Solid State Chem. 79 (1989) 19-27.

[45] E.L. Lee, I.E. Wachs, J. Phys. Chem. C 111 (2007) 14410-14425.

[46] M. Kilo, C. Schild, A. Wokaun, A. Baiker, J. Chem. Soc., Faraday Trans. 88 (1992) 1453-1457.

[47] S. Tanuma, C.J. Powell, D.R. Penn, Surf. Interface Anal. 21 (1994) 165-176.

[48] M.C. Biesinger, B.P. Payne, A.P. Grosvenor, L.W.M. Lau, A.R. Gerson, R.S. Smart, Appl. Surf. Sci. 257 (2011) 2717-2730.

[49] S. Poulston, P.M. Parlett, P. Stone, M. Bowker, Surf. Interface Anal. 24 (1996) 811-820.

[50] W.P.A. Jansen, J. Beckers, J.C. v. d. Heuvel, A.W. Denier v. d. Gon, A. Bliek, H.H. Brongersma, J. Catal. 210 (2002) 229-236.

[51] M.M. Viitanen, W.P.A. Jansen, R.G. van Welzenis, H.H. Brongersma, D.S. Brands, E.K. Poels, A. Bliek, J. Phys. Chem. B 103 (1999) 6025-6029.

[52] J.C. Sharp, Y.X. Yao, C.T. Campbell, J. Phys. Chem. C 117 (2013) 24932-24936.

[53] M.E. Straumanis, L.S. Yu, Acta Crystallogr., Sect. A: Cryst. Phys., Diffr., Theor. Gen. Crystallogr. A 25 (1969) 676-682.

[54] H. Bohlbro, Chem. Eng. World 46 (1970) 5-8.

[55] C. Rhodes, G.J. Hutchings, PCCP 5 (2003) 2719-2723.

[56] S.S. Hla, D. Park, G.J. Duffy, J.H. Edwards, D.G. Roberts, A. Ilyushechkin, L.D. Morpeth, T. Nguyen, Chem. Eng. J. 146 (2009) 148-154.

[57] G. Busca, V. Lorenzelli, React. Kinet. Catal. Lett. 15 (1980) 273-278.

[58] L. Huang, B. Han, Q. Zhang, M. Fan, H. Cheng, J. Phys. Chem. C 119 (2015) 28934-28945.

[59] S.J. Tauster, Acc. Chem. Res. 20 (1987) 389-394.

[60] J. Koy, J. Ladebeck, J.R. Hill, Stud. Surf. Sci. Catal. 119 (1998) 479-484.

[61] F. Domka, M. Laniecki, Z. Anorg. Allg. Chem. 435 (1977) 273-283.

[62] J.A. Rodriguez, J.C. Hanson, D. Stacchiola, S.D. Senanayake, PCCP 15 (2013) 12004-12025.

[63] C.S. Chen, W.H. Cheng, S.S. Lin, Chem. Commun. 37 (2001) 1770-1771.

[64] C.S. Chen, W.H. Cheng, S.S. Lin, Appl. Catal., A 257 (2004) 97-106.

[65] P. Kappen, J.D. Grunwaldt, B.S. Hammershoi, L. Troger, B.S. Clausen, J. Catal. 198 (2001) 56-65.

[66] P. Liu, J.A. Rodriguez, J. Chem. Phys. 126 (2007) 164705

[67] L. Huang, B. Han, Q.F. Zhang, M.H. Fan, H.S. Cheng, J. Phys. Chem. C 119 (2015) 28934-28945.

FIGURES

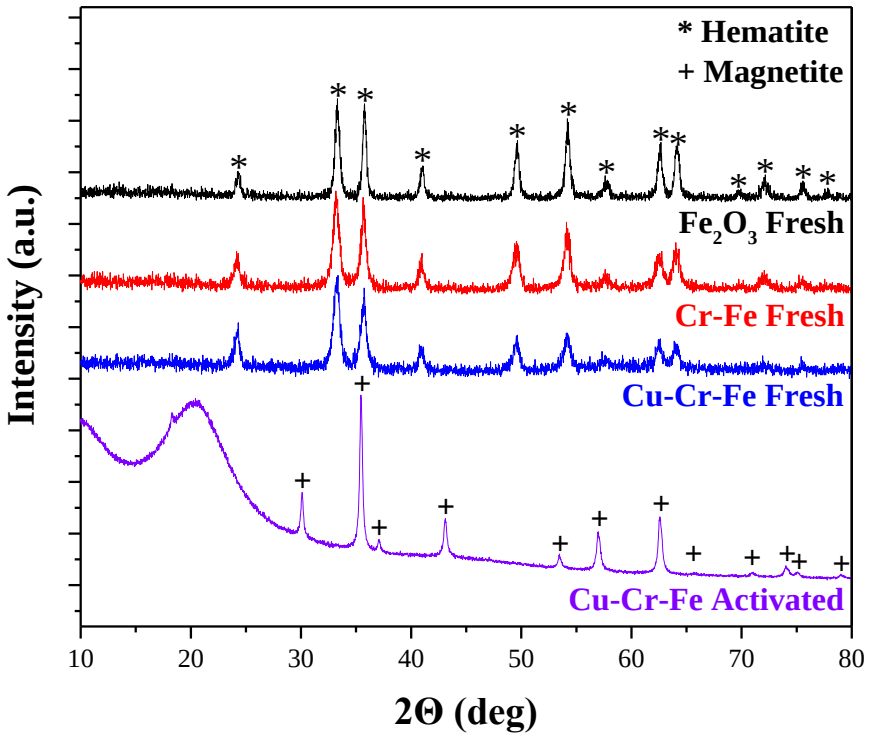

Figure 4.1 XRD diffractograms of fresh Fe_2O_3, Cr_2O_3-Fe_2O_3, CuO-Cr_2O_3-Fe_2O_3 catalysts and activated CuO-Cr_2O_3-Fe_2O_3 catalysts.

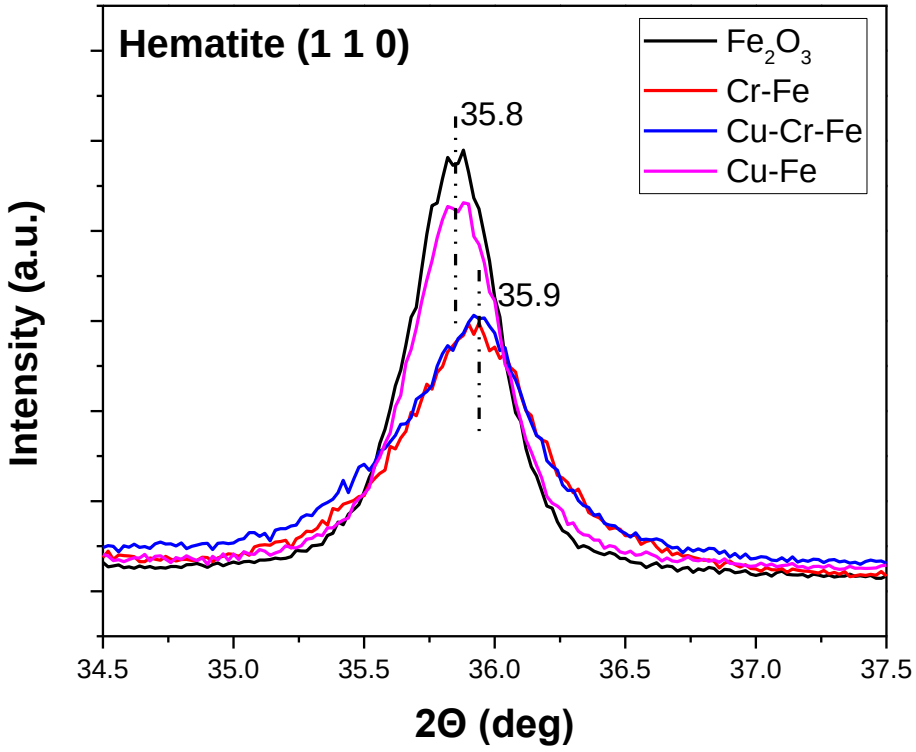

Figure 4.2 XRD main peak spectra of hematite (1 1 0) of the Fe_2O_3, Cu-Fe, Cr-Fe and Cu-Cr-Fe catalyst.

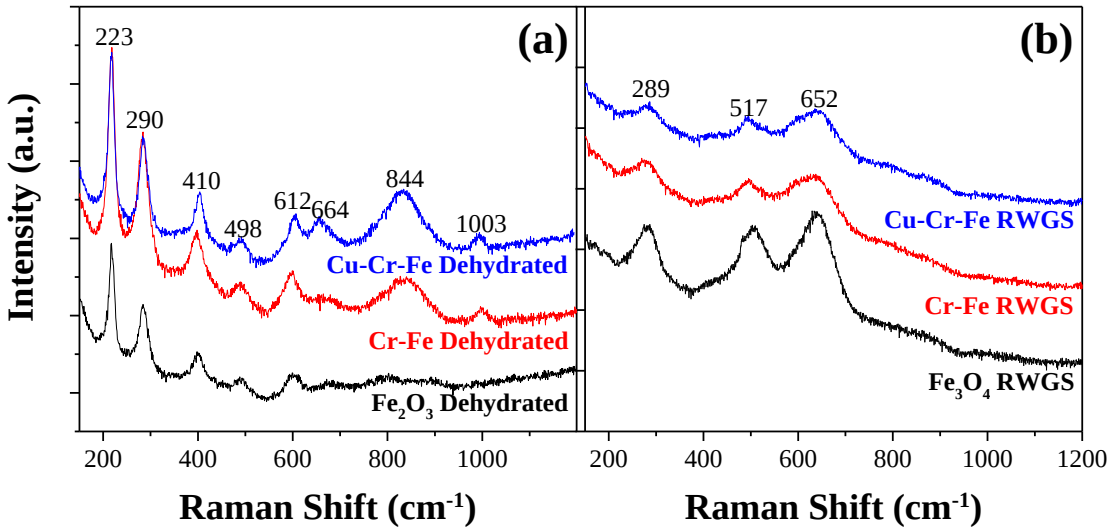

Figure 4.3 The *in situ* Raman spectra of Fe_2O_3, Cr_2O_3-Fe_2O_3 and CuO-Cr_2O_3-Fe_2O_3 under (a) dehydrated conditions (30 ml/min 10% O_2/Ar) and (b) RWGS reaction conditions (10 ml/min CO_2, 10 ml/min H_2 and 10 ml/min Ar).

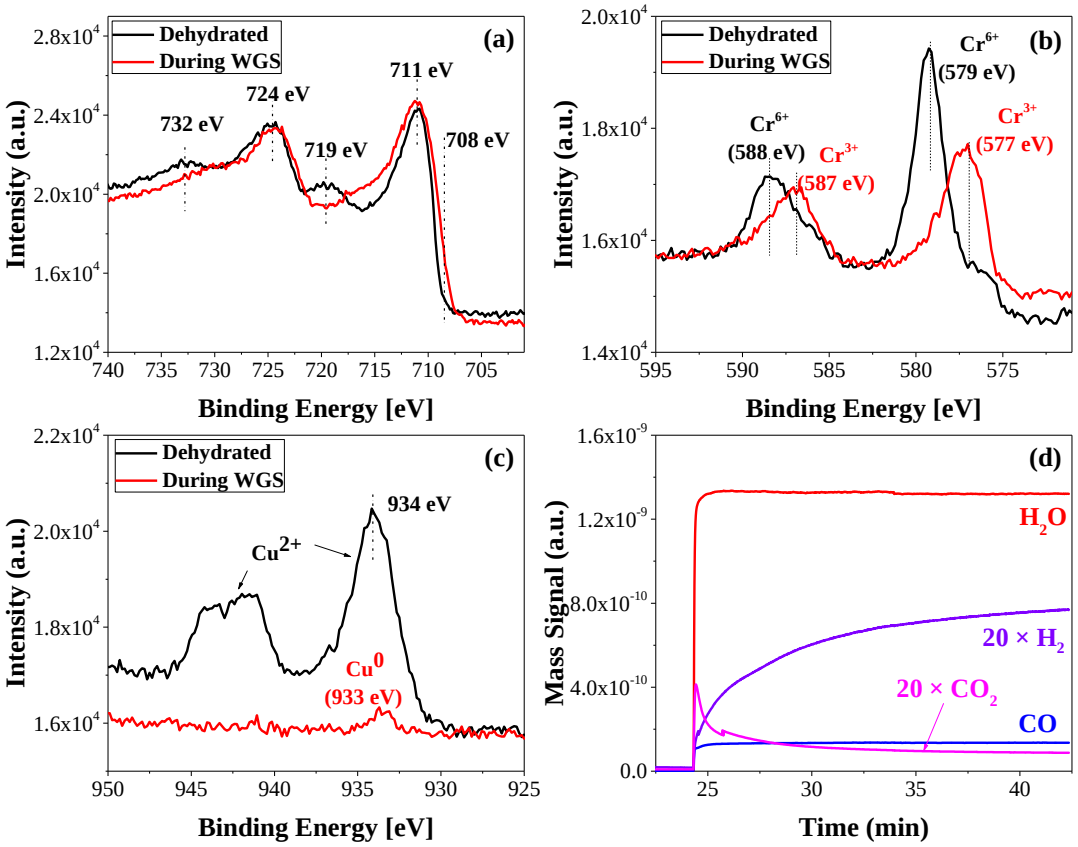

Figure 4.4 The *operando* NAP-XPS-MS spectra of (a) Fe 2p, (b) Cr 2p, (c) Cu 2p regions from the CuO-Cr_2O_3-Fe_2O_3 catalyst under dehydrated conditions at 400°C and during the HT-WGS reaction (P = 0.3 mbar, T = 400°C, and H_2O:CO ratio = 10), and (d) the corresponding mass spectrometer signals as a function of time.

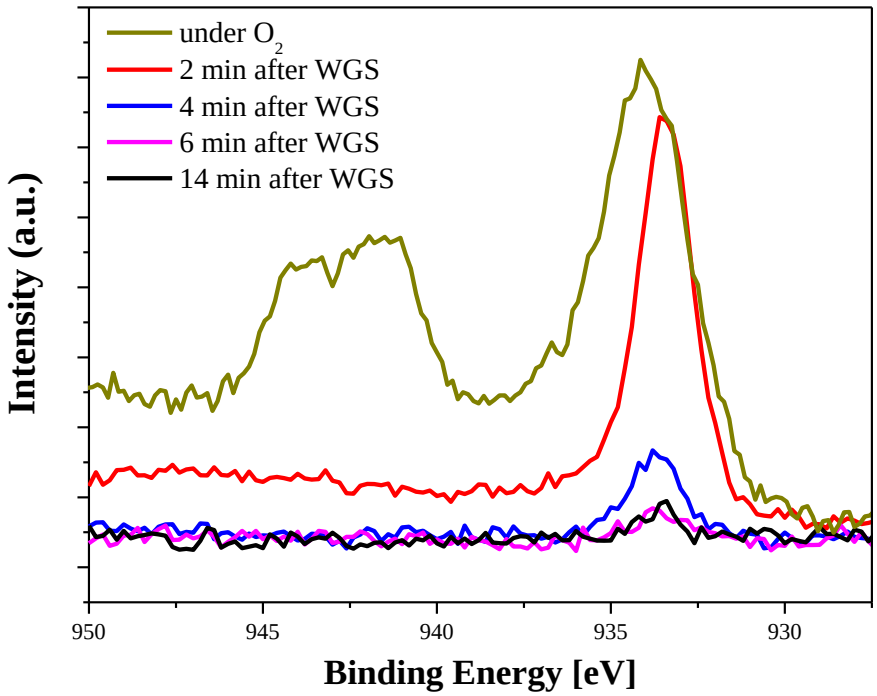

Figure 4.5 Time resolved NAP-XPS Cu 2p region of CuO-Cr_2O_3-Fe_2O_3 upon switching from dehydrated oxidizing conditions to WGS reaction conditions (P = 0.3 mbar, T = 400°C, and H_2O:CO ratio = 10).

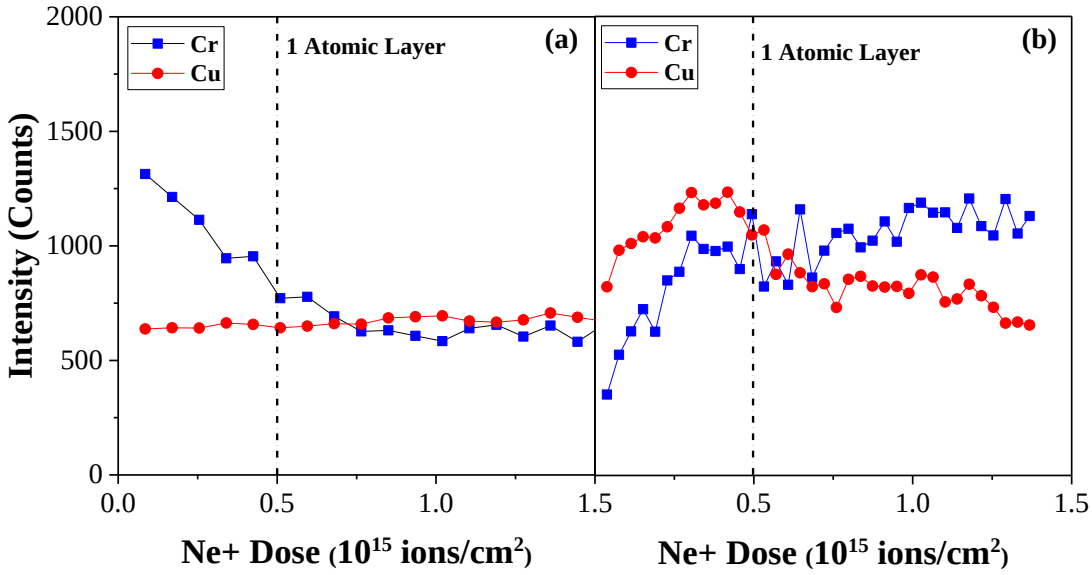

Figure 4.6 The Cr and Cu atomic density of (a) fresh and (b) activated CuO-Cr_2O_3-Fe_2O_3 catalyst as a function of a 5 keV Ne^+ dose.

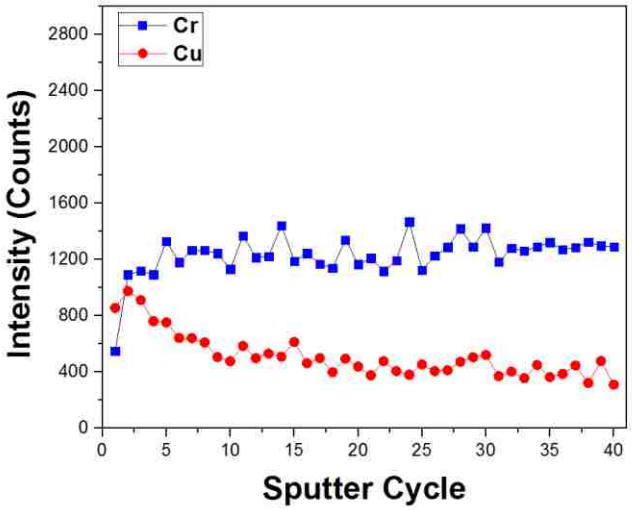

Figure 4.7 Depth profile for Cr and Cu atomic density of activated CuO-Cr_2O_3-Fe_2O_3 catalyst as a function of sputter cycle. (Each sputter cycle corresponds sputtering of ~1 atomic layer)

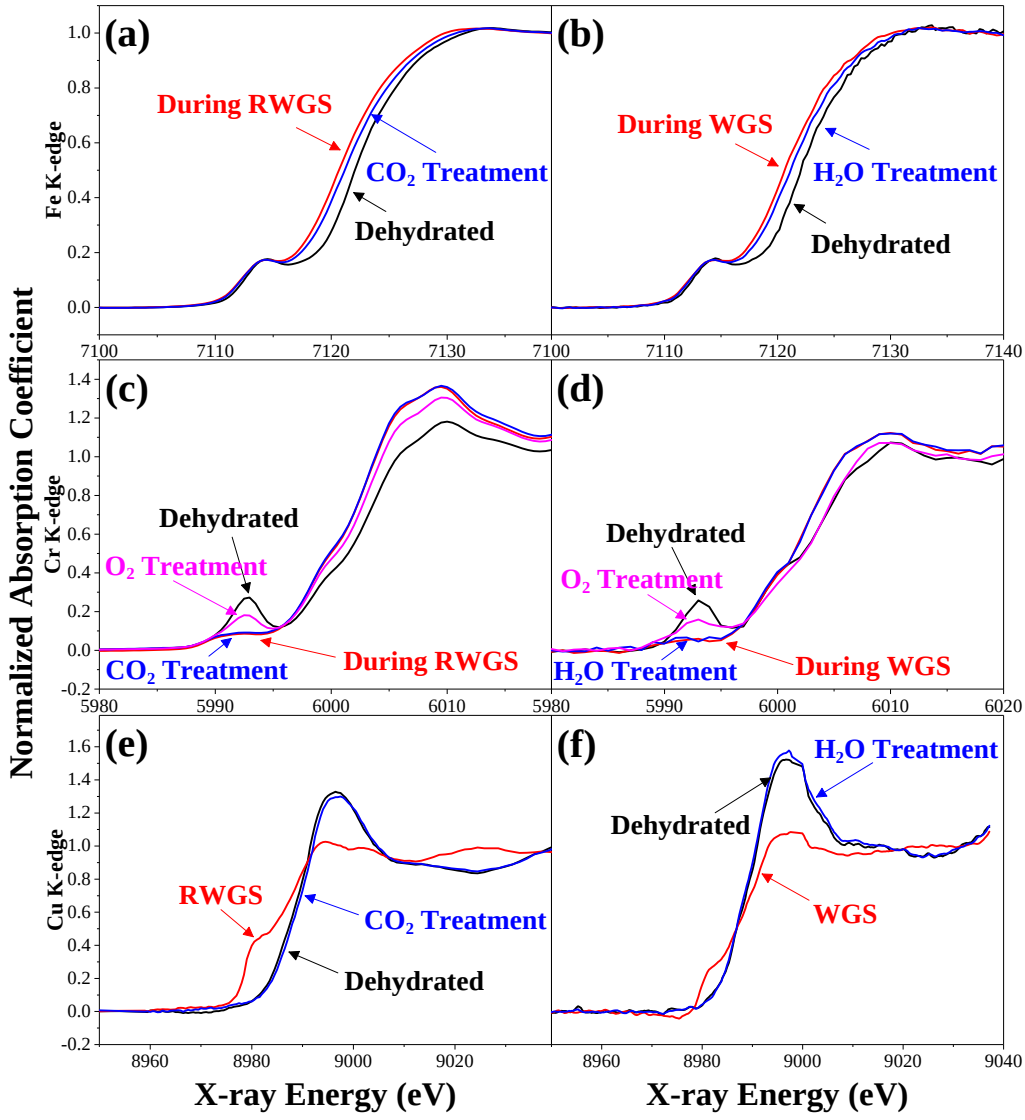

Figure 4.8 *In situ* XANES spectra of CuO-Cr_2O_3-Fe_2O_3 catalyst under different gas environments at 350°C. (a-b) XANES Fe K-edge spectrum; (c-d) XANES Cr K-edge spectrum and (e-f) XANES Cu K-edge spectrum.

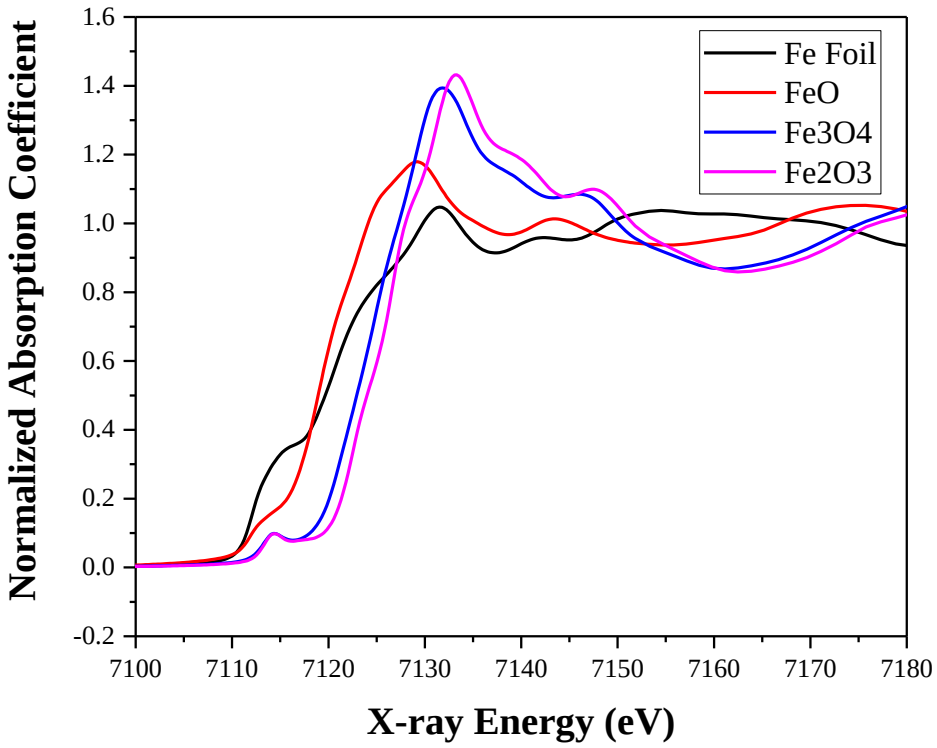

Figure 4.9 XANES spectra of iron reference compounds at room temperature.

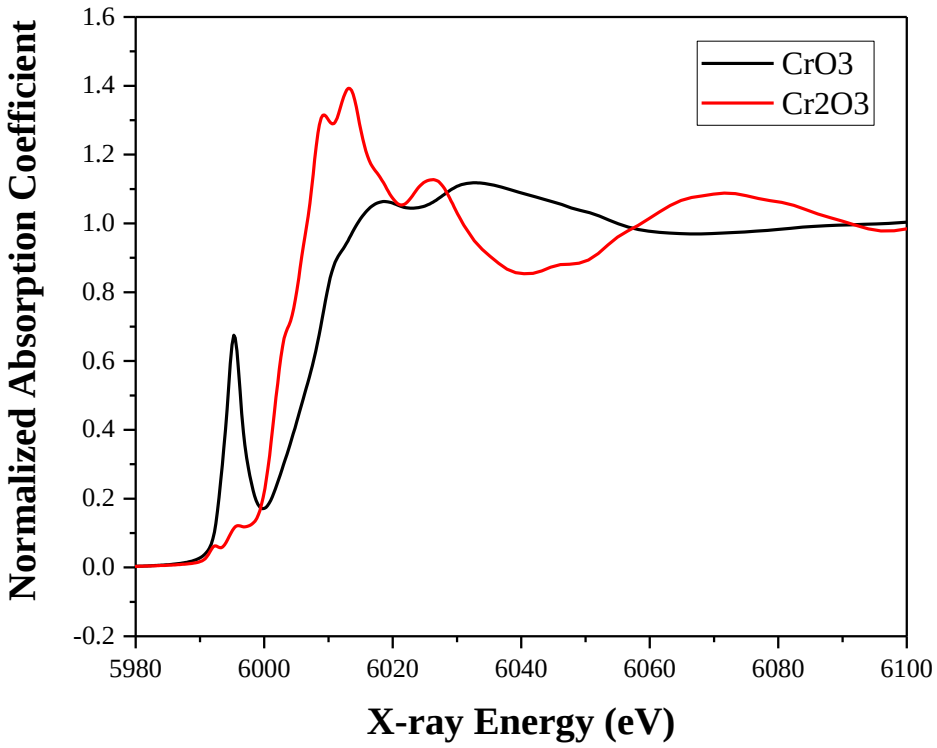

Figure 4.10 XANES spectra of chromium oxide reference compounds at room temperature.

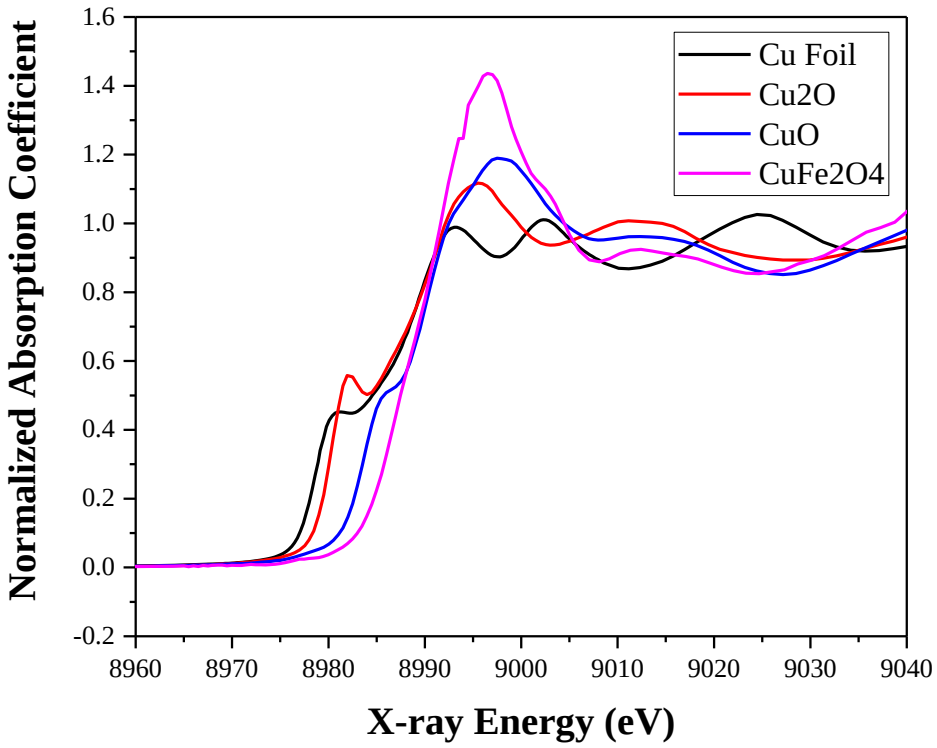

Figure 4.11 XANES spectra of copper reference compounds at room temperature.

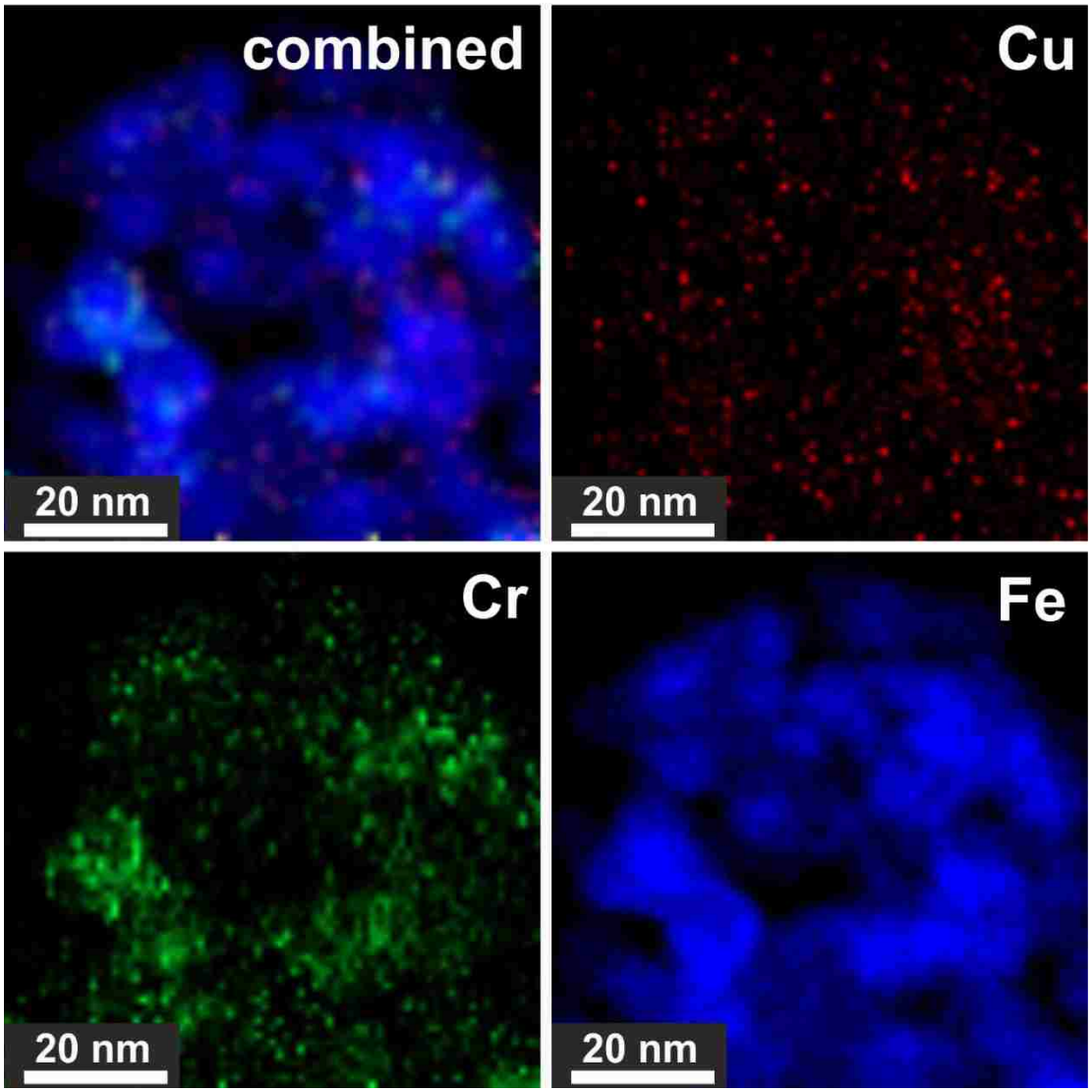

Figure 4.12 EDX map of fresh CuO-Cr_2O_3-Fe_2O_3 catalyst

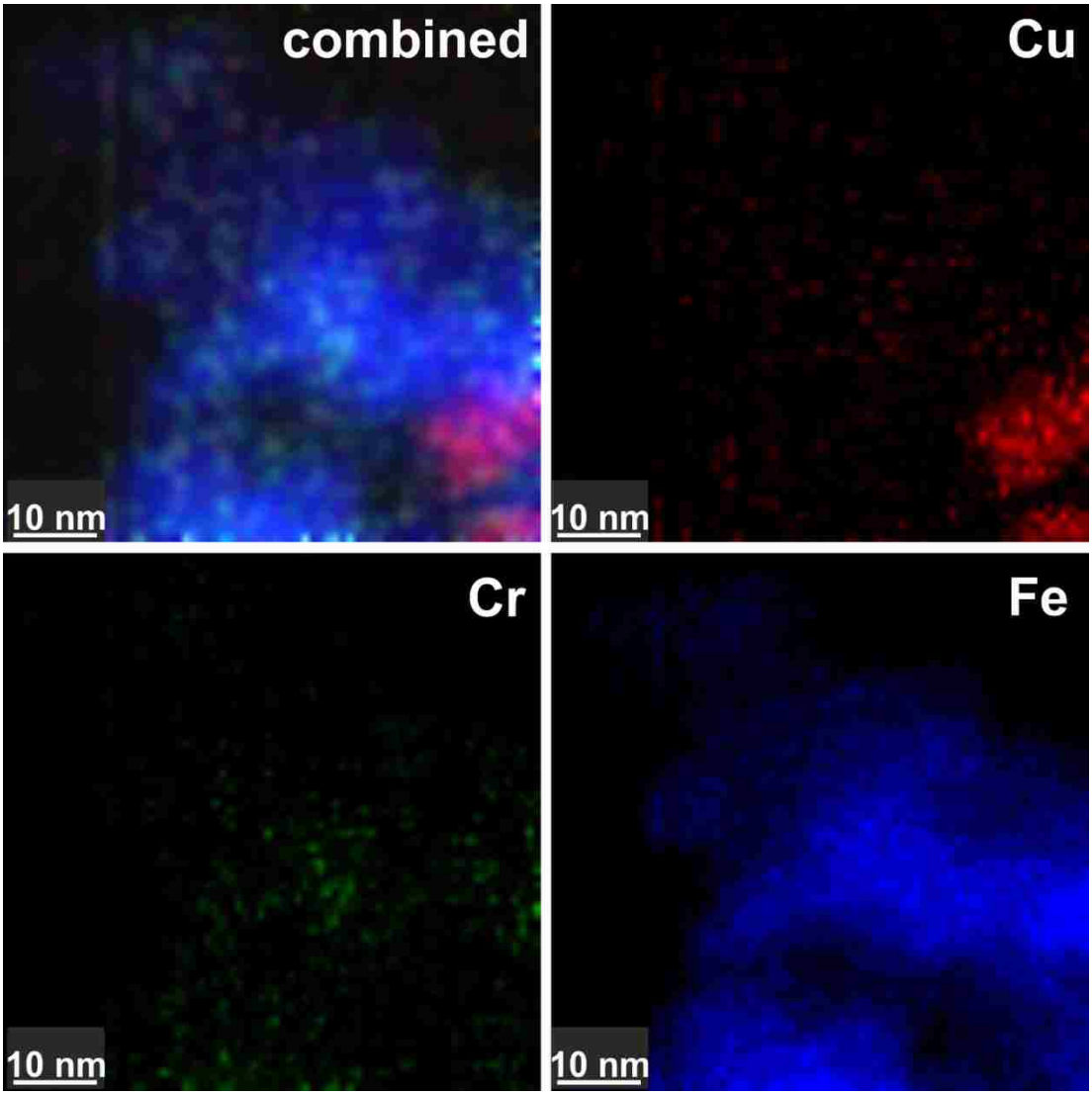

Figure 4.13 EDX map of activated CuO-Cr_2O_3-Fe_2O_3 catalyst

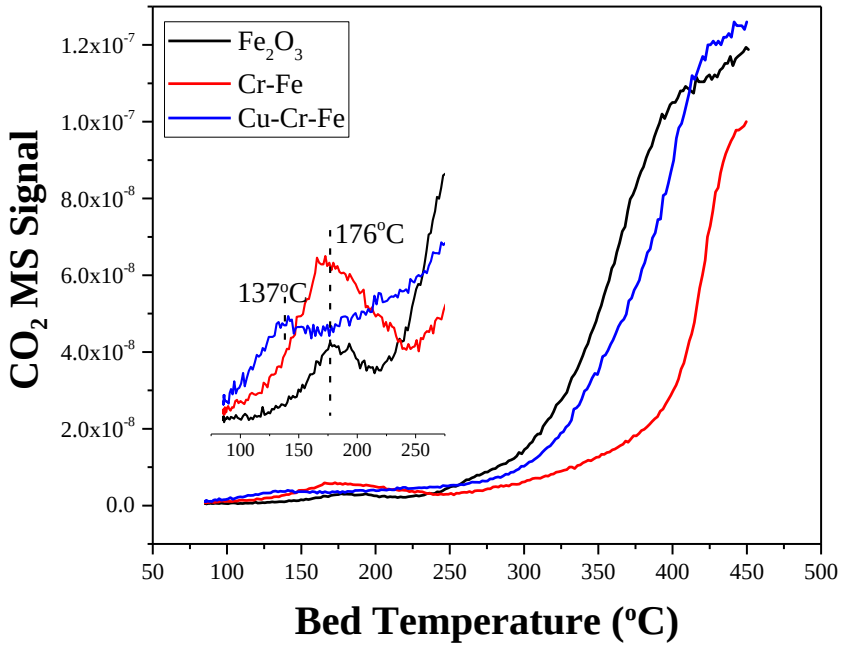

Figure 4.14 The CO-TPR spectra of activated Fe_2O_3, Cr-Fe and Cu-Cr-Fe catalysts activated by WGS reaction conditions at 350°C.

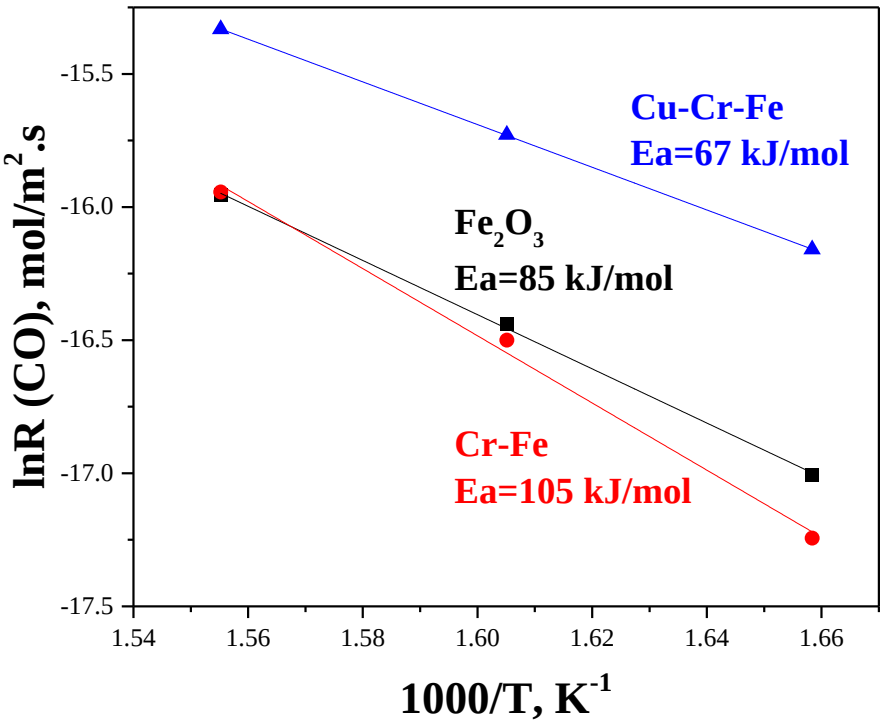

Figure 4.15 Arrhenius plot for steady-state WGS kinetics over Fe_2O_3, Cr-Fe and Cu-Cr-Fe catalysts.

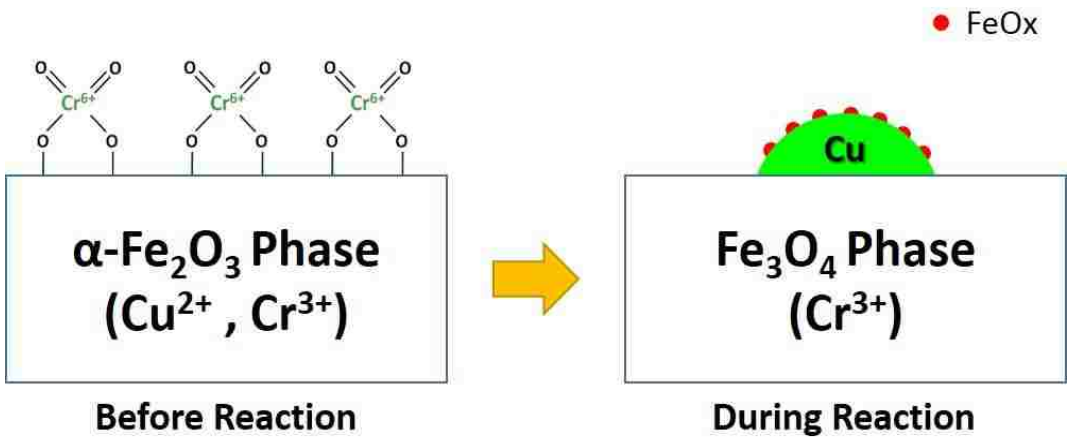

Figure 4.16 Schematics of the copper-chromium-iron oxide catalyst before and during the HT-WGS reaction.

CHAPTER 5

Rational Design of Chromium-Free Iron Oxide-Based Catalysts for the High Temperature Water-Gas Shift Reaction

ABSTRACT

Finding a replacement for the toxic hexavalent chromium oxide present in commercial iron oxide-based high temperature water-gas shift (HT-WGS) catalyst is of current environmental concern. In the present investigation, the possible replacement of chromium with Mg^{+2}, Al^{+3} and Si^{+4} in HT-WGS catalyst was examined. The catalysts were synthesized by co-precipitation of the oxide precursors and followed by impregnation of Cu to form supported $CuO/(MO_x\text{-}Fe_2O_3)$ catalysts (M = Si, Al, Cr and Mg). The catalysts were characterized with *in situ* BET due to the pyrophoric nature of the activated catalysts, *in situ* Raman during HT-WGS, transient $C^{16}O_2 \rightarrow C^{18}O_2$ isotopic studies to determine the number of catalytic active sites (Ns) and TOF values, and steady-state reaction rates. The Si^{+4} promoter exhibited the highest thermostability during HT-WGS, but the lowest activity. The Mg^{+2} promoter resulted in the least thermally stable catalyst during HT-WGS and only modest activity. Only the Al^{+3}

promoter was found to yield a catalyst that possessed comparable thermostability and activity during HT-WGS as the Cr-promoted catalyst. This suggests that Al^{+3} would be an appropriate replacement for Cr in the current supported Cu/iron oxide catalyst system for the HT-WGS reaction.

5.1 Introduction

Industrial H_2 is currently primarily produced by methane steaming reforming (MSR) followed by the water-gas shift (WGS) reaction to increase or control the H_2/CO ratio. The WGS reaction involves reaction of carbon monoxide with steam to produce H_2 and CO_2 and is commercially performed in several temperature stages with different catalysts to optimize the greater CO equilibrium conversion attained at lower temperatures since the reaction is exothermic and reversible [1, 2]. The high temperature water-gas shift (HT-WGS) reaction is commercially performed at ~350-450°C with iron oxide-based catalysts and the low temperature water-gas shift (LT-WGS) reaction is performed at ~190-250°C with supported copper-based catalysts.

$$CO + H_2O \leftrightarrow CO_2 + H_2 \qquad \Delta H = -40.6 kJ/mol \qquad (1)$$

During the HT-WGS reaction, the equilibrated bulk iron oxide phase is present as magnetite (Fe_3O_4), which is produced by the partial reduction of the starting hematite (Fe_2O_3) phase. [3, 4] Chromium oxide is added as a textural promoter to stabilize the surface area and prevent over-reduction of the magnetite phase to metallic iron. Copper

is also added as a promoter in commercial iron-chromium oxide catalysts and increases the catalytic activity that allows operation over a wider temperature range. [5-11] The Cu promoter functions as a chemical promoter by providing new highly active catalytic active metallic Cu^0 sites and Cu-iron oxide interfacial sites.[12]

A concern about the current HT-WGS iron-chromium oxide-based catalyst is the presence of hexavalent chromium (Cr^{+6}), a potent carcinogen that threatens human life and the environment [13]. This concern has motivated intensive research over the past decades to develop Cr-free HT-WGS catalysts that possess comparable performance to the current Cu promoted iron-chromium oxide catalyst. Rethwisch and Dumesic [15] examined the HT-WGS activity of Zn and Mg promoted Cu-free magnetite (Fe_3O_4), but these catalysts exhibited lower activity than iron-chromium oxide catalysts. Chinchen [14] was the first to investigate Cu promoted iron oxide catalysts containing Ca, Ce and Zr oxides that form bulk spinel mixed oxide compounds. Lee *at al*. performed extensive research investigating Ni as a possible replacement for Cr [16-18]. The incorporation of Ni to a Cu promoted iron oxide catalyst increased CO conversion by increasing the surface area of the catalysts. Aluminum also received much attention as a Cr replacement for Cu promoted iron oxide catalysts for better WGS activity. A variety of additional promoters have also been screened (Ba, Ca, Mg, Sr, Ce, La, Zn, Y, and Mn) to further promote Cu-Al-Fe-O

catalyst while most of the reported findings were trial-and-error studies and only discussed the conversion and BET surface areas on fresh samples. [19-25]

In the present study, both Cu-free and Cu promoted iron oxide catalysts were investigated for the HT-WGS reaction. The oxides of MgO (Mg^{+2}), Al_2O_3 (Al^{+3}) and SiO_2 (Si^{+4}) were selected to replace Cr to examine the influence of cation oxidation state. The Cu-free bulk SiO_2-Fe_2O_3, MgO-Fe_2O_3, Al_2O_3-Fe_2O_3 and Cr_2O_3-Fe_2O_3 mixed oxide catalysts were synthesized by co-precipitation. The Cu-promoted SiO_2-Fe_2O_3, MgO-Fe_2O_3, Al_2O_3-Fe_2O_3 and Cr_2O_3-Fe_2O_3 catalysts were synthesized by subsequent impregnation of Cu onto the mixed oxide catalysts. The performance of the series of catalysts for HT-WGS was evaluated based on several criteria: catalytic activity, thermos-stability after ultra-high temperature WGS operation, number of active sites (Ns) and turnover frequency (TOF). The current findings suggest that replacing the toxic Cr with Al results in a comparable performing HT-WGS iron oxide-based supported Cu catalyst.

5.2 Experimental

5.2.1 Catalyst Synthesis and Preparation

The SiO_2-Fe_2O_3, MgO-Fe_2O_3, Al_2O_3-Fe_2O_3 and Cr_2O_3-Fe_2O_3 mixed oxide catalysts used in this study were synthesized using the ammonia assisted co-precipitation method. The employed precursors were iron nitrate (Sigma Aldrich,

99.999% trace metals basis), tetraethyl orthosilicate (Sigma Aldrich, 99.999% trace metals basis), magnesium nitrate (Sigma Aldrich, 99.999% trace metals basis), aluminum nitrate (Sigma Aldrich, 99.997% trace metals basis) and chromium nitrate (Sigma Aldrich, 99.99% trace metals basis). Calculated amounts of metal nitrates were mixed and dissolved in deionized water. Dilute aqueous ammonia was added to the solution dropwise until the pH reached 8.5. The dark brown precipitate formed was further aged overnight and filtered off. The filtered precipitate was then oven-dried at 80°C for 12 h and subsequently calcined at 400°C for 3 h in static air.

The Cu-promoted SiO_2-Fe_2O_3, MgO-Fe_2O_3, Al_2O_3-Fe_2O_3 and Cr_2O_3-Fe_2O_3 catalysts were synthesized by incipient-wetness impregnation of an aqueous solution of copper(II) nitrate (Sigma Aldrich, 99.99% trace metals basis). The catalysts were prepared with a loading of 3 wt.% CuO, allowed to dry overnight under ambient conditions, followed by an oven-drying step at 80°C for 12h and subsequent calcination at 400°C for 3h in static air.

5.2.2 BET Specific Surface Area Measurement

The BET surface areas of both fresh and used catalysts were measured by a 3-point flow BET method with an Altamira Instruments system (AMI-200) equipped with a TCD detector. The N_2 adsorption/desorption amount were measured at three different partial pressures (P/P_0=0.14, 0.22 and 0.30) for the calculation of surface areas. Prior

to measurement, the fresh samples were heated at ~150°C to remove any absorbed moisture. To measure BET surface areas of activated sample, the reactor was flushed with N_2 after the HT-WGS reaction and quenched with liquid nitrogen without exposing the pyrophoric catalyst to air (*in situ* BET).

5.2.3 X-ray Diffraction (XRD) Spectroscopy

Powder X-ray diffraction (XRD) patterns of fresh WGS catalysts were measured with a Rigaku Miniflex II diffractometer using Cu K-α radiation (1.5418 Å). Full scans from 10-80 degrees (2-theta) were performed with a scan rate of 1 deg/min. Additionally, the major XRD peak from the hematite phase at 34.5-37.5 degrees was scanned with a rate of 0.1 deg/min to examine for possible formation of MO_x-Fe_2O_3 and/or CuO-Fe_2O_3 solid solutions (M=Si, Mg, Al and Cr).

5.2.4 *In Situ* Raman Spectroscopy

The *in situ* Raman spectra were collected with a Horiba-Jobin Yvon LabRam-HR spectrometer equipped with a confocal microscope, 2400/900 grooves/mm gratings, and a notch filter. The visible laser excitation at 442 nm (violet) was generated by a He-Cd laser. The lasers were focused on the samples with a confocal microscope equipped with a 50X long working distance objective (Olympus BX-30- LWD). And the scattered photons were directed and focused onto a single-stage monochromator and measured with a UV-sensitive LN2-cooled CCD detector (Horiba CCD-3000V).

The catalyst samples were placed in an environmentally controlled high-temperature cell reactor (Linkam CCR1000) with the temperature controlled by a temperature controller (Linkam TMS94). The spectrum of the dehydrated sample was collect after catalysts treated by 10% O_2/Ar (Airgas, certified, 10% O_2/Ar balance) at 400°C for 1 hour to remove any possible adsorbed organic impurities and adsorbed moisture. For spectra of the activated catalysts during RWGS reaction, the catalysts were first dehydrated with 10% O_2/Ar at 400°C for 1 hour followed by switching to the RWGS reaction conditions (10 ml/min CO_2 (Airgas, UHP certified gas), 10 ml/min H_2 (Airgas, UHP certified gas), 10 ml/min Ar (Airgas, UHP certified gas)). The *in situ* Raman spectra were then collected at 400ºC after the catalysts were equilibrated under the RWGS reaction conditions for 1 hour at 400ºC.

5.2.5 Isotope Switch Experiments

The $C^{16}O_2/C^{18}O_2$ isotope switch experiments were carried out with an Altamira Instruments system (AMI-200) connected to Dymaxion Dycor mass spectrometer (DME200MS). Approximately 20mg of catalyst was loaded into a quartz U-tube and initially dehydrated with 10% O_2/Ar at 400ºC to remove any residual carbonaceous residue and moisture. After dehydration, the catalyst was first equilibrated in the flowing $C^{16}O_2/H_2$ RWGS reaction conditions at 330°C, then flushed with inert He (20 ml/min He) for 10 min to remove residual $C^{16}O_2/H_2$ reactants from the system, and

lastly exposed to a flow of isotopic labelled $C^{18}O_2/H_2$ reaction mixture (10ml/min $C^{18}O_2$, 10 ml/min H_2). The time-resolved reaction products were monitored every 0.5 seconds with the online mass spectrometer (MS).

5.2.6 Steady-State WGS Reaction

The steady-state forward WGS reaction was perform on an Altamira AMI-200 spectroscope equipped with a Dycor Dymaxion DME200MS online quadrupole mass spectrometer. Approximately 10 mg of catalyst was loaded into a U-type quartz tube for the reaction and the catalyst was held in place by quartz wool. Initially the catalyst was treated with 10% O_2/Ar (Airgas, certified, 10% O_2/Ar balance) at 400°C for 1 hour to remove any possible adsorbed organics by combustion. Then the system was flushed with He for 10 min, after which the reaction mixture was introduced (10% CO/Ar (Airgas, UHP certified gas, 10 ml/min), He (Airgas, UHP certified gas, 30 ml/min) and water vapor introduced by flowing the gas through a water bubbler at 25°C). The HT-WGS reaction was performed at different temperatures for each catalyst for 90 min to ensure steady-state reaction conditions. The gases exiting the quartz tube reactor were analyzed with the online mass spectrometer. The following *m/z* ratios were employed for the identification of reaction gases and products: H_2, $m/z = 2$; H_2O, $m/z = 18$; CO (corrected for CO_2 cracking in MS), $m/z = 28$; CO_2, $m/z = 44$.

5.3 Results

5.3.1 Catalyst Structure

The XRD diffractograms of fresh MO_x-Fe_2O_3 and CuO/MOx-Fe_2O_3 catalysts (M=Si, Mg, Al, Cr) calcined at 400°C are presented in Figure 5.1. The bulk phase of all the catalysts is identical and is the crystalline Fe_2O_3 (hematite) phase. [26] The XRD patterns do not show any separate MO_x crystalline phases. All the promoters (Si, Mg, Al, Cr) form solid solution with Fe_2O_3 as indicated by the slight shift in the XRD hematite peak for the MO_x-Fe_2O_3 mixed oxide catalysts (Figure 5.2). It is not apparent from XRD if CuO also forms a solid solution with MO_x-Fe_2O_3 since the amount of CuO is small and only a slight shift in the XRD peak is detected in the presence of CuO.

The *in situ* Raman spectra of the MO_x-Fe_2O_3 mixed oxide and supported CuO/MO_x-Fe_2O_3 catalysts are presented in Figure 5.3 as a function of environmental conditions. The *in situ* Raman spectra of the initial dehydrated iron oxide mixed oxide and Cu-supported catalysts at 400°C are presented in Figures 5.3a and 5.3c, and exhibit Raman bands at 585, 491, 389, 271 and 208 cm^{-1} that are characteristic of the bulk α-Fe_2O_3 phase [27]. The weak Raman band appearing at ~680 cm^{-1} is attributed to the formation of bulk $Fe_{2-x}M_xO_3$ solid solutions. [12] The Cr-containing Cr_2O_3-Fe_2O_3 and supported CuO/(Cr_2O_3-Fe_2O_3) catalysts possesses two new bands from Cr^{+6} surface dioxo $(O=)_2CrO_2$ sites: 839 cm^{-1} (bridging Cr-O-Fe) vibration and 1000 cm^{-1}

(symmetric O=Cr=O stretch) [28]. Under the reverse water-gas shift (RWGS) reaction at 400ºC (presented in Figures 5.3b and 5.3d), the bulk crystalline α-Fe_2O_3 (hematite) phase reduces and transforms to the bulk crystalline Fe_3O_4 (magnetite) phase (characteristic Raman bands at 282, 498 and 634 cm^{-1}) [29]. The initially fully oxidized surface Cr^{6+} species reduces to Cr^{+3} under the RWGS reaction environment and dissolve into the bulk iron oxide lattice to form additional $Fe_{3-x}Cr_xO_4$ as indicated by the absence of vibrations from the surface Cr-O-Fe and O=Cr=O functionalities [12]. Raman bands from CuO_x are not observed under both dehydrated and reaction conditions and is related to the small concentration and lower Raman cross-section of CuO_x relative to the higher amounts and higher Raman cross-sections of iron and chromium oxides [30].

5.3.2 Catalyst Thermostability

The BET surface areas of fresh and used catalysts are listed in Table 5.1. The MO_x-Fe_2O_3 mixed oxide catalysts contains 8 wt.% MO_x (MO_x = SiO_2, MgO, Al_2O_3 or Cr_2O_3). Among all the fresh MO_x-Fe_2O_3 mixed oxide catalysts, the SiO_2-Fe_2O_3 catalyst has the highest surface area of 162 m^2/g, followed by MgO-Fe_2O_3 (130 m^2/g), and Al_2O_3-Fe_2O_3 has a lower surface area (113 m^2/g) that is still slightly higher than Cr_2O_3-Fe_2O_3 (101 m^2/g). Adding CuO slightly decreases the surface areas (~2-14% with the greatest decrease for supported CuO/(Fe_2O_3-Cr_2O_3).

To examine the thermostability of the catalysts under working condition, the catalysts were tested for 5 hours at 500°C during HT-WGS reaction that is much higher than the normal operating temperature of 350-450°C. The BET surface areas were measured *in situ* without exposing the activated pyrophoric catalysts to air. The Si promoted catalysts exhibits the best thermostability (see Table 5.1), closely followed by Cr and Al promoted catalysts. The Mg promoted catalysts, however, exhibited the poorest thermostability with the lowest BET surface areas after the HT-WGS reaction.

5.3.3 Catalytic Activity (Steady-State HT-WGS Reaction Rates)

The steady-state HT-WGS reaction rates in units of 10^{-6} mol/s·g for the HT-WGS reaction by the MO_x-Fe_2O_3 mixed oxide and supported Cu/(MO_x-Fe_2O_3) catalysts are presented in Figure 5.4 as Arrhenius plots and additional information regarding apparent activation energy values and pre-exponential factors are provided in Table 5.2. The Cr_2O_3-Fe_2O_3 mixed oxide catalyst exhibits the highest HT-WGS activity among the MO_x-Fe_2O_3 mixed oxide catalysts, closely followed by Al_2O_3-Fe_2O_3 and MgO-Fe_2O_3. The SiO_2-Fe_2O_3 mixed oxide catalyst shows the lowest activity for the HT-WGS reaction. The supported Cu/(MO_x-Fe_2O_3) catalysts are significantly more active than the Cu-free MO_x-Fe_2O_3 mixed oxide catalysts reflecting the promotion by Cu. The supported Cu/(Al_2O_3-Fe_2O_3) and Cu/(Cr_2O_3-Fe_2O_3) catalysts exhibit comparable HT-WGS activity. The apparent activation energies for the HT-WGS reaction were found

to be ~101–123 kJ/mol for the Cu-free MO_x-Fe_2O_3 mixed oxide catalysts and decreased to ~67-72 kJ/mol for the Cu promoted catalysts. The decrease in apparent activation energy values is somewhat compensated by the 10^3-10^4x decrease in the apparent pre-exponential factors. The significant increase in activity by the Cu promoter, however, is dominated by the decrease in the apparent activation energy. This indicates that Cu promotes the HT-WGS reaction by lowering the apparent activation energy.[12]

5.3.4 Number of Active Sites (Ns)

The number of active sites present for the HT-WGS activated iron oxide-based catalysts was determined by the isotope switch method ($C^{16}O_2/H_2 \rightarrow C^{18}O_2/H_2$) [31]. This transient isotopic method has been shown to count the number of $^{16}O^*$ catalytic active sites participating in the HT-RWGS reaction. The Ns values for the activated Cu-free and Cu-promoted catalysts are indicated in Table 5.3. The Cu-free MO_x-Fe_2O_3 mixed oxide catalysts possess very similar Ns values (1.7-2.3 x10^{-3} mol/g with Mg ~ Si > Al > Cr. Addition of the Cu promoter to the MO_x-Fe_2O_3 mixed oxide catalysts slightly decreases the number of active sites during HT-WGS and tightens the spread in Ns values (1.7-2.0 x10^{-3} mol/g) with Mg > Si ~ Al > Cr.

5.3.5 Turnover Frequency (TOF)

The turnover frequencies for the HT-WGS reaction were determined by dividing

the catalytic activity (mol/s·g) by the number of catalytic active sites (mol/ g) and the TOF values are presented in Table 5.3. For the Cu-free MO_x-Fe_2O_3 mixed oxide catalysts, the TOF values vary from 0.2-1.2 s^{-1} with Cr > Al > Mg > Si. The addition of Cu increases the TOF by ~3x, confirming the chemical promotion effect of copper on the HT-WGS reaction [12]. The TOF values of the Cu-supported MO_x-Fe_2O_3 mixed oxide catalysts varies from 0.5-3.3 s^{-1} with Cr ~ Al > Mg > Si.

5.4 Discussion

5.4.1 Effect of Promoters on Catalysts Thermostability and Catalytic Activity

5.4.1.1 Bulk MO_x-Fe_2O_3 Mixed Oxide Catalysts

The bulk Cr_2O_3-Fe_2O_3, Al_2O_3-Fe_2O_3 and SiO_2-Fe_2O_3 mixed oxide catalysts exhibit comparable BET surface areas after accelerated aging under HT-WGS at 500^{o}C that are higher than the MgO-Fe_2O_3 catalyst. All the bulk mixed oxide catalysts possess comparable N_s values with the highest TOF values for Cr_2O_3-Fe_2O_3 and Al_2O_3-Fe_2O_3. These parameters, especially the thermostability and TOF variations, account for the bulk Cr_2O_3-Fe_2O_3 and Al_2O_3-Fe_2O_3 mixed oxide catalysts being the better performing Cu-free HT-WGS catalysts with the Cr-containing catalyst performing slightly better than the Al-containing catalyst (see Figure 5.4a).

5.4.1.2 Supported Cu/(MO_x-Fe_2O_3) Catalysts

The Cu-supported Cr_2O_3-Fe_2O_3, Al_2O_3-Fe_2O_3, SiO_2-Fe_2O_3, MgO-Fe_2O_3

catalysts exhibit variable BET surface areas after accelerated aging under HT-WGS at 500^{o}C with Si > Al ~Cr > Mg. As for the bulk mixed oxide catalysts, the Cu-supported catalysts possess comparable N_s values with the highest TOF values for supported Cu/(Cr_2O_3-Fe_2O_3) and Cu/(Al_2O_3-Fe_2O_3) catalysts. These parameters, especially the thermostability and TOF variations, account for the supported Cu/(Cr_2O_3-Fe_2O_3) and Cu/(Al_2O_3-Fe_2O_3) catalysts being the better performing Cu-promoted HT-WGS catalysts with the Cr-containing catalyst performing slightly better than the Al-containing catalyst (see Figure 5.4b).

5.4.2 Evaluation of Cr-Free Supported Cu/(MO_x-Fe_2O_3)-based Catalysts for HT-WGS

A suitable Cr-free iron oxide-based HT-WGS catalyst needs to satisfy multiple criteria (thermostability, high Ns and TOF). Although the SiO_2-Fe_2O_3 catalyst possess the best thermostability during HT-WGS, it also exhibits the lowest TOF value making SiO_2 a poor replacement for Cr (see Figure 5.4). In contrast, the MgO-Fe_2O_3 catalyst possess the poorest thermostability during HT-WGS and intermediate TOF values making it a modestly performing replacement for Cr (see Figure 5.4). The supported Cu/(Al_2O_3-Fe_2O_3) catalyst exhibits comparable thermostability during HT-WGS and TOF to the conventional supported Cu/(Cr_2O_3-Fe_2O_3) making Al_2O_3 a suitable replacement for Cr (see Figure 5.4).

5.5 Conclusions

The current concern that hexavalent chromium (Cr^{+6}), a potent carcinogen that threatens human life and the environment, is present in the industrial HT-WGS iron-chromium oxide-based catalyst motivated this study to examine possible Cr-free replacements. Three candidate elements (Mg^{+2}, Al^{+3}, and Si^{+4}) were selected based on their different oxidation states as possible substitutes for Cr in HT-WGS iron oxide-based catalysts. The SiO_2 promoted catalyst was found to yield the best thermostability under HT-WGS, but lowest TOF value that compromised its effectiveness. The poor thermostability under HT-WGS and its modest TOF value of the MgO promoted catalyst compromised the effectiveness of this catalyst. The Al_2O_3 promoted catalyst was found to exhibit comparable thermostability and TOF to the conventional Cr_2O_3-Fe_2O_3 catalysts (both Cu-free and supported Cu) making Al_2O_3 the best substitute for Cr-free HT-WGS supported Cu/iron oxide catalysts.

Acknowledgment

The authors acknowledge financial support from National Science Foundation Grant CBET - 1511689.

References

[1] D.S. Newsome, Catal. Rev.: Sci. Eng. 21 (1980) 275-318.

[2] C. Ratnasamy, J.P. Wagner, Catal. Rev.: Sci. Eng. 51 (2009) 325-440.

[3] M.L. Kundu, A.C. Sengupta, G.C. Maiti, B. Sen, S.K. Ghosh, V.I. Kuznetsov, G.N. Kustova, E.N. Yurchenko, J. Catal. 112 (1988) 375-383.

[4] A. Patlolla, E.V. Carino, S.N. Ehrlich, E. Stavitski, A.I. Frenkel, ACS Catal. 2 (2012) 2216-2223.

[5] A. Andreev, V. Idakiev, D. Mihajlova, D. Shopov, Appl. Catal. 22 (1986) 385-387.

[6] V. Idakiev, D. Mihajlova, B. Kunev, A. Andreev, React. Kinet. Catal. Lett. 33 (1987) 119-124.

[7] G.K. Reddy, K. Gunasekera, P. Boolchand, J.H. Dong, P.G. Smirniotis, J. Phys. Chem. C 115 (2011) 7586-7595.

[8] G.K. Reddy, P. Boolchand, P.G. Smirniotis, J. Phys. Chem. C 116 (2012) 11019-11031.

[9] F. Meshkani, M. Rezaei, Korean J. Chem. Eng. 32 (2015) 1278-1288.

[10] F. Meshkani, M. Rezaei, Chem. Eng. J. 260 (2015) 107-116.

[11] S.M. Latifi, A. Salehirad, Korean J. Chem. Eng. 33 (2016) 473-480.

[12] M. Zhu, T.C.R. Rocha, T. Lunkenbein, A. Knop-Gericke, R. Schlögl, I.E. Wachs, ACS Catal. (2016) 4455-4464.

[13] C. Pellerin, S.M. Booker, Environ. Health Perspect. 108 (2000) A402-A407.

[14] G.C. Chinchen, in: E.B. Catalytic preparation of hydrogen from carbon monoxide and water (Ed.), 1982.

[15] D.G. Rethwisch, J.A. Dumesic, Appl. Catal. 21 (1986) 97-109.

[16] J.Y. Lee, D.W. Lee, K.Y. Lee, Y. Wang, Catal. Today 146 (2009) 260-264.

[17] J.Y. Lee, D.W. Lee, Y.K. Hong, K.Y. Lee, Int. J. Hydrogen Energy 36 (2011) 8173-8180.

[18] J.Y. Lee, D.W. Lee, M.S. Lee, K.Y. Lee, Catal. Commun. 15 (2011) 37-40.

[19] G.C. de Araujo, M.D. Rangel, Catal. Today 62 (2000) 201-207.

[20] Q.S. Liu, W.P. Ma, R.X. He, Z.J. Mu, Catal Today 106 (2005) 52-56.

[21] J.M.T. de Souza, M.D. Rangel, React. Kinet. Catal. Lett. 77 (2002) 29-34.

[22] A.O. de Souza, M.D. Rangel, React. Kinet. Catal. Lett. 79 (2003) 175-180.

[23] J.M.T. de Souza, M.D. Rangel, React. Kinet. Catal. Lett. 83 (2004) 93-98.

[24] A. Khan, P. Chen, P. Boolchand, P.G. Smirniotis, J. Catal. 253 (2008) 91-104.

[25] F. Meshkani, M. Rezaei, M. Jafarbegloo, Mater. Res. Bull. 70 (2015) 229-235.

[26] I.S. Lyubutin, C.R. Lin, Y.V. Korzhetskiy, T.V. Dmitrieva, R.K. Chiang, J. Appl. Phys. 106 (2009) 034311.

[27] J.M. Jehng, I.E. Wachs, F.T. Clark, M.C. Springman, J. Mol. Catal. 81 (1993) 63-75.

[28] E.L. Lee, I.E. Wachs, J. Phys. Chem. C 111 (2007) 14410-14425.

[29] K.F. Mccarty, D.R. Boehme, J. Solid State Chem. 79 (1989) 19-27.

[30] M. Kilo, C. Schild, A. Wokaun, A. Baiker, J. Chem. Soc., Faraday Trans. 88 (1992) 1453-1457.

[31] M. Zhu, I.E. Wachs, ACS Catal. 6 (2016) 1764-1767.

FIGURES

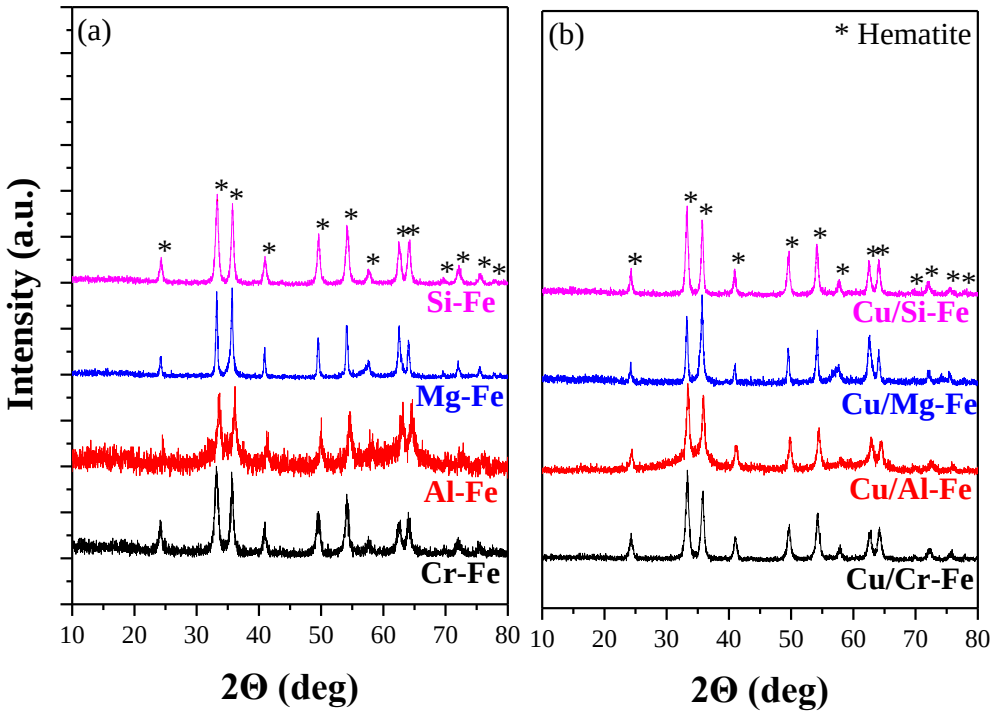

Figure 5.1 XRD diffractograms of fresh calcined (a) MO_x-Fe_2O_3 and (b) CuO-MOx-Fe_2O_3 catalysts (M=Si, Mg, Al and Cr). * represents the XRD peaks of the hematite phase.

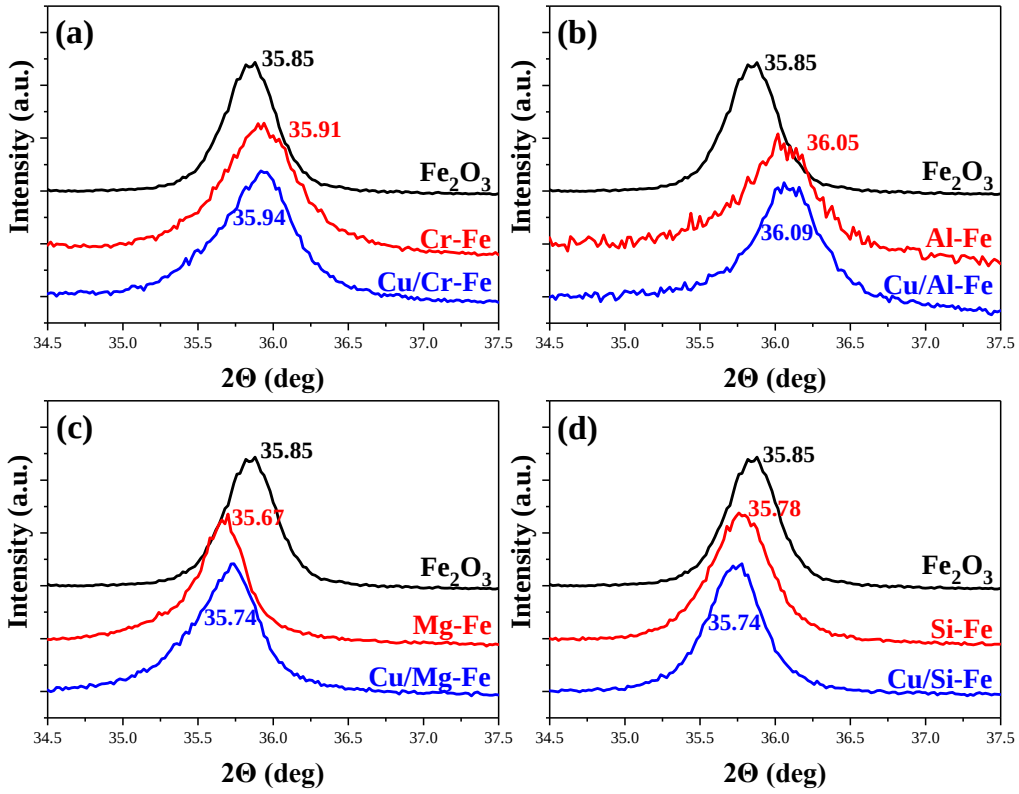

Figure 5.2 Main XRD peak of hematite (1 1 0) of the fresh calcined MO_x-Fe_2O_3 and CuO-MO_x-Fe_2O_3 catalysts (M=Si, Mg, Al and Cr).

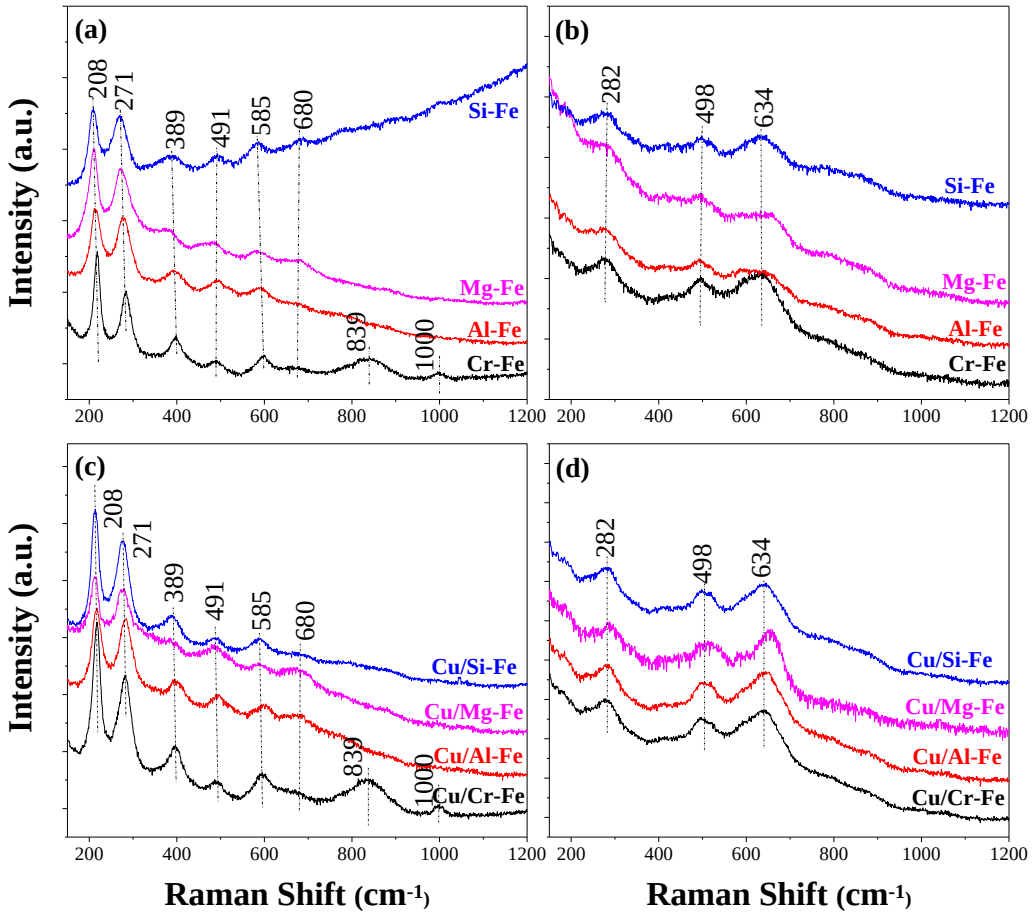

Figure 5.3 The in situ Raman spectra of MO_x-Fe_2O_3 mixed oxide catalysts (M=Si, Mg, Al and Cr) under (a) dehydrated conditions (T=400^{o}C; 10% O_2/Ar) and (b) RWGS reaction conditions (T = 400^{o}C; 10 ml/min CO_2, 10 ml/min H_2 and 10 ml/min Ar) and CuO-MO_x-Fe_2O_3 under (c) dehydrated conditions and (d) RWGS reaction conditions.

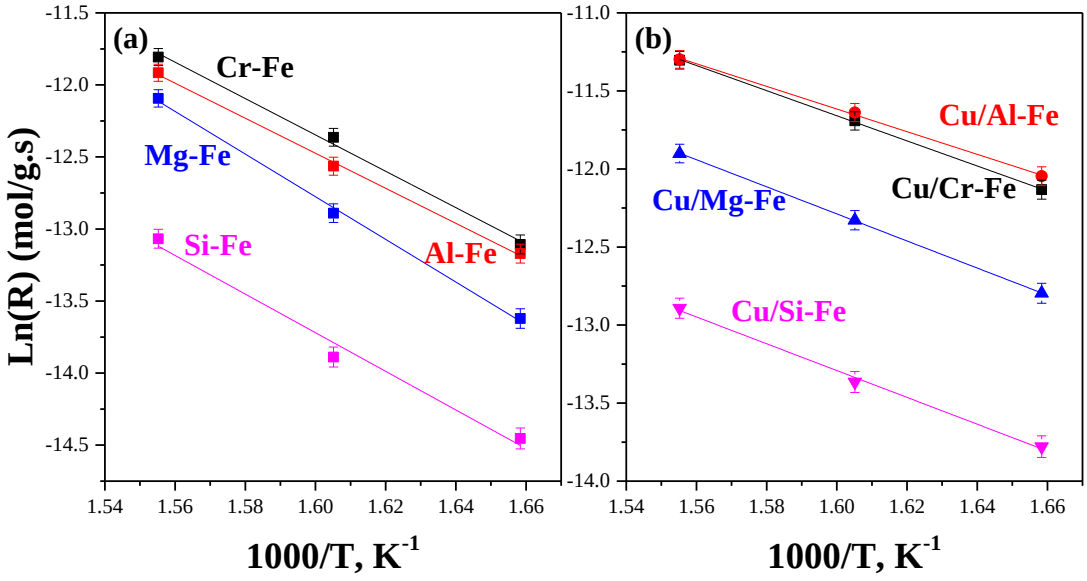

Figure 5.4 Arrhenius plots for steady-state WGS reaction activity for (a) MO_x-Fe_2O_3 mixed oxide catalysts; (b) supported Cu/MO_x-Fe_2O_3 catalysts.

TABLES

Catalyst	BET Surface Area (m^2/g)	
	Fresh	**Used**
SiO_2-Fe_2O_3	162	44
CuO/SiO_2-Fe_2O_3	159	40
MgO-Fe_2O_3	130	29
CuO/MgO-Fe_2O_3	119	23
Al_2O_3-Fe_2O_3	113	42
CuO/Al_2O_3-Fe_2O_3	104	35
Cr_2O_3-Fe_2O_3	101	41
CuO/Cr_2O_3-Fe_2O_3	87	34

Table 5.1 BET surface areas of fresh and used catalysts. The used catalysts were treated under HT-WGS condition at 500°C for 5 hours.

Catalyst	Apparent Activation Energy Ea (kJ/mol)	Pre-exponential A (mol/g·s)
Cr-Fe	105 ± 7	3×10^3
Al-Fe	101 ± 4	1×10^3
Mg-Fe	123 ± 5	5×10^4
Si-Fe	111 ± 14	2×10^3
Cu/Cr-Fe	67 ± 1	3
Cu/Al-Fe	60 ± 2	1
Cu/Mg-Fe	72 ± 1	5
Cu/Si-Fe	71 ± 4	2

Table 5.2 Apparent activation energy and pre-exponential factor for the MO_x-Fe_2O_3 mixed oxide and supported Cu/MO_x-Fe_2O_3 catalysts.

Catalyst	WGS Activity H_2O conversion (10^{-6} mol/s·g)	Ns (10^{-3} mol/ g)	TOF (10^{-3} s^{-1})
Cr-Fe	2.0	1.7	1.2
Cu/Cr-Fe	5.4	1.7	3.3
Al-Fe	1.9	1.9	1.0
Cu/Al-Fe	5.9	1.8	3.2
Mg-Fe	1.2	2.3	0.5
Cu/Mg-Fe	2.8	2.0	1.4
Si-Fe	0.5	2.3	0.2
Cu/Si-Fe	1.0	1.9	0.5

Table 5.3 WGS activity, number of sites, and turnover frequencies (TOFs). (10% CO/Ar (10 ml/min), He (30 ml/min) and water vapor (H_2O/CO ~1); T=330°C)

CHAPTER 6

Conclusions and Future Studies

6.1 Conclusions

The reaction mechanism of the high temperature water-gas shift (HT-WGS) reaction catalyzed by chromium-iron oxide catalysts for H_2 production has been studied for 100 years covering the reaction mechanism, reaction intermediates, rate-determining-step, overall kinetics, catalytic active site and role of promoters. Unlike the Low Temperature Water-Gas Shift (LT-WGS) reaction by Cu/ZnO catalysts that has received intensive analysis with modern *in situ* and *operando* spectroscopy and DFT studies, the corresponding HT-WGS reaction by iron oxide-based catalysts still lacks a fundamental understanding because of the absence of modern catalysis studies of this important catalytic system. Given the role of the WGS catalysts on production of H_2 for a hydrogen economy, it is imperative that the fundamental molecular level understanding of the HT-WGS catalyst be advanced. Recently, there has been much interest in developing a Cr-free iron oxide HT-WGS catalyst because of the presence of toxic hexavalent chromium (VI) oxide in this catalyst. The lack of fundamental understanding of how the HT-WGS catalyst functions, especially the role of Cr oxide,

however, hampers the development of Cr-free HT-WGS iron oxide-based catalysts is covered in the literature review provided in Chapter 1. This dissertation investigated and discussed the fundamental aspects of current the CuO-Cr_2O_3-Fe_2O_3 HT-WGS catalyst. Based on such fundamental understanding, new Cr-free catalysts were rationally designed. The main conclusions of each chapter containing the research performed for this dissertation are summarized below.

Chapter 2

A series of temperature programmed surface reaction (TPSR) spectroscopy (CO-TPSR, CO+H_2O-TPSR and HCOOH-TPSR) with equilibrated Cr_2O_3-Fe_2O_3 catalysts) were used to study the reaction mechanism of the HT-WGS on iron oxide-based catalysts. The evolution of CO_2 and H_2 from the TPSR studies was able, *for the first time*, to demonstrate that the HT-WGS reaction by Cu/CrO_x-FeO_x catalysts follows a redox mechanism where the catalyst surface is alternatively reduced by CO and re-oxidized by H_2O. The alternatively proposed associative reaction mechanism for CO_2 and H_2 formation proceeding through a surface reaction intermediate, such as surface formate, and its decomposition is disproved by the current findings. The new mechanistic insight will be fundamental towards the understanding of copper and chromium promotion mechanism and the discovery of a non-toxic Cr-free HT-WGS catalysts for manufacture of clean H_2 fuel.

Chapter 3

In this chapter, based on the mechanistic understanding from Chapter 2 that the HT-WGS reaction by iron-oxide based catalysts follows a redox mechanism, the Fe_2O_3, Cr_2O_3-Fe_2O_3 and CuO-Cr_2O_3-Fe_2O_3 catalysts were investigated with transient $C^{16}O_2/C^{18}O_2$ isotope switch measurements to determine the number of catalytic active sites participating in the HT-WGS reaction. The HT-WGS reaction by iron oxide-based catalysts was found to follow a redox mechanism primarily involving oxygen atoms from the surface layer and the participating oxygen atoms represent the most abundant reactive intermediate (mari). The isotopic switch experiments allow *for the first time* determination of the number of catalytic active sites and specific catalytic reactivity (TOF). The Cr was found to be a textural promoter that increases the number of participating oxygen sites by stabilizing a higher surface area of iron oxide (the main catalyst component). The Cu was found to be a chemical promoter that increases the specific reaction rate (TOF) of the HT-WGS reaction by iron oxide-based catalysts. The dual promotion of iron oxide by Cr and Cu yields a HT-WGS catalyst that has a specific reaction rate (TOF) that is ~3x greater and a catalyst activity per gram that is ~5x greater than an unpromoted iron oxide catalyst.

Chapter 4

Iron oxide, chromium-iron oxide and copper promoted chromium-iron oxide

catalysts were prepared and extensively studied with modern characterization techniques in this chapter. The catalyst bulk and surface structures both before and during the reaction were analyzed with *operando* NAP-XPS (Near Ambient Pressure X-ray Photoelectron Spectroscopy)-MS, *in situ* Raman, *in situ* XANES (X-ray Absorption Near Edge Spectroscopy), XRD, TEM/EDX and HS-LEIS (High Sensitivity-Low Energy Ion Scattering). The nature of the catalytic active sites and the redox characteristics of the catalyst bulk and surface components during WGS were examined with *in situ* XANES and NAP-XPS-MS. The promotion mechanisms of chromium and copper upon the redox behavior of the iron oxide catalysts were also examined by CO-TPR on catalysts activated under the HT-WGS reaction conditions.

The fresh chromium promoted iron oxide catalysts contain the α-Fe_2O_3 (hematite) bulk phase and surface Cr^{6+} species with Cu^{2+} and some Cr^{3+} migration into the iron oxide bulk lattice. During the HT-WGS reaction, the α-Fe_2O_3 phase is partially reduced to Fe_3O_4 (magnetite) and surface Cr^{6+} reduces to Cr^{3+} that dissolves into the bulk lattice to form a $Fe_{3-x}Cr_xO_4$ solid solution. The initially dispersed Cu^{2+} is reduced to Cu^0 and migrates onto the catalyst surface and forms metallic Cu^0 nanoparticles with average dimension of ~3nm. About 30% of the Cu surface is also covered by an FeO_x overlayer due to a strong metal support interaction (SMSI). The Cr oxide promoter does not function as a redox chemical promoter and only acts as structural stabilizer (textural

promoter) that retards sintering of the working catalyst as well as over-reduction of the bulk iron oxide phase during the HT-WGS reaction. The Cu promoter, however, functions as a redox chemical promoter by providing new highly active catalytic metallic Cu^0 sites and Cu-iron oxide interfacial sites. These new fundamental insights, *for the first time*, provide direct experimental evidence of the promotion mechanisms of chromium and copper upon the iron oxide-based HT-WGS catalysts.

Chapter 5

In this chapter, Cr substitutes were selected because of their earth abundance and variable oxidation states: Mg^{+2}, Al^{+3} and Si^{+4}. The SiO_2-Fe_2O_3, MgO-Fe_2O_3, Al_2O_3-Fe_2O_3 and Cr_2O_3-Fe_2O_3 mixed oxide catalysts were synthesized by the co-precipitation method. The Cu-promoted SiO_2-Fe_2O_3, MgO-Fe_2O_3, Al_2O_3-Fe_2O_3 and Cr_2O_3-Fe_2O_3 catalysts were synthesized by subsequent impregnation of a Cu precursor. The performance of catalysts was evaluated based on activity, Ns, TOF and thermostability after ultra-high temperature operation, allowing a systematic discussion and selection the best promoter candidate to replace toxic chromium. Among the three promoter candidates (magnesium, aluminum and silicon), aluminum appears to be the best substitute providing comparable activity, number of active sites, turnover frequency and thermostability to the Cr-promoted HT-WGS supported Cu/iron oxide catalysts. Hence, the supported Cu/$Fe_{2-x}Al_xO_3$ appears to be a viable alternative for the current

commercial supported $Cu/Fe_{2-x}Cr_xO_3$ HT-WGS catalyst.

6.2 Future Studies

The majority part of work that have been done within this thesis focus on understanding of the current industrially used catalyst which consists of CuO-Cr_2O_3-Fe_2O_3. The understanding of the HT-WGS reaction, catalytic structure, chemical states, copper and chromium promotion mechanisms serve as fundamental knowledge that will guide the development of new chromium-free iron based catalysts as has been illustrated in Chapter 5. There are some more aspects that require more detailed research and discussion to design a better chromium-free iron based catalysts for the high temperature water-gas shift reaction:

1) The importance of copper and the copper - iron oxide interface have been illustrated in Chapter 4. In our study, only 3 wt.% of copper oxide was added as a promoter, corresponding to ~2.5 wt. % of metallic copper during the HT-WGS reaction. With an average dimension of ~3 nm, the surface coverage of copper under working conditions is low, resulting in a limited amount of copper – iron oxide interface. Hence, focuses can be given on how to stabilize the surface of the metallic copper during the HT-WGS reaction. The precursors, preparation methods and promoters are key aspects that should be investigated. Proper *in situ* characterization methods also need to be performed to accurately determine the size of surface copper metal

during reaction. Any *ex situ* measurements suffer the risk of copper re-oxidation and structural change.

2) The copper – iron oxide interface was shown to provide higher HT-WGS activity than either copper or iron oxide individually. It's difficult though to study how the two components synergistically interact with each other. DFT calculations would be an ideal method to resolve this issue by creating copper clusters on a clean Fe_3O_4 surface and examining the influence of decoration of the metallic copper nanoparticles by FeO_x. Per the conclusion of Chapter 2, the redox mechanism should be invoked when DFT calculations are performed. The CO adsorption, H_2O adsorption, H_2O dissociation and CO oxidation are key steps to be calculated and compared among pure Fe_3O_4 surface, pure Cu surface and the Cu-Fe_3O_4 interface.
3) It has been concluded in Chapter 3 that only surface oxygen is involved in the HT-WGS redox reaction. Thus, supported monolayer Fe_3O_4 can be a good direction to improve the WGS activity by spreading Fe_3O_4 on a support with high surface area. To move one step further, supported monolayer Fe_2O_3/CuO may be synthesized to maximize the Fe_2O_3-Cu interface.
4) In Chapter 5, new chromium-free catalysts were discussed based on activity, Ns, TOF and thermostability. During industrial use, however, there are more parameters that should be considered in the rational design of Cr-free supported

Cu/iron oxide HT-WGS catalysts such as tolerance to sulphur and performance under different feed gas compositions, etc. Thus, to better evaluate the catalyst a variety of reaction gas components and composition need to be tested on any new catalyst formulation to determine its efficacy. This will provide more realistic insights about the performance of new Cr-free supported Cu/iron oxide HT-WGS catalysts for industrial applications.

VITAE

Education

Global Study Program, University of California, Davis, **2010**
B.S. in Chemical and Biological Engineering, Zhejiang University, **2011**
Ph.D. in Chemical Engineering, Lehigh University, expected completion **2016**
Advisor: Israel E. Wachs

Research Experience

LEHIGH UNIVERSITY, Bethlehem, PA

Rational Design of High Temperature Water-Gas Shift (HT-WGS) Catalysts with Non-Toxic Earth-Abundant Elements

- Demonstrated *for the first time* that the HT-WGS on iron-based catalysts follows the redox mechanism rather than the associative mechanism, thus resolving the decades-old debate about the mechanism of the HT WGS reaction.
- Elucidated both bulk and surface structure of copper promoted ferrite catalyst before and during HT-WGS reaction.
- Proved experimentally that chromium is only a textural promoter and copper is the chemical promotor.
- Proposed the promotion mechanism of copper for iron based HT-WGS catalysts.
- Discovered new chromium-free iron-based HT-WGS catalyst with better activity and comparable thermo-stability.

Selective Catalytic Reduction (SCR) of NO with NH_3 by Supported V_2O_5-WO_3/TiO_2 Catalysts

- Improved catalyst performance and created new active sites by co-precipitation; characterized supported V_2O_5-WO_3/TiO_2 catalysts synthesized by different methods and provided critical information regarding catalyst bulk and surface.
- Discovered key aspects of the SCR mechanism by a series of isotopically labeled experiments.

Conversion of Ethanol to Butadiene on promoted Zr/SiO_2 catalysts

- Identified reaction pathways from ethanol to butadiene by proving that diethyl ether is not reaction intermediate, and reaction of acetaldehyde with ethanol is required to form butadiene.
- Evaluated efficiency of catalyst promoters on conversion and selectivity to butadiene.

ZHEJIANG UNIVERSITY, Hangzhou, China

Rational Design of Ru/Zn Catalyst for Selective Hydrogenation of Benzene to Cyclohexene

- Discovered catalyst for highest selectivity and conversion of benzene selective hydrogenation to cyclohexene
- Optimized hydrogenation reaction conditions for highest productivity.

UNIVERSITY OF CALIFORNIA, DAVIS, Davis, CA

Synthesis and Characterization of Nanocrystalline Lithium Nickel Oxide

- Synthesized and characterized $LiNiO_2$; demonstrated that formation of NiO and Li_2CO_3 was unavoidable at relatively low temperature; provided an ideal sample to simulate lithium deficient conditions during electrochemical lithium displacement.

AWARDS

ACS CATL Division Travel Award (2016)
Kokes Award - 24th North American Catalysis Society Meeting, Pittsburgh (2015)
3rd prize - Principles of Process Engineering Contest (2010)
Third-Class Scholarship for Outstanding Performance at Zhejiang University (2010)
Third-Class Scholarship for Outstanding Students at Zhejiang University (2010)
Excellent Student Award for Outstanding Performance at Zhejiang University (2008)
Third-Class Scholarship for Outstanding Students at Zhejiang University (2008)

PUBLICATIONS

(1) The Dynamics of CrO_3-Fe_2O_3 Catalysts during the High Temperature Water-Gas Shift Reaction: Molecular Structures and Reactivity
Keturakis, C. J.; Zhu, M.; Gibson, E. K.; Daturi, M.; Tao, F.; Frenkel, A. I.; Wachs, I. E. *ACS Catal.* **2016**.

(2) Promotion Mechanisms of Iron Oxide-Based High Temperature-Water Gas Shift (HT-WGS) Catalysts by Chromium and Copper
Zhu, M.; Rocha, T. C. R.; Lunkenbein, T.; Knop-Gericke, A.; Schloegl, R.; Wachs, I. E. *ACS Catal.* **2016**, *6*, 4455-4464.

(3) Influence of Catalyst Synthesis Method on Selective Catalytic Reduction (SCR) of NO by NH_3 with V_2O_5-WO_3/TiO_2 Catalysts
He, Y.; Ford, M. E.; Zhu, M.; Liu, Q.; Tumuluri, U.; Wu, Z.; Wachs, I. E. *Appl. Catal., B* **2016**, *193*, 141-150.

(4) Resolving the Reaction Mechanism for H_2 Formation from High-Temperature Water-Gas Shift by Chromium-Iron Oxide Catalysts
Zhu, M.; Wachs, I. E. *ACS Catal.* **2016**, *6*, 2827-2830.

(5) Determining Number of Active Sites and TOF for the High-Temperature Water Gas Shift

Reaction by Iron Oxide-Based Catalysts
Zhu, M.; Wachs, I. E. *ACS Catal.* **2016**, *6*, 1764-1767.

(6) Selective Catalytic Reduction of NO by NH_3 with WO_3-TiO_2 Catalysts: Influence of Catalyst Synthesis Method
He, Y.; Ford, M. E.; Zhu, M.; Liu, Q.; Wu, Z.; Wachs, I. E. *Appl. Catal., B* **2016**, *188*, 123-133.

(7) Iron-Based Catalysts for the High-Temperature Water–Gas Shift (HT-WGS) Reaction: A Review
Zhu, M.; Wachs, I. E. *ACS Catal.* **2016**, *6*, 722-732.

(8) Synthesis, size reduction, and delithiation of carbonate-free nanocrystalline lithium nickel oxide
Dearden, C.; Zhu, M.; Wang, B. B.; Castro, R. H. R. *J. Mater. Sci.* **2013**, *48*, 1740-1745.